MICROWAVE INTEGRATED CIRCUIT BROADBAND FILTERS AND CONTIGUOUS MULTIPLEXERS

by

JOHN E. DEAN, B.Sc.

A thesis presented for the degree of Doctor of Philosophy, in the Department of Electrical and Electronic Engineering at the University of Leeds

October 1979

ABSTRACT

A novel design and construction technique for Microwave Integrated Circuit broadband filters and a contiguous multiplexer is presented together with experimental results on a number of devices. The multiplexer is formed from a cascade of diplexers each containing a highpass and lowpass filter. Based on the generalised Chebyshev prototype, selective low loss microwave filters for these diplexers are designed having new suspended substrate configurations. Octave bandwidths are achieved for the highpass channels. The contiguous multiplexer built has three outputs 4 - 8 GHz, 8 - 12 GHz and 12 - 18 GHz and is constructed on a single substrate approximately 2" x 1¼". Experimental results show each channel has low passband loss and highly selective responses at the bandedges and the multiplexer will meet the normal environmental conditions. Also, due to the printed circuit realisation, a high degree of population tracking can be readily achieved. Detailed computer analysis of the devices is presented and results are in very close agreement with the experimental results. Suitable constructional techniques are developed so the final multiplexer could be manufactured on a commercial basis.

ACKNOWLEDGEMENTS

The author wishes to express his sincere gratitude to Professor J.D. Rhodes who supervised the research and took an active part in it. The author would also like to thank Professor P.J. Lawrenson for permission to undertake the research in the Department of Electrical and Electronic Engineering at the University of Leeds and for the use of the facilities offered by the Department. Finally, the author wishes to thank Filtronic Components Ltd., Ferranti Ltd. and the Ministry of Defence for supporting this work.

CONTENTS

Page No.

LIST OF MAIN SYMBOLS

Lumped Lowpass Prototype

C_r, $r = 2,4,\ldots,(n-1)$: Series capacitance in shunt resonant sections.

C'_2: Modified C_2, when prototype is used in a contiguous diplexer.

L_o: Insertion loss in dB.

L_r, $r = 1,3,\ldots,n$: Series inductances.

L_r, $r = 2,4,\ldots,(n-1)$: Series inductance in shunt resonant sections.

L'_1: Modified L_1, when prototype is used in a contiguous diplexer.

f: General frequency

m: Number of resonant sections

n: Degree of prototype

ω: General angular frequency

ω_3: Angular frequency when the insertion loss is 3 dB

ω_o: Angular frequency of finite transmission zeros

ω_{40}: Angular frequency closest to bandedge where the insertion loss reaches 40 dB.

ϵ: Passband ripple level of amplitude response (i.e. of $|S_{12}|^2$)

Frequency Transformations

a_H: Simple scaling factor for the distributed quasi highpass prototype, determining the actual cut-off frequency.

a_L: Simple scaling factor for the distributed quasi lowpass prototype, determining the actual cut-off frequency.

p : Lumped complex frequency variable.

t : Distributed complex frequency variable

α_H: Constant in the reciprocal of Richards frequency transformation. It determines the ratio of passband bandwidth to bandedge frequency for the distributed highpass prototype. In this work $\alpha_H = \omega_o$.

α_L: Constant in Richards frequency transformation. It determines the ratio of stopband bandwidth to bandedge frequency for the distributed lowpass prototype. In this work $\alpha_L = 1/\omega_o$.

Distributed Quasi Lowpass Prototype

f_{bL}: Bandedge frequency, i.e. first frequency where the insertion loss just increases above the passband ripple level (N.b. $\omega_{bL} = 2\pi f_{bL}$)

f_{40L}: Frequency closest to bandedge where the insertion loss reaches 40 dB.

f_{cL}: Centre frequency of stopband.

S_L : Selectivity of skirt characteristic. In this work, $S_L = (f_{40L} - f_{3L})/f_{3L}$, where f_{3L} is the 3 dB frequency of the distributed quasi lowpass prototype. For a diplexer, selectivity is expressed in terms of the crossover frequency.

Y_r, $r = 2,4,\ldots,(n-1)$: Characteristic admittance of shunt resonant o/c stubs, normalised to 1 Ω terminations.

Z_r : $Z_r = 1/Y_r$

λ_{cL}: Wavelength of TEM propagation at f_{cL}. Depends on dielectric constant of medium.

Distributed Quasi Highpass Prototype

f_{bH} : Bandedge frequency (N.b. $\omega_{bH} = 2\pi f_{bH}$)

f_{40H}: Frequency closest to bandedge where the insertion loss reaches 40 dB.

f_{cH} : Centre frequency of passband.

S_H : Selectivity of skirt characteristic. In this work $S_H = (f_{3H} - f_{40H})/f_{3H}$, where f_{3H} is the 3 dB frequency of the distributed quasi highpass prototype.

Z_{in} : Input impedance seen looking towards the source/load at a plane immediately left/right of the first/last shunt resonator

Z_{rH}, $r = 1,3,\ldots,n$: Impedance of the series o/c stubs at a frequency f.

λ_{cH} : Wavelength of TEM propagation at f_{cH}

Printed Circuit Filters and Multiplexers

(a) Quantities common to both highpass and lowpass filters

C'_f : Fringing capacitance for an isolated rectangular strip in a homogeneous medium.

C'_{fe}: Even mode fringing capacitance for coupled rectangular strips in a homogeneous medium

C'_{fo}: Odd mode fringing capacitance for coupled rectangular strips in a homogeneous medium

(N.b. These fringing capacitances are shown in the Appendix, section A2).

b : Ground plane spacing of housing containing printed circuit. In this work, b = 0.07"

h : Thickness of substrate. In this work, h = 0.005"

t : Thickness of copper conductors on substrate. In this work, t ≈ 0.00085".

ε : Absolute permittivity of a medium

ε_o : Absolute permittivity of free space = 8.854×10^{-12} F/m.

ε_r : Dielectric constant of a medium. Normally, ε_r = dielectric constant of duroid 5880 = 2.22

u : Velocity of light in free space = 2.998×10^8 m/s

(b) Lowpass filter

ℓ_{rL}, r = 1,3,...,n: Designed length of unit elements

ℓ'_{rL}, r = 1,3,...,n: Physical length of unit elements, i.e. distance between neighbouring resonators.

ℓ_{rL}, r = 2,4,...,(n-1): Designed length of shunt resonators

ℓ'_{rL}, r = 2,4,...,(n-1): Physical length of shunt resonators, i.e. length of shunt arm not including any extension into the T-junction.

L_{rL}, r = 1,3,...,n: Lumped inductance of series inductors which have the same bandedge impedance as the corresponding series s/c stubs of the distributed lowpass prototype.

s : Distance of unit elements from nearest side box wall.

w_L : Width of unit elements

w_{rL}, r = 2,4,...,(n-1): Width of shunt resonators

w'_{rL} : Modified width of shunt resonators to account for interaction between the fringing fields of the resonator

Z_L : Characteristic impedance of the unit elements.

(c) Highpass filter

ℓ_{rH}, r = 2,4,...,(n-1) : Designed length of shunt resonators

ℓ'_{rH}, r = 2,4,...,(n-1) : Physical length of shunt resonators

w_{rH}, r = 2,4,...,(n-1) : Width of shunt resonators.

w'_{rH}, r = 2,4,...,(n-1) : Modified width of shunt resonators to account for interaction between fringing fields of the resonator.

The following symbols apply to each inhomogeneous section; the suffix r is used to denote each section and takes the values 1,3,..., (n-1) :

C_{oor} : Per-unit-length capacitance-to-ground of each coupled line operating in the odd mode, not including end effects.

f_c : Frequency (s) where the <u>total</u> shunt admittances of the highpass become zero.

ℓ_{rH} : Length

s_1 : Distance of the inhomogeneous sections from the nearest side box wall.

u_{or} : Phase velocity of the odd mode.

u_{er} : Phase velocity of the even mode. In this work $u_{er} \approx u = 2.998 \times 10^8$ m/s.

w_r : Width

w_{er} : Effective width when calculating Z_{oor} to account for finite strip thickness. In this work $w_{er} = w_r + t$.

w'_{er} : Different effective width when calculating ε_{er}. In this work $w'_{er} = w_r - t$

$Y'_r(f)$: Shunt admittance of equivalent pi-network of inhomogeneous section at frequency f.

Z'_{in} : Input impedance seen looking towards the source/load at a plane immediately to the left/right of the first/last shunt resonator.

Z_{oer} : Characteristic impedance of each coupled line for the even mode.

Z_{oor} : Characteristic impedance of each coupled line for the odd mode.

Z'_{rH} : Series impedance of equivalent pi-network of inhomogeneous section at frequency f.

ε_{er} : Effective dielectric constant of the medium for the odd mode.

$\varepsilon_{er}(f)$: Variation of ε_{er} with frequency, i.e. dispersion effects.

θ_{er} : Electrical length of the coupled lines for the even mode.

θ_{or} : Electrical length of the coupled lines for the odd mode.

η_o : Characteristic impedance of free space = 376.73 Ω .

1. INTRODUCTION

1.1 Advantages of Printed Circuit Multiplexers

One of the key components for Electronic Warfare signal sorting is the broadband microwave contiguous multiplexer. In this country there is a current and an increasing demand for such multiplexers, with the only source of supply being in the USA. In Ref. [1.1], H.L. Schumacher describes a multioctave contiguous channel multiplexer supplied from the USA. This multiplexer is constructed of coaxial lowpass and highpass filters and consists of a main body with several components internally milled and with additional discrete components to form the complete electrical circuit. Due to the frequent requirement of population tracking between devices, great skill is required in the assembly and alignment of these multiplexers.

For operation up to 18 GHz, precision construction techniques must be used and great advantages were forseen in printed circuit realisations. The initial aim of this thesis was to develop a highly selective broadband low loss contiguous channel multiplexer printed on a single substrate with little or no external tuning, and to meet the normal environmental requirements associated with such components. Definite advantages over the coax counterparts would be achieved by this realisation. Not only would there by a considerable reduction in the size and weight of the multiplexer, but there would

also be a much higher level of population tracking in both amplitude and phase. Also, the printed form opens up the real possibility of designing complete sub system receivers on a single substrate.

Although the initial aims were very high, this thesis shows that after encountering several different problems, complex multiplexers can now be produced on a single substrate with a performance which surpasses all expectations. This performance is comparable to that achieved by the conventional coaxial multiplexers. However, the printed circuits designed in this thesis could easily be extended to produce superior performances than the coax multiplexers, as well as possessing the reduced size and better population tracking properties.

1.2. Choice of the Basic Medium for the Printed Circuits

For many years, some types of microwave filters have been built in stripline or microstrip. These have normally been in cases where the bandwidths have not been too narrow and where the selectivity has not been severe. For the broadband multiplexers considered here, however, the impedance variation is very difficult to realise in microstrip. Moreover for these highly selective devices, the variation of the dielectric constant of microstrip with temperature, would produce a temperature stability insufficient to meet most environmental requirements. In addition, microstrip structures are quite susceptible to higher ordered modes. This can be serious when the

filters are required to provide a wide frequency rejection band beyond the passband. Stripline also fails to meet the temperature requirement and has high dielectric loss, an inability to fine tune and suffers from compression of components at the higher microwave frequencies.

Taking these points into consideration, it was immediately seen that the solution was to use the suspended substrate stripline as shown in Fig. 1.2.1. The substrate chosen was RT/duroid* 5880 which is a non-woven glass microfiber - reinforced polytetrafluorethylene (PTFE) structure. Duroid 5880 was chosen for a number of reasons. Firstly, it has a suitably fairly low dielectric constant of 2.22, closely held within 2% at any point on the substrate, from d.c. to 18 GHz. Secondly, it has a low dissipation factor of 0.0004 → 0.0009 from 1 MHz → 18 GHz, which is unexcelled by any stripline material except irradiated polyolefin. Thirdly, the substrate will remain dimensionally stable in extreme environments. This is because the coefficient of thermal expansion of the substrate is typically only 0.000032 → 0.000056/^{o}C for a temperature range of -100^{o}C → + 100^{o}C. The substrate will withstand temperatures up to 280^{o}C without warping. Finally, copper-clad duroid has excellent etching properties and can be easily plated. This is due to its high average peel strength of 14 lbs/inch width at ambient temperature, which only reduces to

* Trademark of Rogers Corporation.

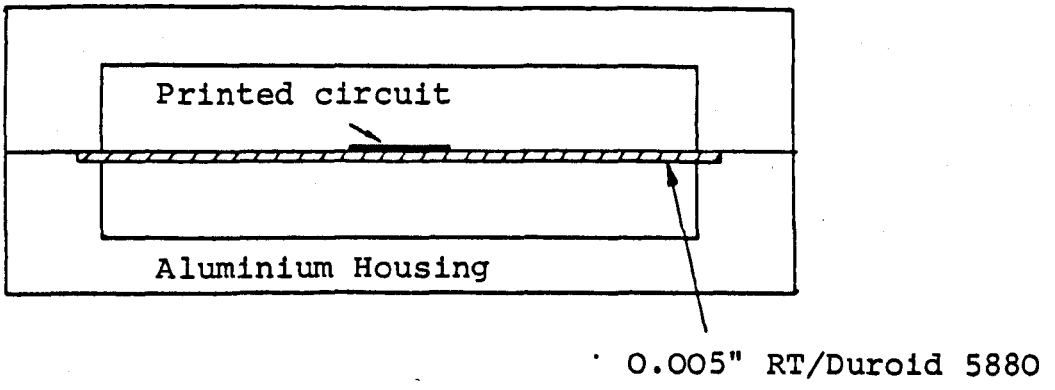

Fig. 1.2.1 The basic suspended substrate stripline configuration

6 lbs/inch width at 150°C. Indeed an experiment at room temperature has shown that two planar coupled lines 0.16" long, but only .007" wide and separated by .004" to form a d.c. block, can be etched successfully.

A substrate thickness of 0.005" (tolerance = ± 0.0005") is used throughout the work since this produces reasonable physical dimensions for the high-pass filters and, moreover, ensures that the critical resonant sections are realised in an air medium. Hence the filter will have good temperature properties. Both sides of the substrate are ½ oz. copper-clad, which is the minimum thickness available and is about 0.00085". Thus the suspended substrate structure is obviously capable of achieving an electrical performance comparable to coax and although the circuits are printed, fine tuning is possible with screws in the main housing.

1.3. Electrical Structure of the Printed Circuit Multiplexer

Having established the basic medium which would be necessary to develop the printed circuit multiplexer, attention was focussed on the electrical structure best suited to the printed circuit form. The original approach for coax multiplexers is shown in Fig. 1.3.1 and is described in Ref. [1.1]. This essentially consists of a cascade of contiguous highpass - lowpass diplexers. The cascade may start with a lowpass filter to prevent

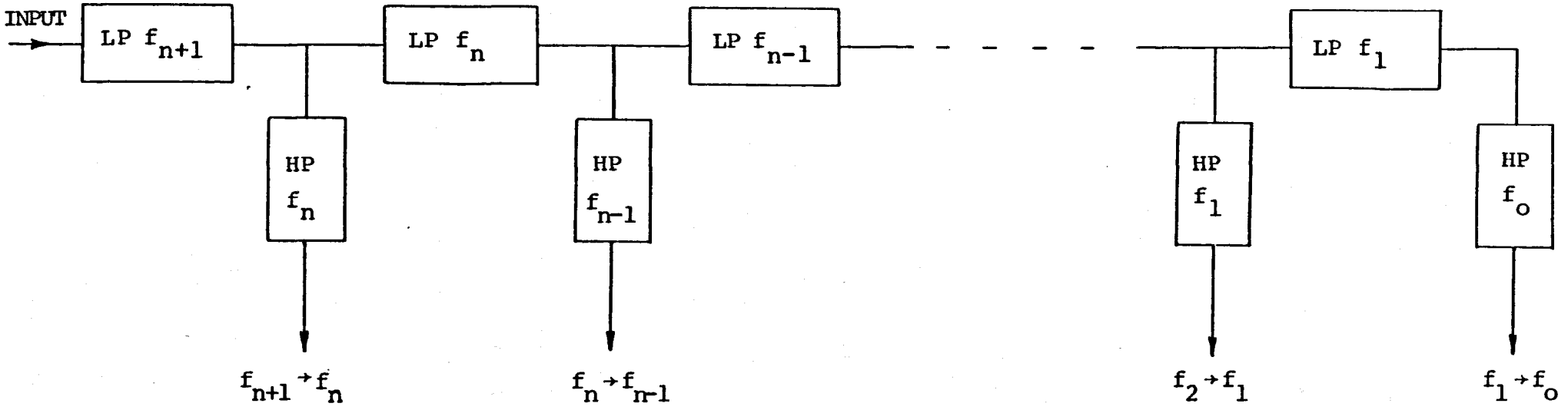

Key: LP f_n = Lowpass filter with cut-off frequency f_n.

HP f_n = Highpass filter with cut-off frequency f_n.

Fig. 1.3.1 Block diagram of a general contiguous n channel multiplexer using highpass and lowpass filters.

the passband of the highest frequency channel extending beyond a frequency limit set in the specification, and also to enhance the attenuation of all channels above this frequency. A highpass filter may also be used at the end of the cascade to reject any signals from d.c. to the crossover frequency of the highpass. This filter would also have to pass signals in the lowest frequency band of the multiplexer.

The signal flow in this structure can best be understood by considering the 4 - 18 GHz triplexer to be designed in this thesis. In cascade form, the triplexer is shown in Fig. 1.3.2. This triplexer has outputs over the bands 4 → 8, 8 → 12 and 12 → 18 GHz, with all channels rejecting signals between 0 and 4 GHz. The triplexer is composed of two diplexers having crossovers of 3 dB at 12 and 8 GHz respectively and a highpass filter with its 3 dB frequency at 4 GHz. Consider signals in the range 0 → 18 GHz entering this triplexer. Signals in the range 12 → 18 GHz are channelled by the 12 GHz diplexer to port 1. After passing through the 12 GHz lowpass filter, signals in the range 0 → 12 GHz are channelled by the 8 GHz diplexer: 8 → 12 GHz signals go to port 2 whereas 0 → 8 GHz signals pass through the 8 GHz lowpass. Signals in the range 0 → 4 GHz are then reflected back to the source by the 4 GHz highpass, whilst the remaining signals in the 4 → 8 GHz range pass through the 4 GHz highpass filter to port 3. Although the isolated filters must be modified before they can be used in the contiguous diplexers, the basic requirements which must be satisfied by these filters can now be summarised:

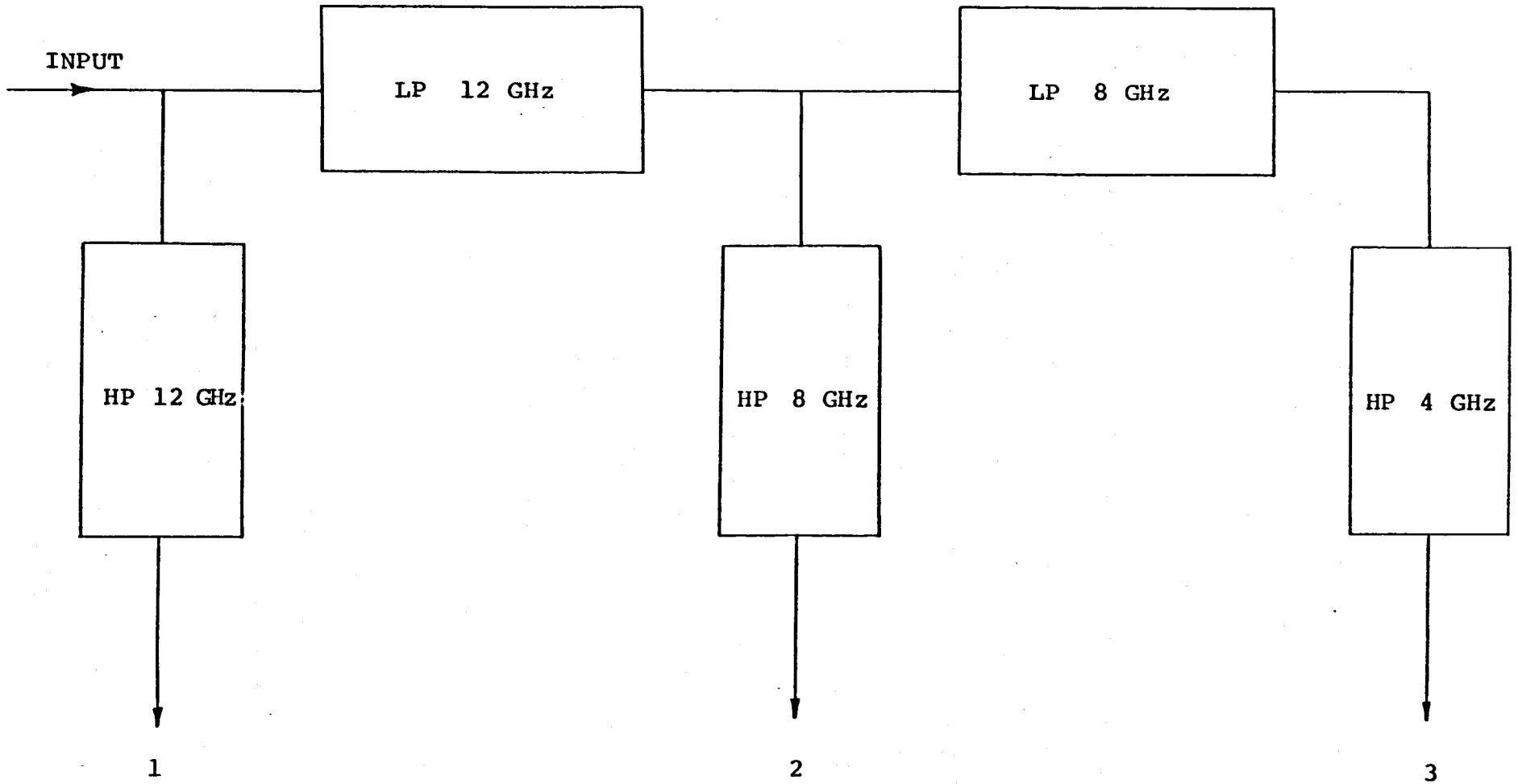

Fig. 1.3.2 Triplexer covering the bands 4 → 8, 8 → 12 and 12 → 18 GHz

Filter	Very good VSWR	Good VSWR	Stopband
12 GHz highpass	-	12 → 18	0→12
12 GHz lowpass	0 → 8	8 → 12	12→18
8 GHz highpass	-	8 → 12	0→ 8
8 GHz lowpass	-	4 → 8	8→12
4 GHz highpass	-	4 → 8	0→ 4

In conclusion, the lowpass filters must provide a very good VSWR over the lower frequency part of their passband, to prevent interactions between the diplexers and the highpass when these are cascaded together. Otherwise a poor match at the common port of the triplexer will occur at these frequencies, producing large insertion loss ripples in the affected passbands. The other requirement of each lowpass filter is that it need only maintain its stopband up to an octave. (In some cases, only a half octave is necessary). For a typical highpass filter, its stopband must be maintained from d.c. to its crossover frequency and its passband need only be maintained up to an octave. These points are extremely important for determining the simplest form of printed circuit to be used.

An alternative approach to the above is the use of bandpass filters. However, the periodic passbands of the lower frequency channels have to be suppressed and this implies the use of large shunt capacitors which affects the cut-off frequencies and the temperature performance. Furthermore, it is difficult to simultaneously produce two crossover frequencies to the close tolerance

which is required when using a printed circuit form.

Thus it was decided to use the cascaded arrangement of the triplexer. The problem now was to produce basic lowpass and highpass filters which would satisfy the requirements summarized in the preceding table and would enable the specification outlined in Fig. 1.3.3 to be achieved. This figure shows the main electrical requirements of a specification produced by the Ministry of Defence and is used as a basis for this work. It should be noted from this specification that the minimum stopband insertion loss of 35 dB of any channel must be achieved within 5% of the crossover frequencies. This high selectivity is comparable to that obtained in the coax multiplexers, which produce 60 dB attenuation within 10-15% of the crossover frequencies.

1.4. Development of Suitable Lowpass Prototype

The coax multiplexers use channel filters of the elliptic function type having transmission zeros very close to bandedge and an optimum equiripple performance. Thus to achieve a performance with similar severe selectivities, it is at least necessary to realise characteristics similar to the elliptic function type. One could consider the exact elliptic function lowpass prototype [1.2], whose characteristic has the maximum number of ripples in the passband and stopband. For given ripple levels in the stopband and passband and a prescribed selectivity, this prototype is the minimum

Passbands

Output	1	(LO)	4 → 8 GHz
Output	2	(MID)	8 → 12 GHz
Output	3	(HIGH)	12 → 18 GHz

Crossover Frequency Tolerance

8 GHz ± 80 MHz
12 GHz ± 120 MHz

In Band Losses

4.16 → 7.68 GHz , less than 1 dB
8.32 → 11.52 GHz , less than 1 dB
12.48 → 18.00 GHz , less than 1 dB

Crossover Loss

At 4 GHz ± 40 MHz , 4.5 dB ≤ loss ≤ 3 dB
At 8 GHz and 12 GHz , 4.5 dB maximum

Rejection

Output 1 : 1 → 3.8 GHz and 8.4 → 18 GHz, 35 dB min
Output 2 : 1 → 7.6 GHz and 12.6 → 18 GHz, 35 dB min
Output 3 : 1 → 11.4 GHz , 35 dB min

Input port VSWR

4.00 GHz → 4.16 GHz, input port VSWR = 8 : 1 max.
4.16 GHz → 18.00 GHz, input port VSWR = 2 : 1 max.

Fig. 1.3.3. Main parts of electrical specification for 4 → 18 GHz triplexer

degree solution and is therefore optimum. However, when this prototype is used to design a microwave distributed filter with a 2 : 1 bandwidth or more, the impedance variation in the filter can be up to 10 : 1. This is mainly due to the section producing the transmission zero most remote from bandedge and would obviously cause severe problems with a printed circuit realisation.

Attention was therefore focused on the odd degree generalised Chebyshev prototype, which has the maximum number of finite transmission zeros at one frequency close to bandedge and an optimum equiripple passband characteristic. It was anticipated that this prototype should lead to a much smaller impedance change through the network. Element values for the prototype have recently been derived at Leeds [1.3] and the impedance variations in it are typically only 2 : 1. The prototype is shown in Fig. 1.4.1 with its insertion loss characteristic given in Fig. 1.4.2; equation (1.4.1) was provided by Professor Rhodes. This prototype is considerably more selective than the same degree ordinary Chebyshev lowpass prototype, with the same passband ripple level, and is only slightly less selective than the exact elliptic function prototype (N.b. Selectivity expresses the frequency where the minimum stopband insertion loss is first achieved as a percentage of a frequency near bandedge, usually the 3 dB frequency).

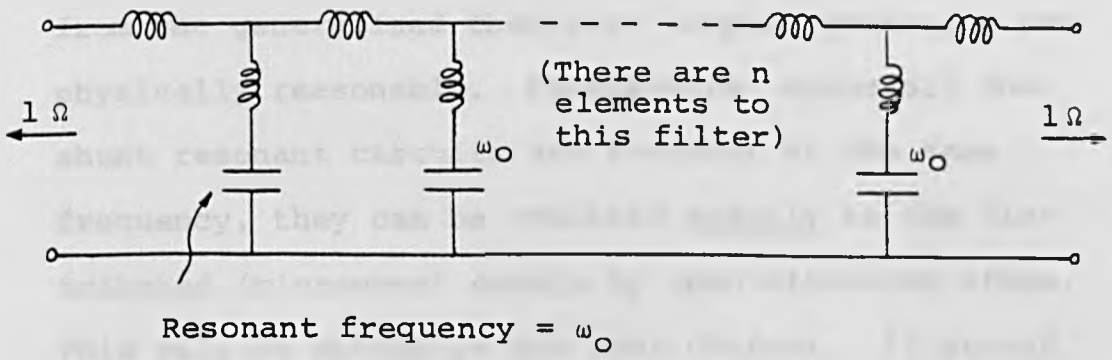

Fig. 1.4.1 The generalized Chebyshev lowpass prototype

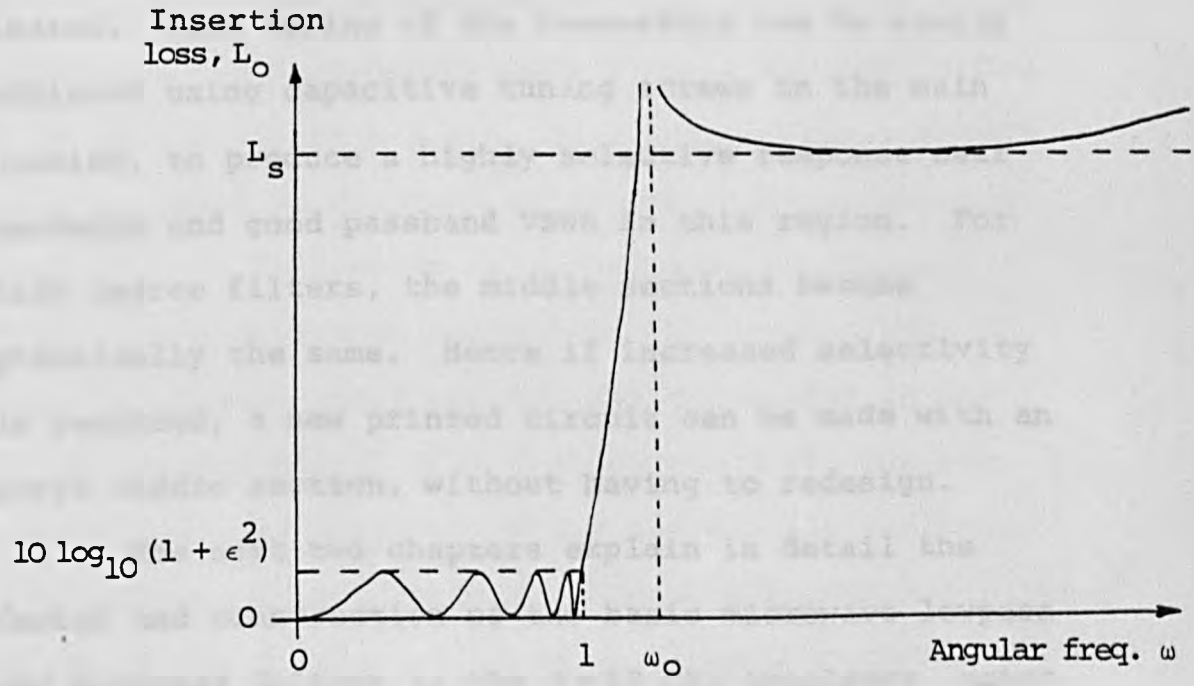

$$L_o = 10 \log_{10}\left[1 + \epsilon^2 \cos^2\left\{(n-1)\cos^{-1}\left(\frac{\omega\sqrt{1-\omega_o^2}}{\sqrt{\omega^2-\omega_o^2}}\right) + \cos^{-1}\omega\right\}\right] \qquad (1.4.1)$$

Fig. 1.4.2 Insertion loss characteristic of generalised Chebyshev lowpass prototype

The dimensions of the microwave filters produced from the generalised Chebyshev lowpass prototype are physically reasonable. Furthermore, since all the shunt resonant circuits are resonant at the same frequency, they can be realised exactly in the distributed (microwave) domain by open circuited stubs. This will be proved in the next chapter. It should be noted that the shunt resonant circuits in the exact elliptic function microwave filter can only be approximated. Fine tuning of the resonators can be simply achieved using capacitive tuning screws in the main housing, to produce a highly selective response near bandedge and good passband VSWR in this region. For high degree filters, the middle sections become practically the same. Hence if increased selectivity is required, a new printed circuit can be made with an extra middle section, without having to redesign.

The next two chapters explain in detail the design and construction of the basic microwave lowpass and highpass filters in the 4 → 18 GHz triplexer, using the generalised Chebyshev prototype. Chapter 4 then gives the design and construction of the 8 and 12 GHz diplexers using these basic microwave filters, with suitable modifications for correct diplexing operation. The design and construction of the single substrate triplexer is then given in the same chapter. The experimental results presented agree extremely well with the detailed computer analysis given in chapter 5.

2. DESIGN OF M.I.C. BROADBAND LOWPASS FILTERS

2.1. Introduction

It should be noted that the dual form of the lowpass prototype in Fig. 1.4.1 is not really suitable for a multiplexer application. The main problem is that the finite transmission zeros of the microwave filter produced from this prototype depend mainly upon the characteristic impedances of the resonant elements and hence the bandedge frequency would be very difficult to tune. Also, in a p.c.b. realisation, the resonant sections must be realised by strong coupling through dielectric. This means large temperature changes, producing significant changes in the permittivity of the dielectric, could produce serious shifts in the bandedge frequency. A seventh degree 8 GHz MIC lowpass filter was constructed and indeed, the bandedge frequency could not be tuned. Results showed a minimum passband return loss of 13 dB, a minimum stopband insertion loss of 43 dB up to 12 GHz and a selectivity of 18.6%. Attention was therefore focused on the prototype form shown in Fig. 1.4.1.

2.2. Distributed Quasi Lowpass Prototype Filter

In order to meet the required insertion loss levels given in specification (Fig. 1.3.3), element values for the prototype are found for $\epsilon = 0.1$ (minimum passband return loss is 20 dB) and a minimum

stopband insertion loss of 40dB. To approximately meet the selectivity requirement, a degree nine prototype is used (this will be shown later, see p. 20). The required prototype is shown in Fig. 2.2.1.

To transform the prototype into a distributed lowpass prototype which is a necessity for broadband microwave filters, the Richards frequency transformation must be used:

$$p \rightarrow t/\alpha_L \qquad (2.2.1)$$

where p is the lumped complex frequency variable, $t = \tanh(a_L p)$ and a_L and α_L are constants (α_L controls the ratio of the first stopband bandwidth to bandedge frequency and a_L is a simple scaling factor determining the stopband centre frequency)

$$\text{i.e.} \qquad \omega \rightarrow \frac{\tan(a_L \omega)}{\alpha_L} \qquad (2.2.2)$$

The quasi lowpass response is shown in Fig. 2.2.2.

Consider now the transformation of the shunt series resonant circuits of the prototype under (2.2.1). Suppose L_r and C_r ($r = 2,4,\ldots,(n-1)$) are the lumped inductance and capacitance values of each shunt series resonant circuit in this prototype. The impedance of this circuit is,

$$Z = \frac{1 + L_r C_r p^2}{C_r p}$$

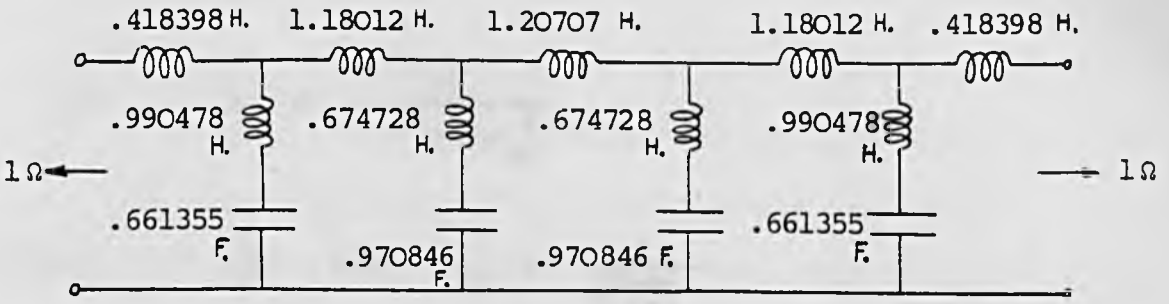

Fig. 2.2.1 Degree nine generalised Chebyshev lowpass prototype (ϵ = .1, L_s = 40 dB)

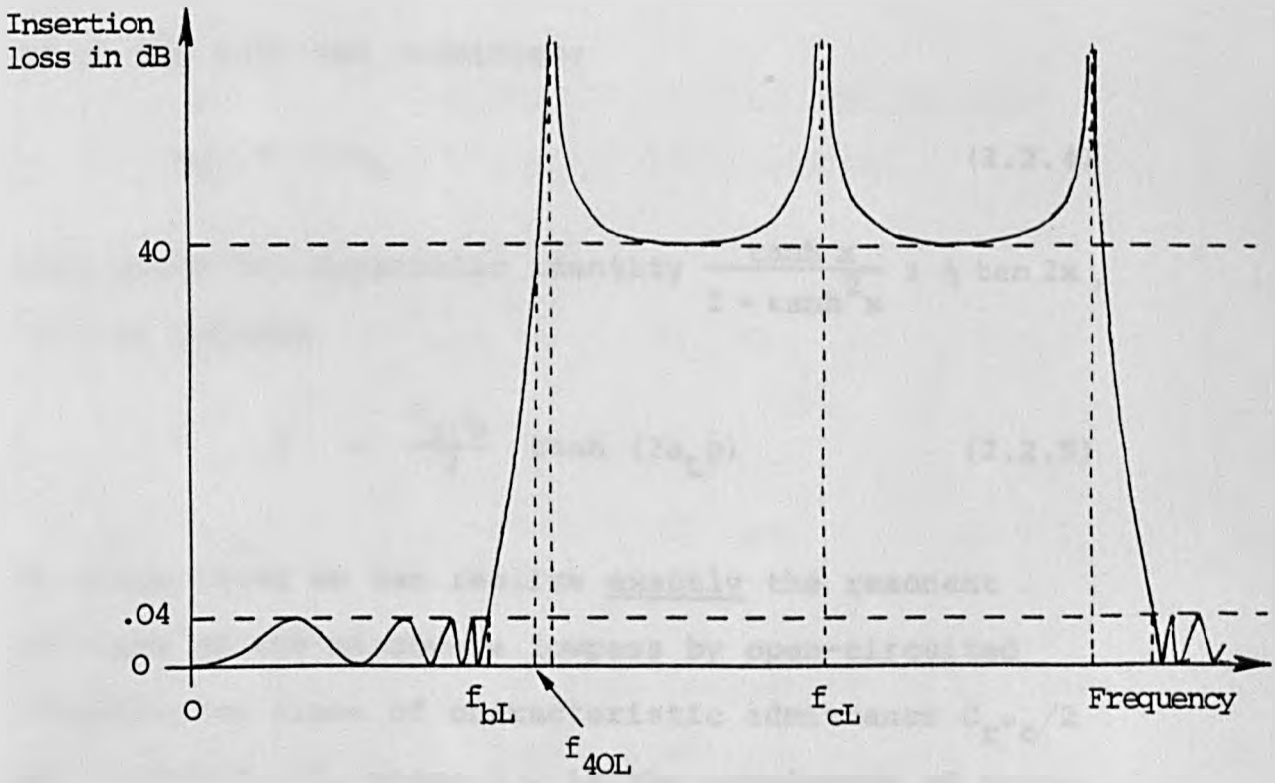

(N.b. this response is periodic with frequency)

Fig. 2.2.2 Quasi lowpass insertion loss response in the distributed domain

$$\text{or} \qquad Y = \frac{C_r p}{1 + p^2/\omega_o^2}$$

where $Y = \frac{1}{Z}$ and $\omega_o = \frac{1}{\sqrt{L_r C_r}}$

Under (2.2.1), this admittance becomes

$$Y = \frac{C_r t/\alpha_L}{1 + \frac{t^2}{\alpha_L^2 \omega_o^2}} \qquad (2.2.3)$$

If we now make the condition:

$$\alpha_L = 1/\omega_o \qquad (2.2.4)$$

then using the hyperbolic identity $\frac{\tanh x}{1 + \tanh^2 x} \equiv \frac{1}{2} \tan 2x$, (2.2.3) becomes

$$Y = \frac{C_r \omega_o}{2} \tanh (2a_L p) \qquad (2.2.5)$$

In other words we can realise <u>exactly</u> the resonant circuits of the microwave lowpass by open-circuited transmission lines of characteristic admittance $C_r\omega_o/2$ and length $\lambda_{cL}/2$, where λ_{cL} is the wavelength of stop-band centre frequency. Note that this result is only true if $\alpha_L = 1/\omega_o$ and such a result cannot be obtained for the elliptic function filter. In this latter filter, since the transmission zeros are all different the shunt resonators can only be approximated. We

now see an immediate advantage of this prototype over its dual in that the transmission zeros close to bandedge are controlled by the lengths of the resonators and so it should be possible to shift the bandedge frequency by capacitive tuning.

Fig. 2.2.3 shows the transformation of the series lumped inductors of the lowpass prototype under (2.2.1). Using this transformation and (2.2.5), results in the degree nine distributed prototype filter shown in Fig. 2.2.4.

Calculation of the stopband centre frequency, bandedge frequency and selectivity for a 8 GHz lowpass

From (2.2.2) we have,

$$f_{bL} = \frac{\tan^{-1}(\alpha_L)}{\tan^{-1}(\alpha_L \omega_3)} \quad 8 \quad \text{GHz.} \qquad (2.2.6)$$

and

$$f_{4oL} = \frac{\tan^{-1}(\alpha_L \omega_{40})}{\tan^{-1}(\alpha_L \omega_3)} \quad 8 \quad \text{GHz.} \qquad (2.2.7)$$

where ω_3 and ω_{40} are the angular frequencies of the 3dB and 40dB points of the lowpass prototype respectively, and where f_{bL} and f_{4oL} are the bandedge and 40dB frequencies of the microwave lowpass filter respectively. (N.b. these equations imply that the 3dB frequency of the microwave filter is 8 GHz).

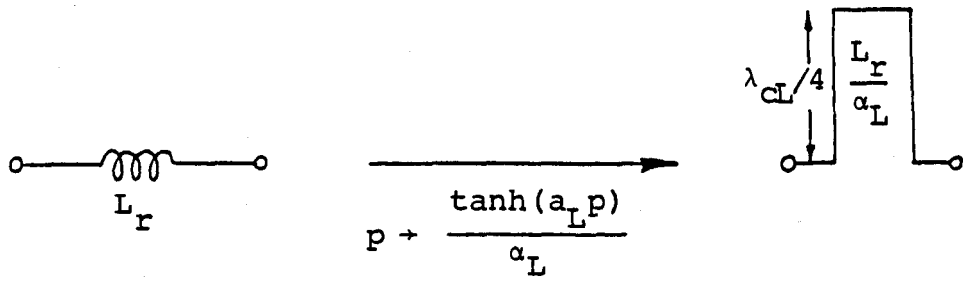

i.e. Series inductor, L_r, of lumped lowpass prototype ($r = 1,3,\ldots,n$) → $\lambda_{cL}/4$ short-circuited stub of characteristic impedance L_r/α_L.

Fig. 2.2.3 Transformation of lumped inductor under $p \to (\tanh(a_L p))/\alpha_L$

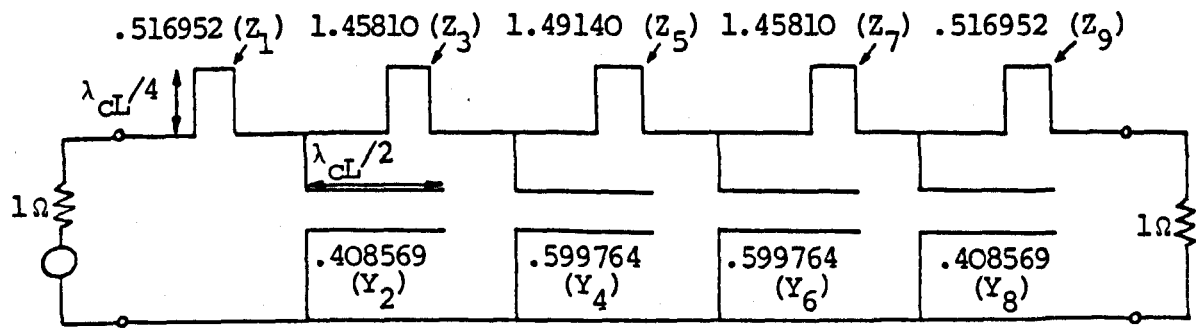

Key:

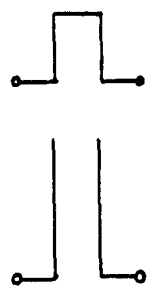

Short-circuited stub

Open-circuited stub

Z_r ($r = 1,3,\ldots,9$) are characteristic impedances in ohms

Y_r ($r = 2,4,\ldots,8$) are characteristic admittances in mhos

Fig. 2.2.4 Distributed quasi lowpass prototype filter

ω_3 and ω_{40} are found by solving (1.4.1), in turn, for $L_o = 3$ and $L_o = 40$dB respectively using the Newton-Raphson technique. We find

$$\omega_3 = 1.01999 \qquad (2.2.8)$$

and $$\omega_{40} = 1.0137 \qquad (2.2.9)$$

whence $$f_{bL} = 7.888 \text{ GHz} \qquad (2.2.10)$$

$$f_{40L} = 8.440 \text{ GHz} \qquad (2.2.11)$$

The selectivity with respect to the 3dB frequency is,

$$S_L = \frac{(f_{40L} - 8)}{8} \ 100\% \qquad (2.2.12)$$

We find $S_L = 5.50\%$ (2.2.13)

The centre frequency of the stopband is,

$$f_{cL} = \frac{(\pi/2)}{\tan^{-1}(\alpha_L \omega_3)} \ 8 \text{ GHz}$$

i.e. $$f_{cL} = 18.21 \text{ GHz} \qquad (2.2.14)$$

We require the stopband of the low channel of the 8GHz diplexer to be maintained up to 12GHz, but this is easily satisfied here since the value of α_L ensures a theoretical stopband up to 27.98GHz. Although the theoretical selectivity is slightly worse than required, it should improve to around 5% when the lowpass is diplexed with its highpass filter.

2.3. Suspended Substrate Realisation of Lowpass Filter

The suspended substrate realisation decided upon for the lowpass is shown in Fig. 2.3.1. The series stubs of the distributed prototype are realised by u.e.'s - this will be explained later.

Attention was given to a microstrip realisation, but this was rejected for a number of reasons. First and foremost, if microstrip resonators are used then the variation of effective dielectric constant with temperature, producing shifts in the resonant and bandedge frequencies, would be too great to meet most military environmental specifications. Secondly, the impedance levels in the filter cannot be satisfactorily realised in microstrip. That is, for the necessary small lengths of the series elements (less than one-eighth of one wavelength at 12GHz) their widths become too narrow to be etched using 0.005" duroid. Infact the width of the middle element becomes only 0.0031" and undercutting would not only affect its impedance but the element would be lossy. There would also be difficulty in etching the high impedance end resonators in microstrip, since their widths would be only 0.00275" using 0.005" duroid. Increasing the substrate thickness to 0.01" would possibly still not solve the etching problems and moreover the highpass would be difficult to physically realise using this substrate thickness.

Returning to the suspended substrate realisation, the physical dimensions are,

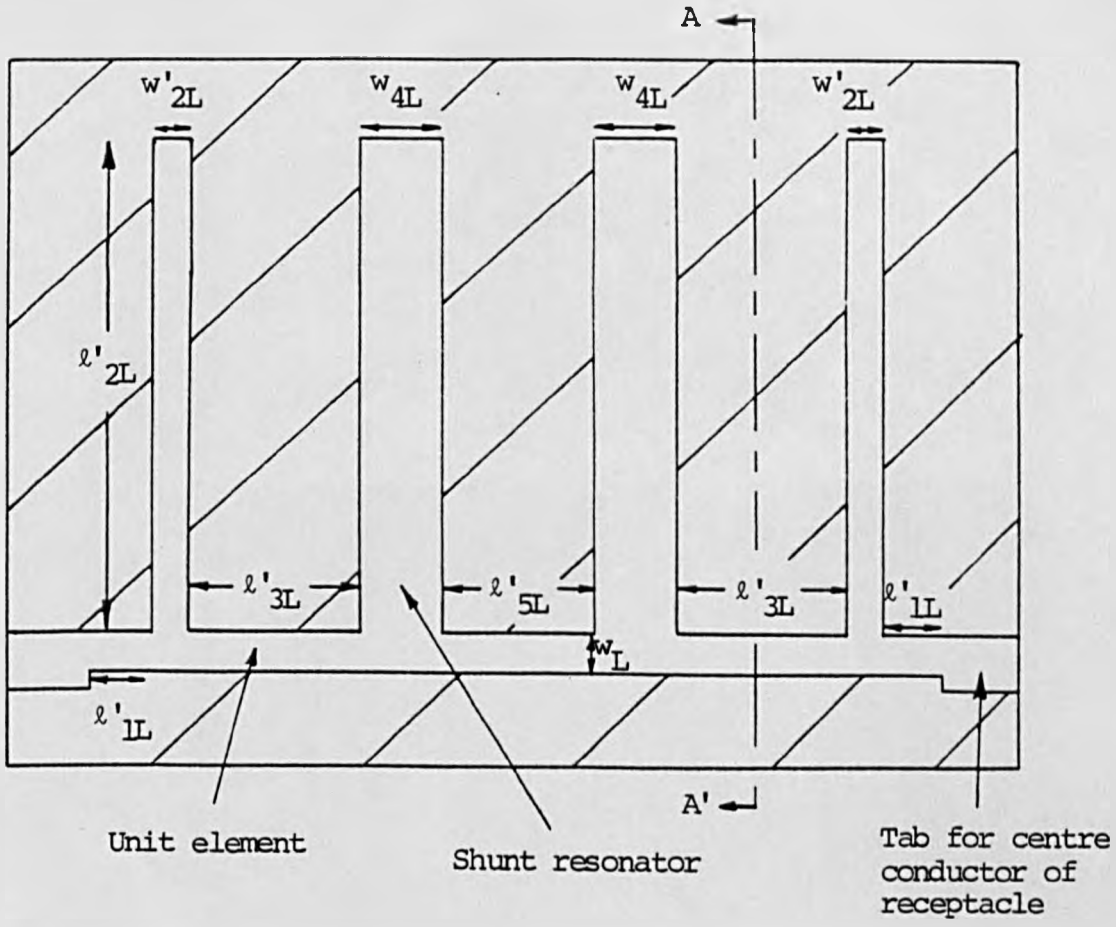

Printed circuit board

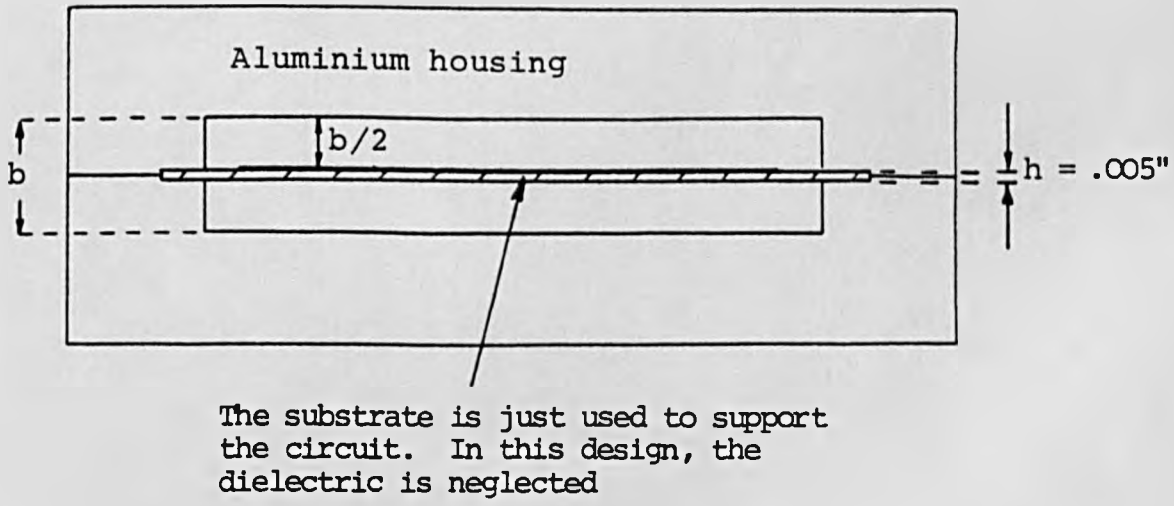

Cross-section of filter box along A - A'

Fig. 2.3.1 Physical realisation of 8 GHz lowpass filter. (See also photograph no. 1)

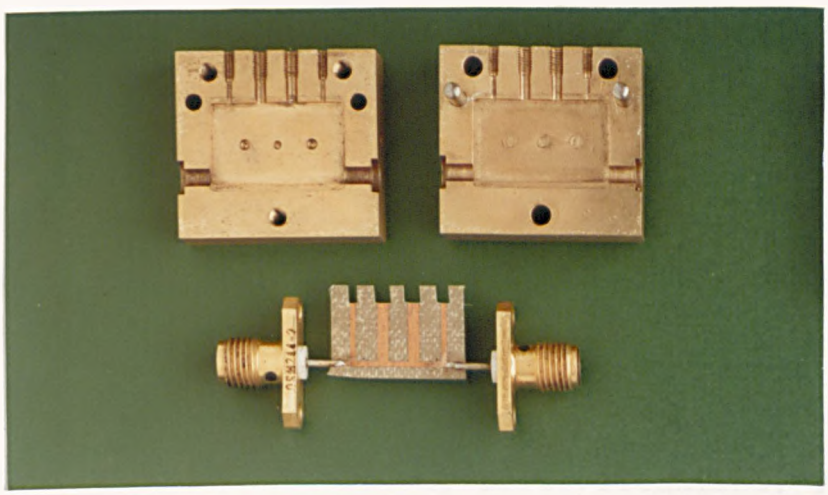

Photograph No. 1 Suspended substrate stripline 8 GHz lowpass filter.

infact, quite reasonable. For example, the shunt resonators are not too wide, therefore not causing serious discontinuities, because of the comparatively large fringing capacitances to ground (N.b. the ground plane spacing is not made too large). The final printed form is very simple with the circuit on only one side of the substrate and virtually uniform impedance lines throughout; the whole p.c.b. is then suspended in a simple box of moderate ground plane spacing. An important point to note is that since the ground plane spacing is much greater than the dielectric thickness and the dielectric constant of duroid, viz. 2.22, is comparable to air, the shunt resonators are essentially in an air medium not in a strong field situation. Therefore temperature changes should only produce a slight variation in the effective dielectric constant. Hence changes in the resonator electrical lengths, which critically determine the performance of the filter around bandedge, should be minimised and the temperature properties approximate airline coax systems. This is an essential requirement if the multiplexer is to meet most environmental specifications.

Consider now the realisation of the series elements. Recall that from (2.2.1) these are short circuited stubs. which produce an infinite impedance when a quarter of a wavelength long. This quarter wavelength frequency occurs at twice the frequency of the finite transmission zeros i.e. at about 2-3 times the

cut-off frequency. At this frequency, the shunt resonators are on open circuit and the attenuation of the filter is entirely due to the series elements. Now a direct realisation of the series short circuited stubs in printed form is difficult due to the distributed coupling to ground. However, we recall from p. 12 that for the contiguous multiplexer application we need only preserve the low channel stopband upto below an octave above the cut-off frequency which is well below the resonant frequency of the series elements. Therefore we only need approximate the short circuited stubs over this band and the simplest solution is to use the series inductive effect of a short length of high impedance transmission line. This effect is detailed in the π-equivalent circuit representation of a length of transmission line and is found in Ref.[2.1.].

2.4. Design of Physical Dimensions of 8 GHz Lowpass

It should be noted that no known exact synthesis for the lowpass structure cited here exists! The design begins my making the following choices for the ground plane spacing b and the width of the unit elements, w_L:

$$\text{Choose} \quad b = 0.07" \qquad (2.4.1)$$

$$\text{and} \quad w_L = 0.025" \qquad (2.4.2)$$

This value of b ensures $b \gg h$ and this fact coupled with the low relative permittivity of duroid means we can neglect the dielectric and assume the resonators

are effectively in air. Another point is that the resonators will not be too wide because b is not too large. This means that any errors introduced because of uncertainties in the reference plane locations of the transmission lines at each T junction, will be minimised. Equation (2.5.2) ensures that each unit element is long enough to produce negligible coupling between the resonators, but not long enough to prevent a comparatively broadband lumped series inductive effect. Before these final choices were made, a few values of b and w_L were tried and the filter designed (as shown below) until suitable physical dimensions were achieved.

2.4.1. Design of resonators

Assuming each resonator can be considered in isolation, the cross-section for any resonator is as shown in Fig. 2.4.1. This assumption is reasonable since we do not want any distributed coupling between the resonators. The substrate and any side walls are not shown since we assume these can be neglected. Each resonator is symmetrically positioned between the ground planes. The fringing capacities shown in Fig. 2.4.1 are found using Getzinger's graphs [2.2].
Now the following ratio is needed:

$$\frac{t}{b} = \frac{0.00085}{0.07} = 0.012 \qquad (2.4.3)$$

Using this ratio and Getzinger's graphs, we find $\frac{C'_f}{\varepsilon_o} = 0.46$.

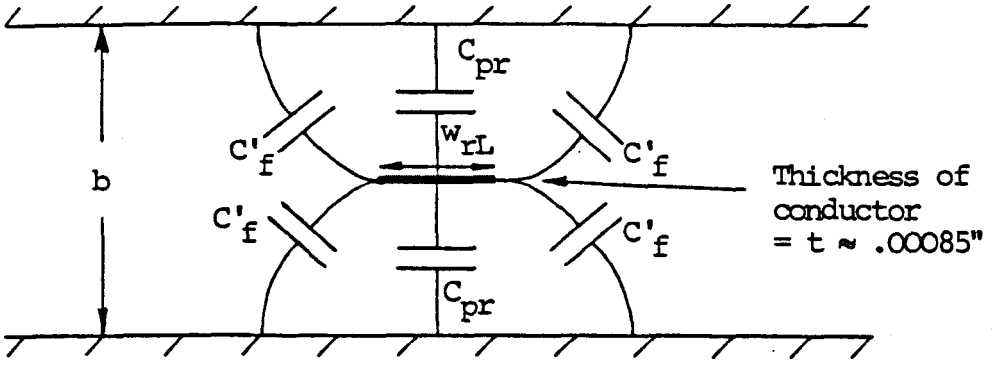

Fig. 2.4.1 Cross-section of resonator in filter box

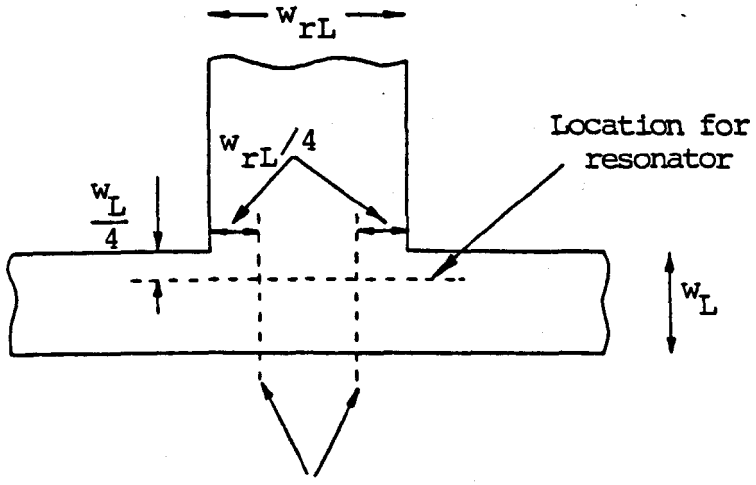

Fig. 2.4.2 Reference plane locations at the T junction discontinuities

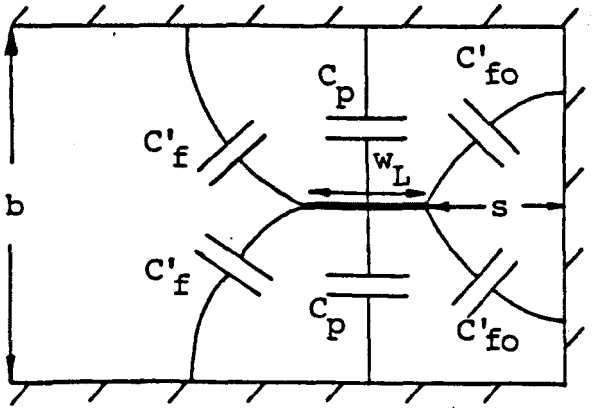

Fig. 2.4.3 Cross-section of unit element

Now the total static capacitance/unit length for each resonator is,

$$\frac{C_{rs}}{\varepsilon_o} = \frac{2C_{pr}}{\varepsilon_o} + \frac{4C'_f}{\varepsilon_o} \quad (r = 2,4,\ldots 8) \quad (2.4.4)$$

where C_{pr}/ε_o = parallel-plate capacitance between one side of the stripline resonator and ground

$$= \frac{w_{rL}}{\frac{1}{2}(b-t)} \quad (2.4.5)$$

Now the admittance, Y, of a transmission line (normalised to 1Ω terminations), operating in the TEM mode, is related to its static capacitance per unit length, C, between conductors of the line by [2.2]

$$\frac{C}{\varepsilon} = \frac{7.534\ Y}{\sqrt{\varepsilon_r}} \quad (2.4.6)$$

where ε is the absolute permittivity of the medium containing the conductors of the line

where ε_r is the relative permittivity of the medium containing the conductors of the line

Substituting (2.4.4) and (2.4.5) into (2.4.6) yields

$$w_{rL} = \frac{1}{4}(b-t)\left[7.534\ Y_r - 4\frac{C'_f}{\varepsilon_o}\right] \quad (2.4.7)$$

For the first shunt resonator $Y_r = Y_2 = 0.408659$. Using (2.4.7),

$$W_{2L} = 0.0236" \quad (2.4.8)$$

Checking to see if $w_{2L} > 0.35\,(b-t)$ (This condition is necessary if the fringing fields of the resonator are not to interact - see reference [2.2], we find $.35\,(b-t) = 0.242"$. To correct for interaction of the fringing fields, a new width w_{2L} is used where

$$w'_{2L} = \frac{.07(b-t) + w_{2L}}{1.2}, \quad 0.1 < \frac{w'_{2L}}{(b-t)} < .35 \qquad (2.4.9)$$

$$\text{i.e.} \quad w'_{2L} = 0.0237" \qquad (2.4.10)$$

Proceeding in the same way, but with $r = 4$ and $Y_4 = 0.599764$ in (2.4.7), we find

$$w_{4L} = 0.051" \qquad (2.4.11)$$

By the symmetry of the filter, the widths of the third and fourth resonators are w_{4L} and w_{2L} respectively. The length of each resonator is given by

$$\ell_{rL} = \lambda_{cL}/2 \quad (r = 2 \text{ or } 4)$$

$$= \frac{u}{2f_{cL}} \qquad (2.4.12)$$

where u = velocity of propagation of TEM waves in air.

$$\text{We find } \ell_{rL} = 0.3241" \qquad (2.4.13)$$

Assuming the effective length of each resonator starts from a reference line as shown in Fig. 2.4.2, the required physical length of each resonator is,

$$\ell'_{rL} = \ell_{rL} - \tfrac{1}{4} w_L = 0.318" \qquad (2.4.14)$$

2.4.2. Design of unit elements

The series lumped inductance , L_{rL} (r = 1,3...9), required to approximate each series short circuited stub of the distributed prototype is found by equating the impedance of the lumped inductor and series stub at the bandedge frequency. That is,

$$j\omega_{bL} L_{rL} = j\, Z_r \tan(a_L \omega_{bL}) \qquad (r = 1,3,5)$$

where Z_r is the characteristic impedance of each series short circuited stub of the distributed prototype and $\omega_{bL} = 2\pi f_{bL}$

Since $\alpha_L = \tan(a_L \omega_{bL})$ (from 2.2.2)

then $$L_{rL} = \frac{Z_r \alpha_L}{\omega_{bL}}$$

$$= \frac{L_r}{\omega_{bL}} \quad , \quad \text{since } Z_r = \frac{L_r}{\alpha_L} \text{ (see Fig. 2.2.3),} \qquad (2.4.15)$$

Now the series lumped inductance approxiated by each u.e. of length ℓ_{rL} (r = 1,3,5) ($\ell_{rL} < \lambda / 8$, where λ is the wavelength of operation) and high characteristic impedance Z_L is [2.1]

Series lumped inductance approximated by each u.e. $= \frac{Z_L \ell_{rL}}{u}$ (2.4.16)

where u is the velocity of propagation along the u.e.

Equating (2.4.15) and (2.4.16) we find,

$$\ell_{rL} = \frac{L_r u}{Z_L \omega_{bL}} \qquad (2.4.17)$$

This equation determines the lengths of the u.e.'s, once Z_L is known. The design given here should ensure a good passband VSWR since we are providing a suitable approximation to the required series impedances around the critical bandedge frequency.

The characteristic impedance of the unit elements must now be determined. The cross section of the unit elements in the filter box is shown in Fig. 2.4.3. This figure shows the static capacitances per unit length between the stripline and ground. Before we can determine all the fringing capacitances we must know s. In order to produce a low VSWR transition from coax to stripline, the centre conductor of each feed terminal is soldered onto the p.c.b. in the position shown in Fig. 2.4.4. Distance s and diameter d can now be found to ensure that the transmission line formed by each centre conductor and the box walls is 50Ω. Fig. 2.4.5 shows the cross-section for this line. Notice that to keep the situation symmetrical, the distance of the centre conductor from the side wall is made b/2. The characteristic impedance of the line can then be found by the simple formula: [2.3]

$$Z = \frac{138}{\sqrt{\epsilon_r}} \log_{10} 1.17\rho \qquad (2.4.18)$$

where $\rho = b/d$

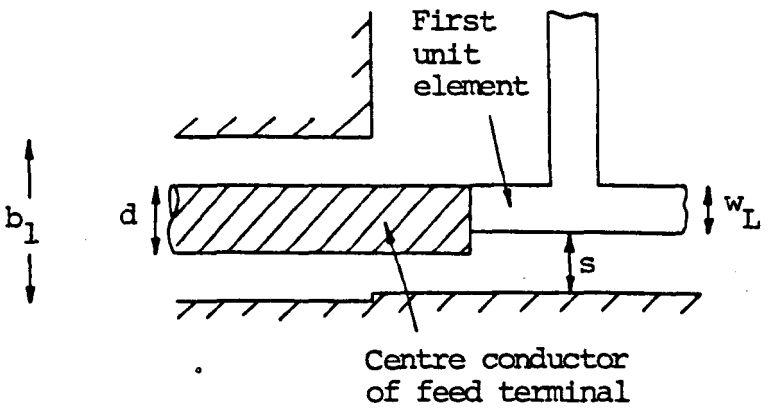

Fig. 2.4.4 Position of centre conductor of feed terminal in relation to first unit element of filter

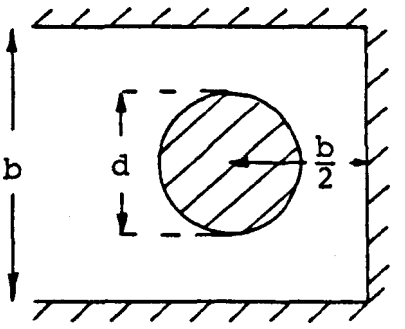

Fig. 2.4.5 Cross-section of centre conductor of feed terminal inside box

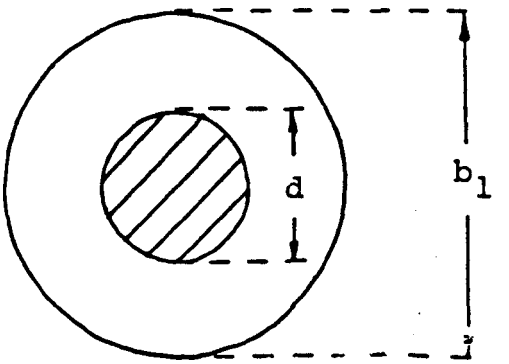

Fig. 2.4.6 Cross-section of centre conductor of feed terminal in side wall hole

We require $Z = 50\,\Omega$, so with $b = 0.07"$ and $\varepsilon_r = 1$,

$$d = 0.0356" \qquad (2.4.19)$$

Now $$s = d - w_L + (\frac{b}{2} - \frac{d}{2})$$

i.e. $$s = 0.03" \qquad (2.4.20)$$

The characteristic impedance of the transmission line formed by the centre conductor and the hole drilled in the side box wall for this conductor is (see Fig. 2.4.6) [2.3]

$$Z = \frac{138}{\sqrt{\varepsilon_r}} \log_{10} \frac{b_1}{d} \qquad (2.4.21)$$

This line must be 50Ω, so with $Z = 50\,\Omega$, $\varepsilon_r = 1$ and $d = 0.0356"$,

$$b_1 = 0.082" \qquad (2.4.22)$$

The length of each centre conductor inside the box was made 0.05".

To find the fringing capacitances shown in Fig. 2.4.3 we need the following ratios: $\frac{t}{b} = 0.012$, $\frac{2s}{b} = \frac{0.06}{0.07} = 0.857$

Using Getzinger's graphs [2.2]

$$C'_f/\varepsilon_o = 0.46 \quad \text{and} \quad C'_{f_o}/\varepsilon_o = 0.51$$

The total static capacitance per unit length between conductors of each u.e. is,

$$\frac{C_L}{\varepsilon_o} = \frac{2C'_f}{\varepsilon_o} + \frac{2C'_{fo}}{\varepsilon_o} + \frac{2C_p}{\varepsilon_o} \qquad (2.4.23)$$

where $$\frac{C_p}{\varepsilon_o} = \frac{W_L}{\frac{1}{2}(b-t)} = 0.714$$

Using (2.4.6) with $\varepsilon_r = 1$ we find for 1 Ω terminations,

$$Z_L = 2.236\ \Omega \qquad (2.4.24)$$

The lengths of the series inductors can now be found from (2.4.17) (n.b. u = velocity of propagation of TEM waves in <u>air</u> = 2.998×10^8 m/s). We find,

$$\ell_{1L} = 0.0462" \quad (\text{i.e. } \lambda_{12L}/21.29)$$
$$\ell_{3L} = 0.1268" \quad (\text{i.e. } \lambda_{12L}/7.76)$$
$$\ell_{5L} = 0.1220" \quad (\text{i.e. } \lambda_{12L}/8.06)$$

where λ_{12L} is the wavelength in air at 12 GHz.

Assuming the reference plane locations for the T junctions as shown in Fig. 2.4.2, the physical lengths of the u.e.'s are (refer to Fig. 2.3.1),

$$\ell'_{1L} = 0.04"$$
$$\ell'_{3L} = 0.108" \qquad (2.4.25)$$
$$\ell'_{5L} = 0.097"$$

Referring to Getzinger's graphs we can see that for the separations between the resonators in this filter, there is negligible coupling between the resonators.

Hence it was justifiable to consider each resonator in isolation.

A breakdown of the filter is shown in photograph no. 1 and note that the p.c.b. is only ≈ .45" x .64". Note the capacitive tuning screws at the ends of the resonators. These tuning screws enable a good passband VSWR to be achieved near bandedge, whilst virtually unaffecting the rest of the passband (viz. 90%) which is determined entirely by the printed circuit. The bandedge frequency can also be shifted by about 3.5% using these tuning screws whilst maintaining a good passband VSWR.

2.5. Practical Results and Discussion of 8GHz Low-pass

First results produced a 3dB frequency at 7.07 GHz. However, by scaling the resonators, the response shown in Figs. 2.5.1 and 2.5.2 was achieved. The dimensions of the modified p.c.b. are shown in Fig. 2.5.3. The original low 3dB frequency was due partly to inaccurate reference plane locations used for the resonators but mainly the effect of fringing capacitances at the ends of the resonators, unaccounted for in the design. No known information exists for the discontinuities of stripline T junctions treated in terms of reference plane locations and a shunt impedance, for frequencies from d.c. to 18 GHz. A better approximation to the reference plane locations than used in

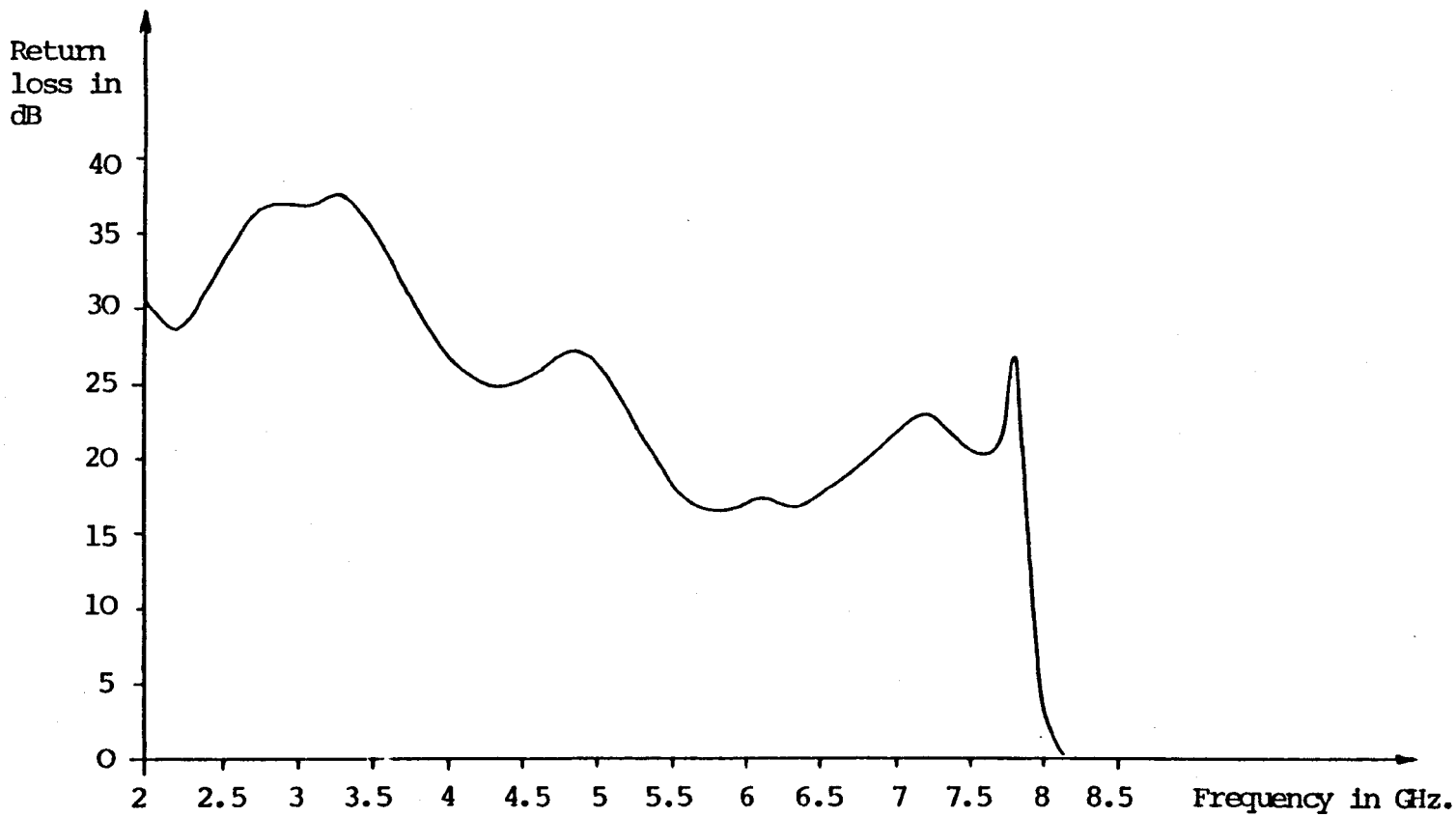

Fig. 2.5.1 Measured return loss of 8 GHz. lowpass filter

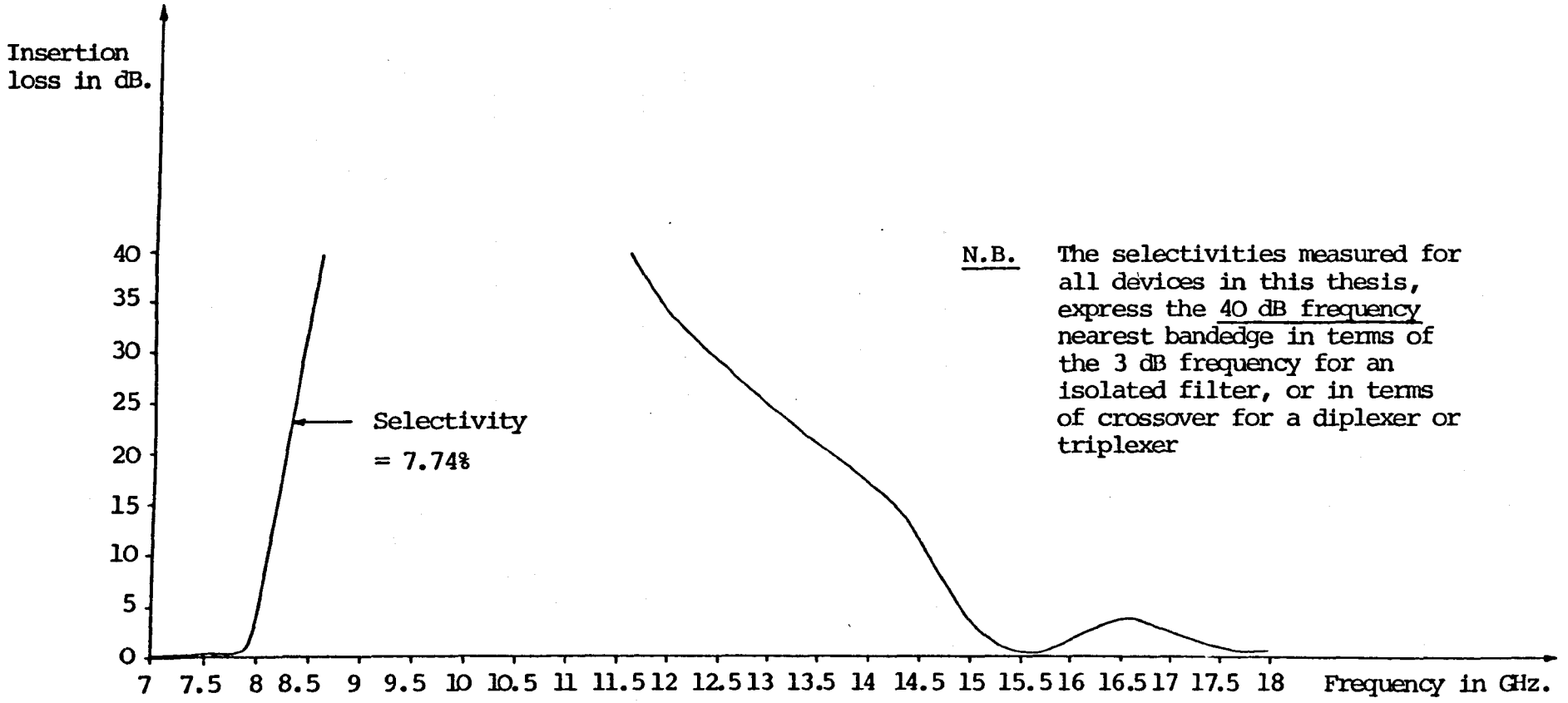

Fig. 2.5.2 Measured insertion loss of (unplated) 8 GHz. lowpass filter

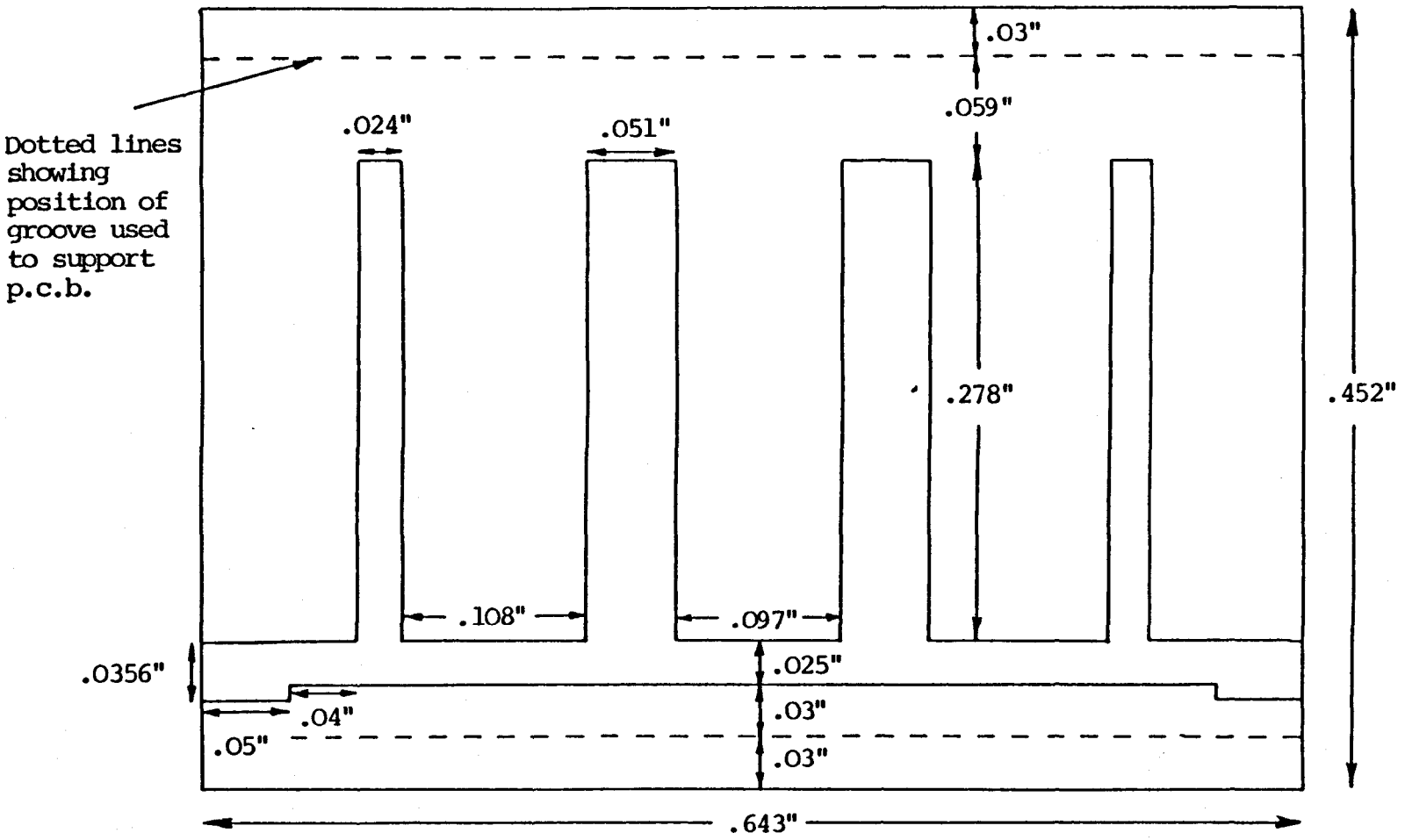

Fig. 2.5.3 Dimensions of printed circuit of 8 GHz lowpass filter

this design can be found in Ref. [2.4] and will be used when designing the diplexers. It should also be noted that no accurate information exists for the fringing capacitances at the ends of the resonators. These problems are not serious in practical terms because the designed resonator lengths are not in serious error and can easily be directly shortened on the p.c.b. or lengthened (using high conductivity silver paint) until the correct bandedge frequency is found.

Figs. 2.5.1 and 2.5.2 show a 3dB frequency at 8.0 GHz, a selectivity of 7.74% with respect to this frequency and a stopband insertion loss of at least 34 dB. maintained up to 12GHz. Note the very good return loss over the lower frequency part of the passband, which is an essential requirement for a triplexer consisting of cascaded diplexers. Since the selectivity will be improved to around 5% in the 8GHz diplexer and that the almost half octave 40dB stopband level is sufficient for the triplexer, this filter essentially meets the specification required for the low channel of the 8GHz diplexer. (N.B. the stopband should be improved to at least half an octave in the diplexer).

Consider now the next passband of the filter between 15.5GHz and at least 18.2GHz. The cut-off and resonant frequencies of the first possible waveguide mode, TE_{101}, propagating through the filter box are 13.05GHz and 15.97GHz respectively. This would possibly

suggest that the second passband is due to this mode. However, placing earthed walls in between the resonators made no difference to the insertion loss response. The passing is due to the circuit and can be explained as follows. At f_{cL} (i.e. at 18.21 GHz), the resonators become open circuits and the lowpass filter becomes a cascade of unit elements whose overall transfer matrix can be written, for 1 Ω terminations:

$$(T) = \begin{bmatrix} \cos(a\omega_{cL}) & jZ_L \sin(a\omega_{cL}) \\ j(1/Z_L)\sin(a\omega_{cL}) & \cos(a\omega_{cL}) \end{bmatrix}$$

where $\omega_{cL} = 2\pi f_{cL}$ and $a\omega_{cL}$ is the electrical length of the cascade of u.e.'s at f_{cL}.

The insertion loss of the filter is then,

$$L_A = 10 \log_{10}(1 + \tfrac{1}{4}(Z_L - \frac{1}{Z_L})^2 \sin^2(a\omega_{cL}))$$

$$\text{i.e. } L_A \leq 10 \log_{10}(1 + \tfrac{1}{4}(Z_L - \frac{1}{Z_L})^2)$$

Substituting for Z_L,

$$L_A \leq 2.55 \text{ dB}$$

Clearly the filter is passing around 18 GHz. In chapter 5, a computer frequency analysis of this lowpass is presented and its results agree very closely with the practical results given here.

3. DESIGN OF M.I.C. BROADBAND HIGHPASS FILTERS

3.1. Distributed Quasi Highpass Prototype Filter

The two filters for the 8GHz diplexer are based on the same lumped lowpass prototype (see chapter 4). To transform this prototype into a distributed quasi highpass prototype, the following frequency transformation is used:

$$p \rightarrow \alpha_H / t \qquad (3.1.1)$$

where for this filter, $t = \tanh(a_H p)$ and α_H and a_H are constants which have similar meaning to those constants in the lowpass distributed frequency transformation.

$$\text{i.e.} \quad \omega \rightarrow -\alpha_H / \tan(a_H \omega) \qquad (3.1.2)$$

The quasi highpass response is shown in Fig. 3.1.1. Following the same method as for the distributed lowpass resonators, given on pp.17-18 we find that provided $\alpha_H = \omega_o$ then

$$\text{Admittance of each distributed shunt highpass resonator} = \frac{C_r \alpha_H \tanh(2a_H p)}{2} \qquad (3.1.3)$$

This condition is true if $\alpha_H = \omega_o$ $\quad (r = 2,4,\ldots 8)$

Therefore we can once again realise the distributed shunt resonators by uniform impedance open circuited

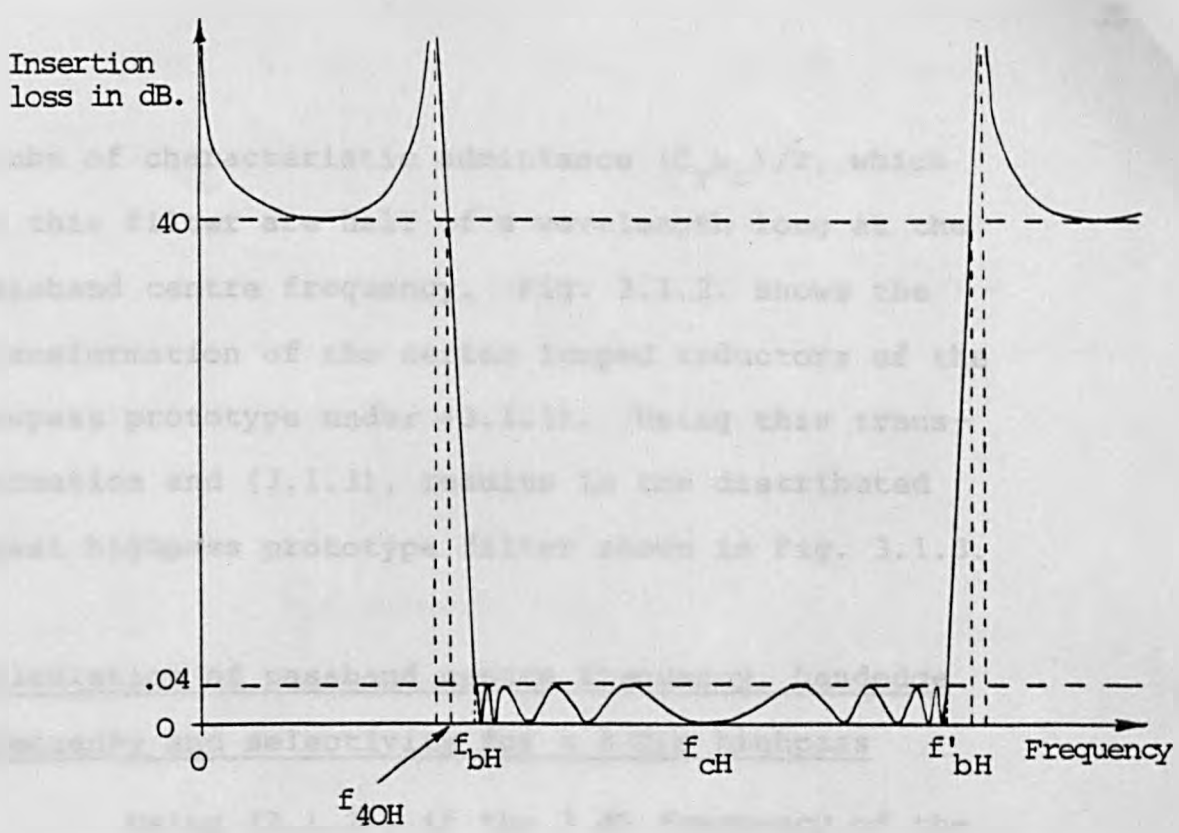

N.B. This response is periodic with frequency

Fig. 3.1.1 Quasi highpass insertion loss response

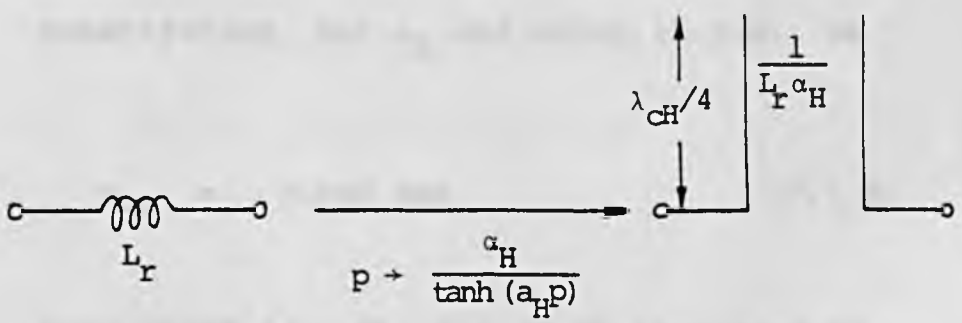

i.e. Series inductor, L_r, of lumped lowpass prototype, ($r = 1,3,\ldots,9$) → $\lambda_{cH}/4$ open-circuited stub of characteristic admittance $1/(L_r \alpha_H)$

(λ_{cH} is the wavelength at passband centre frequency, f_{cH})

Fig. 3.1.2 Transformation of lumped inductor under $p \rightarrow \alpha_H / (\tanh(a_H p))$

stubs of characteristic admittance $(C_r\omega_o)/2$, which in this filter are half of a wavelength long at the passband centre frequency. Fig. 3.1.2. shows the transformation of the series lumped inductors of the lowpass prototype under (3.1.1). Using this transformation and (3.1.3), results in the distributed quasi highpass prototype filter shown in Fig. 3.1.3.

Calculation of passband centre frequency, bandedge frequency and selectivity for a 8 GHz highpass

Using (3.1.2), if the 3 dB frequency of the highpass is at 8 GHz , then the bandedge frequency is,

$$f_{bH} = \frac{\tan^{-1}\alpha_H}{\tan^{-1}(\alpha_H/\omega_3)} \quad 8 \quad \text{GHz} \qquad (3.1.4)$$

Substituting for α_H and using (2.2.8), we have

$$f_{bH} = 8.088 \text{ GHz} \qquad (3.1.5)$$

Also using (3.1.2), the 40 dB frequency is given by

$$f_{40H} = \frac{\tan^{-1}(\alpha_H/\omega_{40})}{\tan^{-1}(\alpha_H/\omega_3)} \quad 8 \quad \text{GHz} \qquad (3.1.6)$$

Substituting for α_H and for ω_{40} and ω_3 from (2.2.9) and (2.2.8) respectively,

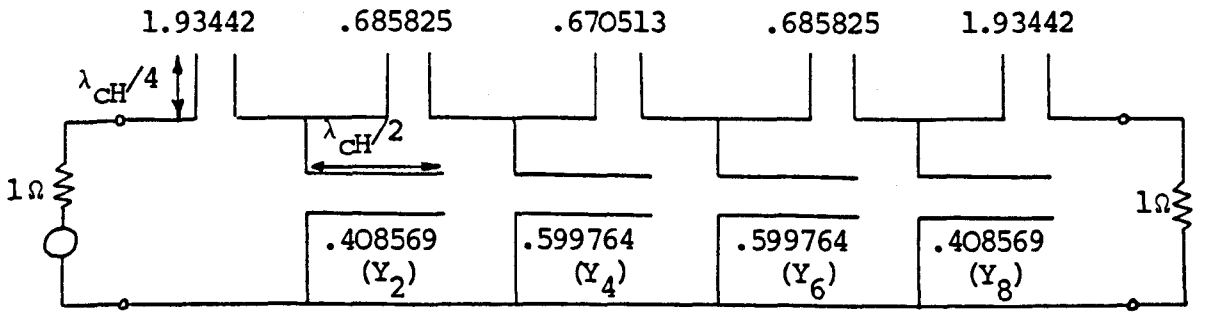

(Numbers shown are characteristic admittances in mhos)

Key:

= Open circuited stub

Fig. 3.1.3 Distributed quasi highpass prototype filter

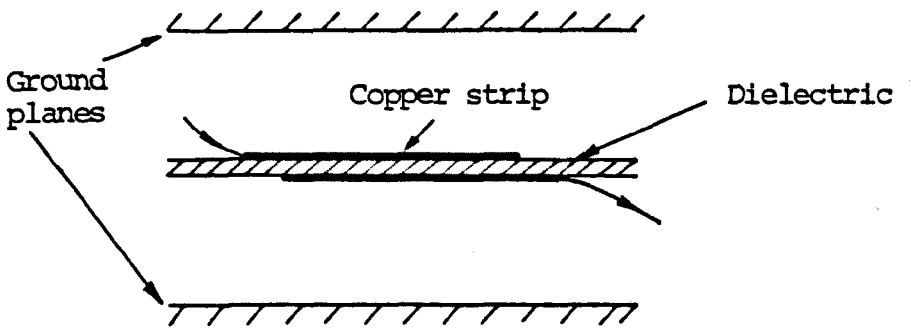

Cross section of inhomogeneous section

Plan view of inhomogeneous section

N.b. Arrows show input and output of section

Fig. 3.2.1 Series coupling element for the highpass filter

$$f_{4OH} = 7.655 \text{ GHz} \qquad (3.1.7)$$

The selectivity of the highpass with respect to its 3 dB frequency is

$$S_H = \frac{8 - f_{4O}}{8} \times 100\%$$

$$\text{i.e. } S_H = 4.31\% \qquad (3.1.8)$$

Since the fractional bandwidth of this highpass is smaller than that of the lowpass, due to $\alpha_H > \alpha_L$, its selectivity is better than that of the lowpass. The passband centre frequency is given by,

$$f_{cH} = \frac{(\pi/2)}{\tan^{-1}(\alpha_H/\omega_3)} \quad 8 \quad \text{GHz}$$

$$= 14.27 \text{ GHz} \qquad (3.1.9)$$

For the high channel of the 8 GHz diplexer we require a passband to only 12 GHz, so clearly this distributed prototype meets this requirement. The prototype also has a good enough selectivity and has the required minimum passband return loss and stopband insertion loss levels. (see specification, Fig. 1.3.3).

3.2. Suspended Substrate Realisation of Highpass Filter

The series elements of the distributed prototype are open circuited stubs which produce zero

impedance at twice the frequency of the finite transmission zeros, which is about 1.8 times the cut-off frequency. Since such a stub is difficult to realise in printed circuit form, an alternative solution must be sought. The distributed coupling between the resonators is insufficient to synthesis the series open circuited stub when a printed form is used. Now for the 4 - 8 GHz channel of the triplexer, the zero impedance frequency occurs in the passband, so this region of frequency behaviour must be simulated if a reasonable VSWR is to be maintained. Furthermore, for the broad bandwidth, a significant amount of capacitance must be realised. This can only be achieved by coupling through the 0.005" thick substrate from conductors on the other side. In chapter 5, a computer analysis is presented which shows that a pure capacitor simulation of the series open circuited stubs is inadequate, because the impedance of the capacitor does not decrease rapidly enough with frequency in the passband. Clearly it is at least necessary to produce an effective series combination of an inductor and capacitor, which approximates to a large capacitor at low frequencies but resonates to produce a zero impedance at about 1.8 times the cut-off frequency. An obvious choice for this element is shown in Fig. 3.2.1. Unfortunately this is a complex inhomogeneous section but can be described electrically by its even and odd mode characteristic impedances and

group velocities plus a large fringing capacitance. Chapter 5 shows that correct design of this complex section can accurately simulate an open circuited stub beyond its quarter wavelength frequency.

The suspended substrate realisation of the highpass is shown in Fig. 3.2.2. The shunt resonators are essentially in air, as with the lowpass resonators, so the filter will have good temperature properties. The only strong fields in dielectric occur in the series elements, but these are in a nonresonant situation near bandedge. Hence temperature changes affecting these elements will only very slightly alter the return loss for the device, not the bandedge frequency.

3.3. Design of Physical Dimensions of 8 GHz Highpass

The ground plane spacing of 0.07" chosen for the 8 GHz lowpass filter is used here, thereby simplifying the diplexer box to be designed later. Also this will lead to reasonable dimensions for the resonators since they have the same impedances as the corresponding lowpass resonators. Walls are placed in between the resonators to prevent distributed coupling between them. However, these walls are removed later without any deterioration in the electrical performance. In chapter 5, computer analysis shows that for all the filters in the triplexer, the effect of coupling between the resonators is negligible; only when the resonators

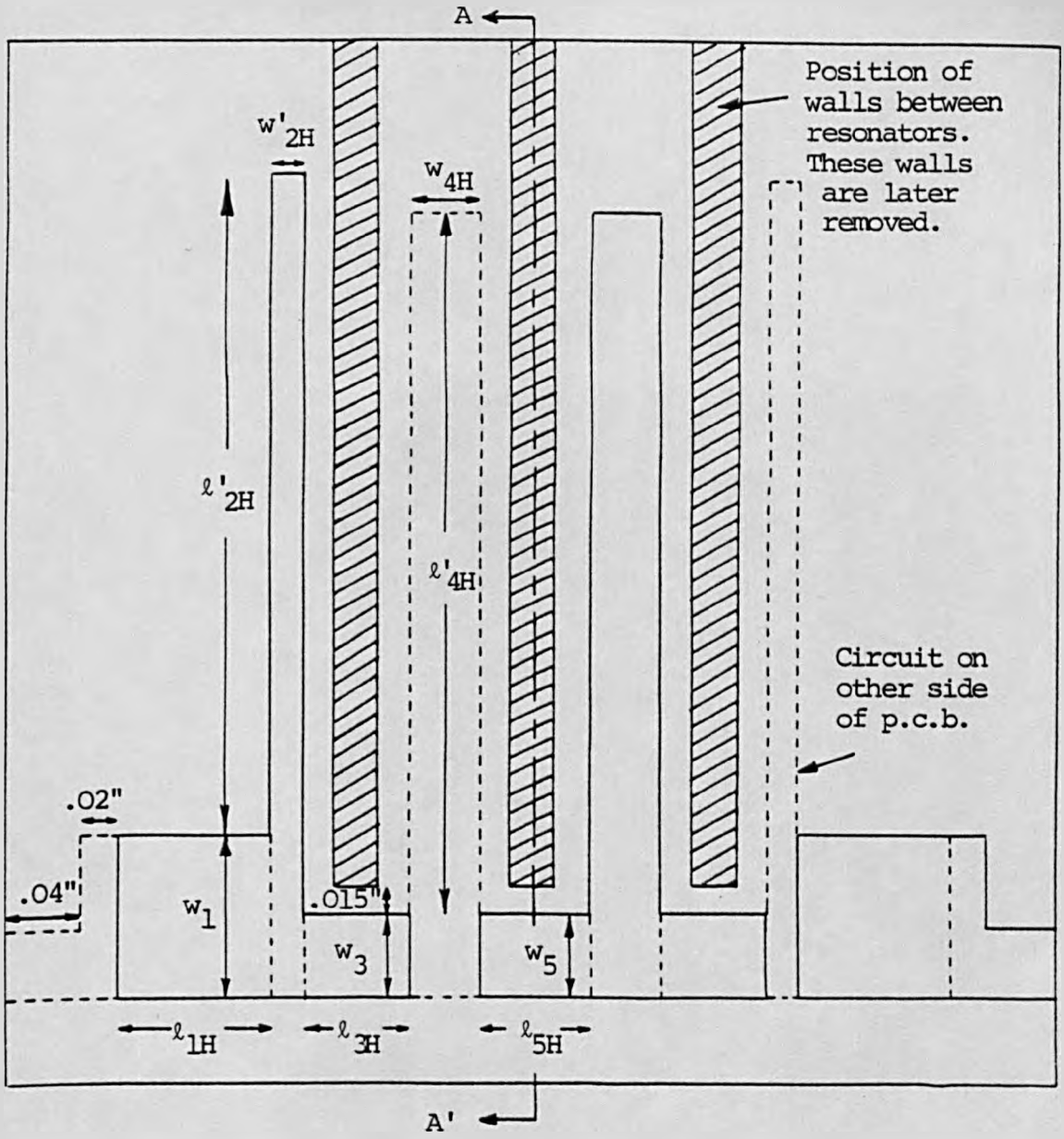

Printed circuit board

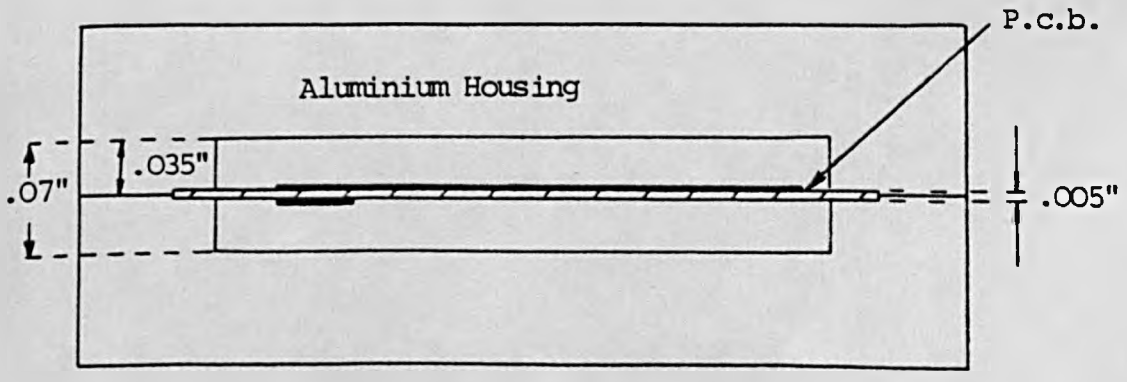

Cross-section of filter box along A - A', without walls between the resonators

Fig. 3.2.2 Suspended substrate realisation of 8 GHz highpass filter

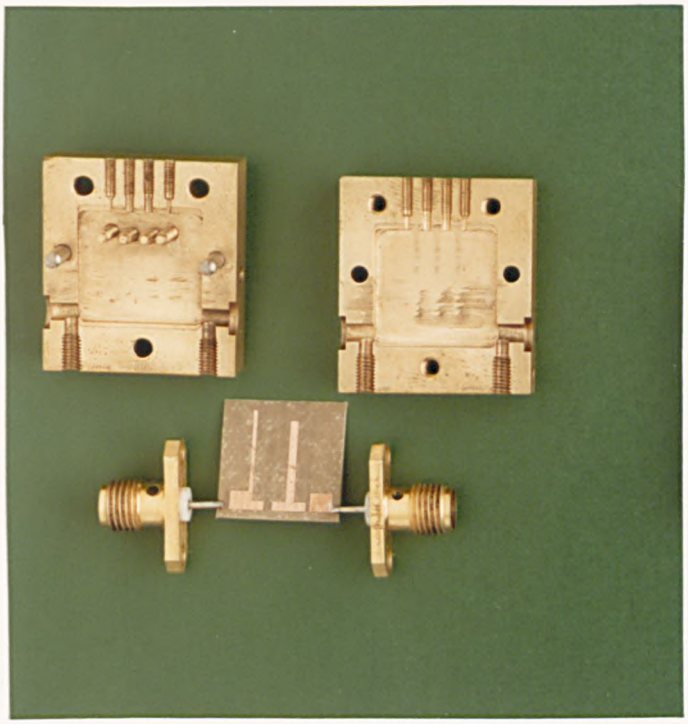

Photograph No. 2 Suspended substrate stripline 8 GHz highpass filter

are brought quite close together does the distributed coupling degrade the electrical performance.

3.3.1. Design of series elements

At this stage an accurate design for the series elements had not yet been developed. However, although the design presented below is somewhat intuitive it does lead to a working broadband highpass. Firstly we assume that at bandedge the series inductance effect of the inhomogeneous coupled lines is negligible and that the coupled lines approximate to a series lumped capacitor. The required lumped capacitance, C_{rH}, is then found by equating the impedance of the capacitor to the impedance of the corresponding series stub of the distributed prototype, at the bandedge frequency f_{bH}. That is,

$$j\omega_{bH}C_{rH} = j\frac{1}{L_r\alpha_H} \tan(a_H\omega_{bH}) \quad (r=1,3,5) \qquad (3.3.1)$$

where $\omega_{bH} = 2\pi f_{bH}$

But from (3.1.2), $\tan(a_H\omega_{bH}) = \alpha_H$

$$\therefore \quad C_{rH} = \frac{1}{L_r\omega_{bH}} \qquad (3.3.2)$$

Substituting for L_r and ω_{bH} we find that the required lumped series capacitances for 1Ω terminations are,

$$C_{1H} = 47.03 \text{ pF}; \quad C_{3H} = 16.67 \text{ pF}; \quad C_{5H} = 16.30 \text{ pF} \qquad (3.3.3)$$

The static capacitance between each pair of overlapping strips is now estimated. The fields between these strips, including end effects, are complex and three dimensional and it should be noted that no known information exists for the capacitance of the complex structure considered here. Therefore assume that the fringing capacitance at the ends of the strips, $2C_f$, (see Fig. 3.3.1(a)) is equivalent to 10% of the total capacitance between the strips. We now assume that the remaining capacitance can be calculated by considering the situation shown in Fig. 3.3.1(b) which shows two infinitely long coupled lines of width w_r (r = 1,3,...,9) (Note that the box walls are neglected in this argument. However, the side walls are a distance .0172" away - see section 3.3.2 - and the top and bottom walls 0.03165" away, so this is a reasonable assumption). To calculate the capacitance per unit length between the infinitely long strips consider Fig. 3.3.1(c). In this figure, the strips are at a potential V and -V respectively, so placing a ground plane as shown will not affect the electric fields since it is placed on an equipotential surface. The top strip is now in a true microstrip situation and its static capacitance to ground per unit length is given by,

$$C_{oor} = \frac{1}{u_{or} Z_{oor}} \qquad (r = 1,3,5) \qquad (3.3.4)$$

where u_{or} = group velocity in the microstrip

" Z_{oor} = microstrip impedance of the top strip

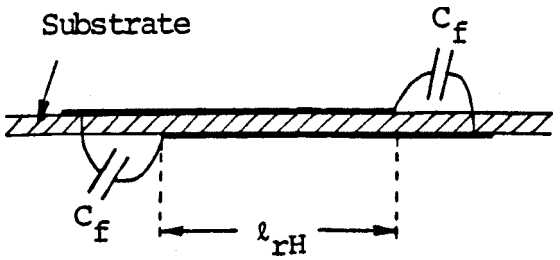

Width w_r goes into the plane of the paper.

(a) End fringing capacitances

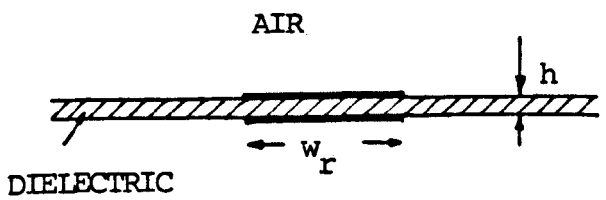

Length extends infinitely into the plane of the paper

(b) Mixed dielectric transmission line

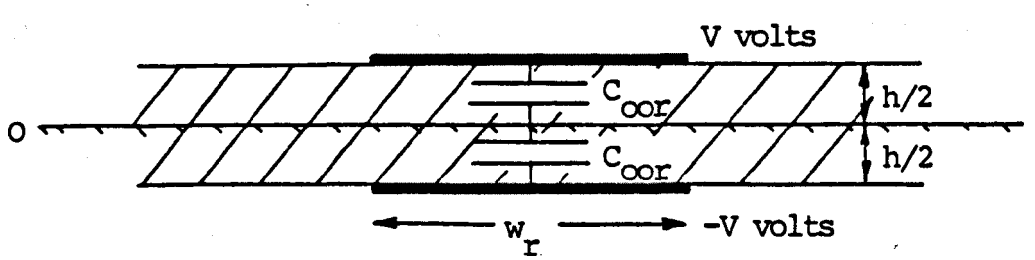

(c) Distributed static capacitance of infinitely long mixed dielectric transmission line

Fig. 3.3.1 Approximations used in estimating series lumped capacitances of 8 GHz highpass filter

$$\text{i.e. } C_{oor} = \frac{\sqrt{\varepsilon_{er}}}{u\, Z_{oor}} \qquad (3.3.5)$$

where u = group velocity in air

and ε_{er} = effective dielectric constant of the microstrip

The static capacitance per unit length between the infinitely long lines is $C_{oor}/2$ so we require,

$$0.9\, C_{rH} = \frac{C_{oor}}{2}\, \ell_{rH} \qquad (3.3.6)$$

$$\text{or } \ell_{rH} = \frac{1.8\, u\, Z_{oor}\, C_{rH}}{\sqrt{\varepsilon_{er}}} \quad (r = 1,3,5) \qquad (3.3.7)$$

(n.b. Z_{oo} assumes 1Ω terminations).

Using (3.3.2),

$$\ell_{rH} = \left(\frac{1.8\, u}{\omega_{bH}}\right) \frac{Z_{oor}}{\sqrt{\varepsilon_{er}}\, L_r} \qquad (3.3.8)$$

This equation determines the lengths of the inhomogeneous sections. However before it can be solved, the widths of these sections must be determined from inductance considerations.

Clearly, the middle inhomogeneous sections must have a greater series inductance than the end sections if they are to resonate at bandcentre, because the middle sections have a smaller series lumped capacitance. This means that the middle sections must be

narrower than the end sections. The following widths are chosen for the inhomogeneous sections, hoping that these lead to the required inductance levels (The widths of the end sections came, infact, from an early design where it was assumed that the inhomogeneous sections approximated to a stripline in air around band-centre. This line was made 50 Ω):

$$\text{Make} \quad w_1 = 0.0899" \tag{3.3.9}$$

$$\text{and} \quad w_3 = w_5 = 0.045" \tag{3.3.10}$$

The odd-mode characteristic impedance and effective dielectric constant of each inhomogeneous section are calculated using Hammerstad's equations (Z_{oor} is calculated for 1Ω terminations) [3.1]:

$$Z_{oor} = \begin{cases} \dfrac{\eta_o}{100\pi\sqrt{\varepsilon_{er}}} \ln\left(8\dfrac{(h/2)}{w_{er}} + 0.25\dfrac{w_{er}}{(h/2)}\right), & \dfrac{w_{er}}{(h/2)} \le 1 \\ \dfrac{\eta_o}{50\sqrt{\varepsilon_{er}}} \left[\dfrac{w_{er}}{(h/2)} + 1.393 + 0.667\ln\left(\dfrac{w_{er}}{(h/2)} + 1.444\right)\right]^{-1}, & \dfrac{w_{er}}{(h/2)} \ge 1 \end{cases}$$

where η_o = wave impedance of free-space = 376.73 Ω

ε_r = dielectric constant of duroid = 2.22

w_{er} = effective widths of the strip conductor accounting for its finite thickness

(3.3.11)

Also,

$$\varepsilon_{er} = \tfrac{1}{2}(\varepsilon_r + 1 + (\varepsilon_r - 1)F)$$

$$\text{where} \quad F = \begin{cases} (1+12\frac{(h/2)}{w'_{er}})^{-\frac{1}{2}} + 0.04\,(1-\frac{w'_{er}}{(h/2)})^{2}, & \frac{w'_{er}}{(h/2)} \leq 1 \\ (1+12\frac{(h/2)}{w'_{er}})^{-\frac{1}{2}}, & \frac{w'_{er}}{(h/2)} \geq 1 \end{cases}$$

and w'_{er} = different effective width of the strip conductor (see below)

(3.3.12)

These equations are the most accurate available and will calculate the impedances to within 1% for most strip widths [3.1]. They are essentially for zero thickness conductors but thick conductors can be considered by modifying their physical widths. The strip thickness increases the fraction of the total energy propagating in air, thereby decreasing the effective dielectric constant. This is equivalent to an effective decrease in the physical width of the strip conductor when calculating ε_{er}, so $w'_{er} < w_r$. The static capacitance of the microstrip is increased by the strip thickness and this is accounted for in Hammerstad's equations by an increase in the physical width, i.e. $w_{er} > w_r$. This produces a definite decrease in Z_{oor} which is only slightly cancelled by the increase in effective dielectric constant due to strip thickness. At present accurate equations for thick conductors exist for $t/(h/2) < 0.2$ (see Ref. [3.2]) but for the microstrips considered in this work, this ratio is 0.34.

We will assume that,

$$w_{er} = w_r + t \tag{3.3.13}$$

$$w'_{er} = w_r - t \tag{3.3.14}$$

The errors produced by this assumption will be small since in this work we are dealing with wide microstrips (i.e. $w_r \gg t$ and $w_r \gg h$).

Using the above equations with (h/2) = 0.0025", t = 0.00085", w_1 = 0.0899", w_3 = 0.045" and w_5 = 0.045", we find,

$$\varepsilon_{e1} = 2.138 \tag{3.3.15}$$

$$Z_{oo1} = 0.12846\,\Omega \quad (1\,\Omega \text{ terminations}) \tag{3.3.16}$$

$$\varepsilon_{e3} = \varepsilon_{e5} = 2.081 \tag{3.3.17}$$

$$Z_{oo3} = Z_{oo5} = 0.2404\,\Omega \tag{3.3.18}$$

The effect of dispersion should be considered. Results of Edwards and Owen, for the dispersion in ε_{er}, may be written as, [3.3]

$$\varepsilon_{er}(f) = \varepsilon_r - \frac{\varepsilon_r - \varepsilon_{er}}{1 + G(f/f_p)^2} \tag{3.3.19}$$

where,

$$G = \left(\frac{Z_{oor} - 5}{60}\right)^{\frac{1}{2}} + 0.004 Z_{oor}$$

$$f_p \text{ (in GHz)} = \frac{15.66\, Z_{oor}}{(h/2)}$$

In these equations, h is in mils, f is frequency in GHz and Z_{oor} and ε_{er} are the quasistatic values given by

equations (3.3.11) to (3.3.14), with Z_{oor} scaled to 50Ω terminations. Using (3.3.15) to (3.3.19),

$$\varepsilon_{e1}\,(18\,\text{GHz}) = 2.141 \qquad (3.3.20)$$

$$\varepsilon_{e3}\,(18\,\text{GHz}) = 2.084 \qquad (3.3.21)$$

Clearly the effect of dispersion upto at least 18GHz can be neglected.

Finally equation (3.3.8) is solved for the lengths of the inhomogeneous sections, since all quantitites in this equation are now known.

$$\ell_{1H} = 0.0847" \qquad (3.3.22)$$

$$\ell_{3H} = 0.0585" \qquad (3.3.23)$$

$$\ell_{5H} = 0.0608" \qquad (3.3.24)$$

3.3.2. Design of centre conductors of input and output terminals

Input and output connections to the p.c.b. are made using Jack receptacles as shown in photograph no. 2. The transmission lines formed by the centre conductors of these terminals with the box walls must be made 50 Ω. The position of each centre conductor in relation to the filter circuit is shown in Fig. 3.3.2, for which the dimensions of the coaxial feeds have already been found when designing the lowpass. That is,

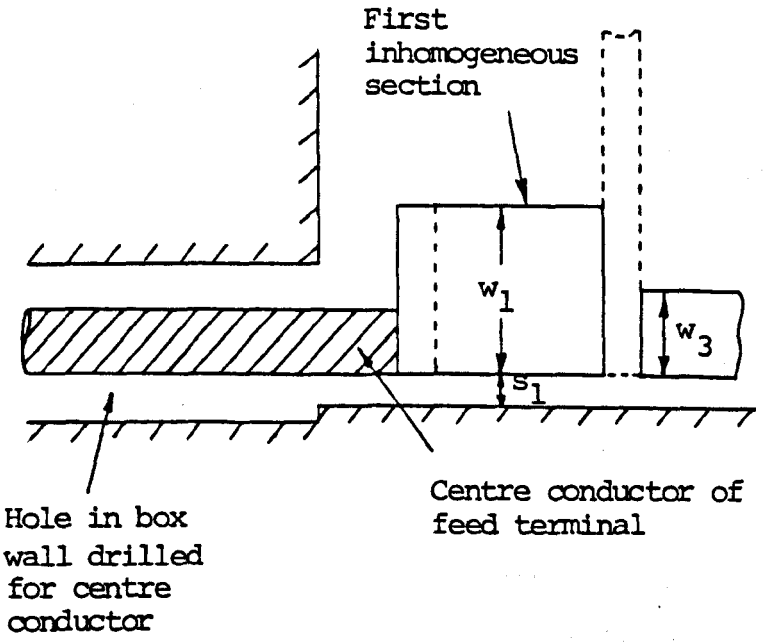

Position of centre conductor of feed terminal in relation to filter circuit

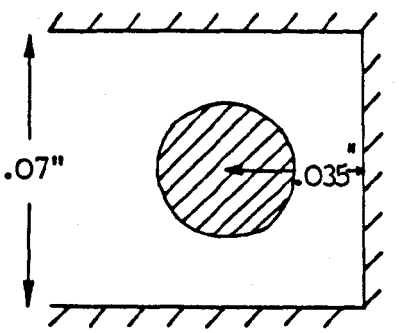

Cross section of the centre conductor inside the box

Fig. 3.3.2 Input and output connections to p.c.b.

$$d = 0.0356"$$

$$\text{and } b_1 = 0.082"$$

$$\text{whence } s_1 = \frac{b-d}{2} = 0.0172"$$

The length of each centre conductor inside the box is made 0.04".

3.3.3. Design of shunt resonators

Let the thickness of the walls between the resonators be 0.025". Although 0.01" thick walls can be accurately milled, the above thickness ensures a better grounding of these walls. The various static fringing capacitances per unit length for each resonator are as shown in Fig. 3.3.3. The distances, shown in the figure, of the resonators from their nearby walls are calculated using the lengths of the inhomogeneous sections given in (3.3.22) - (3.3.24). Due to the length of the first section, the left hand box wall for the first resonator can be neglected so the left hand fringing capacitance for this resonator is C'_f. Using the ratios, $2s_2/b = 0.479$, $2s_4/b = 0.511$ and $t/b = 0.012$ in Getzinger's curves [2.2] we find,

$$C'_f/\varepsilon_o = 0.46; \quad C'_{fo2}/\varepsilon_o = 0.63; \quad C'_{fo4}/\varepsilon_o = 0.61 \tag{3.3.25}$$

Calculating the total capacitance between the first resonator and ground and using (2.4.6), yields the width of the first resonator:

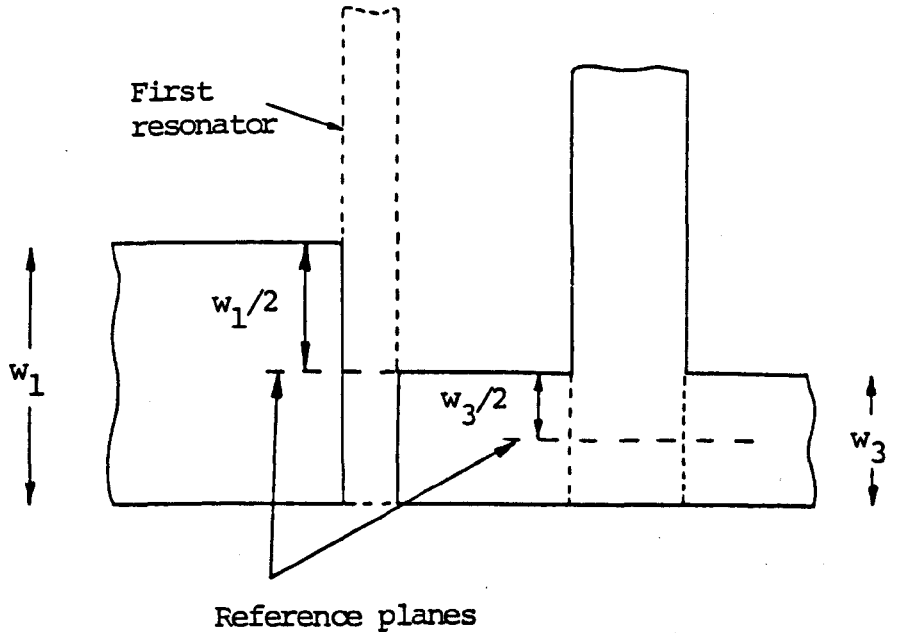

Fig. 3.3.4 Reference planes for shunt resonators of highpass

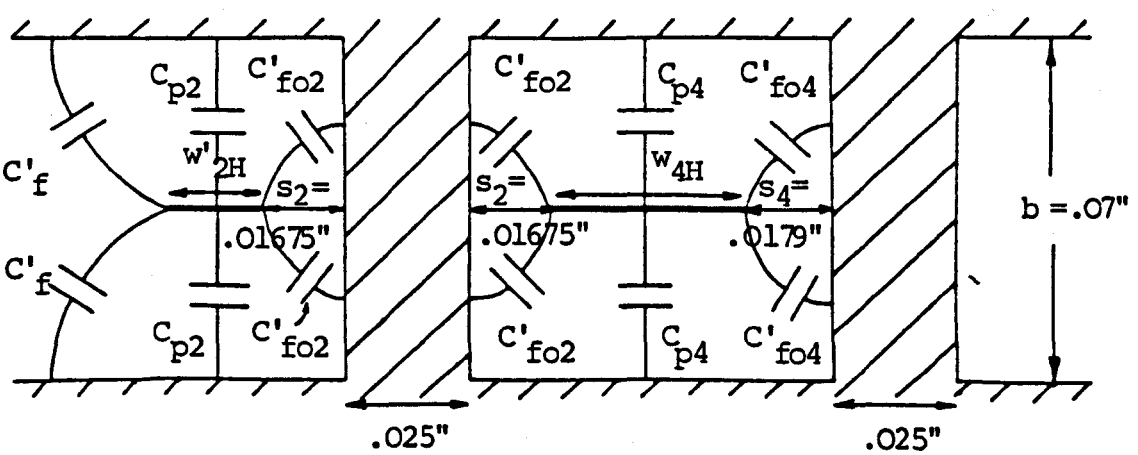

Fig. 3.3.3 Capacitance per-unit-length between each resonator and the ground planes.

$$w_{2H} = \tfrac{1}{4}(b-t)\left(7.534\,Y_2 - \frac{2C'_f}{\varepsilon_o} - \frac{2C'_{fo2}}{\varepsilon_o}\right) \quad (3.3.26)$$

where Y_2 is the normalised characteristic admittance of the first resonator = 0.40856 (from Fig. 3.1.3).

We find $w_{2H} = 0.01741"$ (3.3.27)

But $w_{2H} < 0.35\,(b-t)$, so the fringing fields will interact. Getzinger's correction formula, equation (2.4.9), is now used to produce a greater width to compensate for the loss of fringing due to interaction:

$$w'_{2H} = 0.0185" \quad (3.3.28)$$

$$\left(\text{N.b.} \quad 0.1 < \frac{w'_{2H}/b}{(1-t/b)} < 0.35\right)$$

Repeating the above method, but with Y_2 replaced by Y_4 and C'_f by C'_{fo4}, the width of the second resonator is,

$$w_{4H} = 0.0391" \quad (3.3.29)$$

By symmetry of the filter, the widths of the third and fourth resonators are w_{4H} and w_{2H} respectively.

To complete the design the lengths of the resonators must be determined. The required length of each resonator is,

$$\ell_{rH} = \frac{\lambda_{cH}}{2} = \tfrac{1}{2}\frac{u}{f_{cH}} \qquad (r = 2,4,\ldots 8) \quad (3.3.30)$$

i.e. $\ell_{rH} = 0.4136"$

To calculate the physical lengths of the resonators, the reference plane locations for the resonators must be considered. No known information exists on the 'T' junctions in this highpass and there is also uncertainty in the calculation of the fringing capacitances at the ends of the resonators (N.b. It has been assumed when designing the series elements that the dominant circuit effect, produced by the T-junction discontinuity, in series with each inhomogeneous section is a large lumped fringing capacitance). To produce a 3 dB frequency exactly at 8 GHz will almost certainly require a little experimentation, so the above uncertainties in the effective resonator length are not a problem in practical terms. Therefore assume the simple reference plane locations shown in Fig. 3.3.4 to yield the following physical lengths of the shunt resonators,

$$\ell'_{rH} = \ell_{rH} - \frac{w_{rH}}{2} \qquad (\ell'_{rH} \text{ is defined in Fig. 3.2.2}) \tag{3.3.31}$$

$$\text{i.e. } \ell'_{2H} = 0.369" \tag{3.3.32}$$

$$\ell'_{4H} = 0.392"$$

The complete filter is shown in photograph no. 2 and note that the p.c.b is only $\approx$ .58" x .58". Capacitive tuning screws are placed in the main housing at the ends of the resonators to fine tune the bandedge frequency and VSWR near bandedge. The non-resonator tuning screws at the input and output of the filter

improve the passband VSWR especially at midband (see next section). Note that the distance between adjacent strips of neighbouring inhomogeneous sections is equal to the widths of the resonators, so there should be negligible coupling between these adjacent strips. Also, the distance from the top strip of the first inhomogeneous section to the centre conductor of the Jack receptacle is made 0.02" (see Fig. 3.2.2) to prevent unwanted coupling between these elements.

3.4. Practical Results and Discussion of 8 GHz Highpass

By shortening the end resonators from .369" to 0.360", it was possible using the resonator screws to produce a return loss near bandedge of 9 dB. However, the return loss near bandcentre was only 5½ dB. Placing large capacitive tuning screws in the main housing at the input and output of the printed circuit (see photograph no. 2), considerably improved the midband return loss and slightly improved the return loss near bandedge. The tuned response, given in Fig.(3.4.1), shows that a VSWR of at least 1.9 : 1 was achieved over more than an octave bandwidth. Also, the return loss could be further improved over the first half octave, which is the only bandwidth necessary for the 8 - 12 GHz. channel of the triplexer, to 13 dB minimum upto 13.8 GHz. However, for this response the return loss fell below 10 dB in the next half octave.

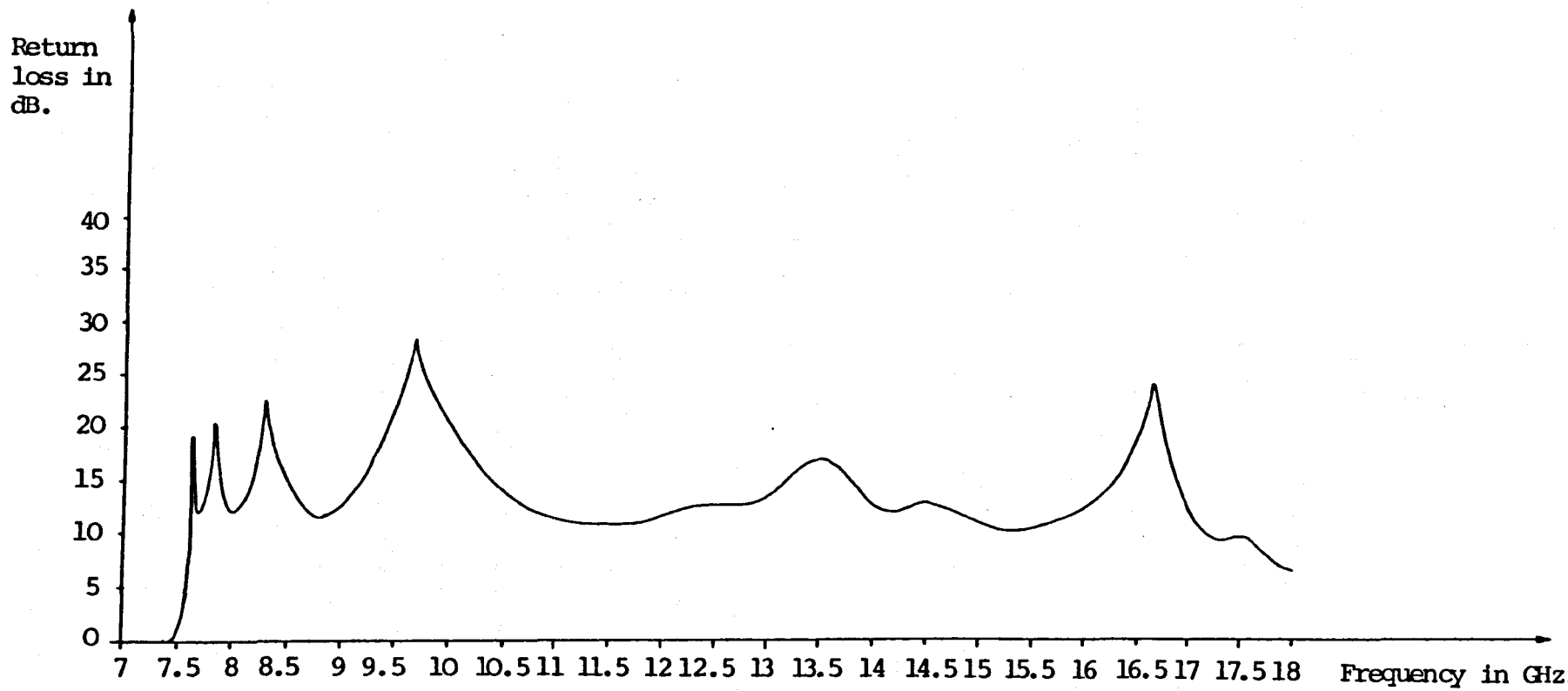

Fig. 3.4.1 Measured return loss of 8 GHz. highpass filter

Clearly the series elements, in particular the end elements, are not quite correct and are, infact, later modified when developing a working single substrate triplexer. In the latter the nonresonator screws are unnecessary. In this highpass these screws are correcting the reactive impedance seen looking towards the nearest termination at the junction of each end resonator and end section. The errors in these end sections are thereby corrected (The change in the resistive impedances seen looking towards the terminations will not be serious). These problems are further considered in chapter 5 where a detailed computer analysis and improved design for this highpass are presented.

If the separation between the ends of the resonator walls and the inhomogeneous sections is increased from 0.015" to 0.06", then the minimum passband return loss improves by 0.5 dB. It appears therefore that this separation should be comparable to the ground plane spacing if the lumped capacitances between the inhomogeneous sections and the resonator walls is to be negligible. Removing these walls entirely, slightly improved the ripples near bandedge, unaffected the selectivity or stopband performance, but allows a box mode to pass at 14.8 GHz.

The stopband and selectivity performance of the filter without walls is shown in Fig. 3.4.2. The low 3 dB frequency is later scaled to 8 GHz by simply shortening the resonators when developing the 8 GHz diplexer.

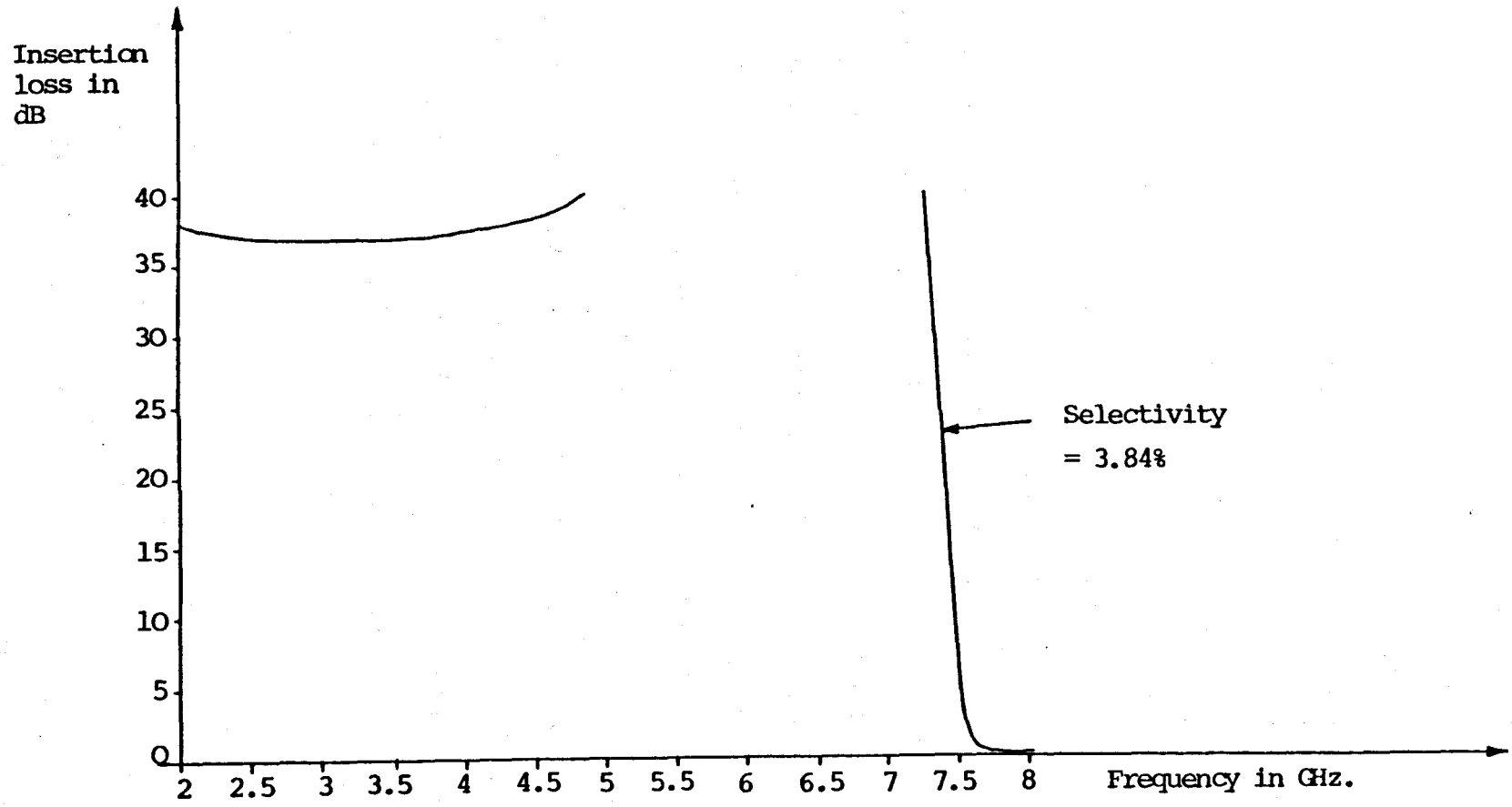

Fig. 3.4.2 Measured insertion loss of (unplated) 8 GHz. highpass filter

Fig. 3.4.2 shows that the highpass is slightly more selective than the distributed prototype highpass, a result which is confirmed by computer analysis in chapter 5. This analysis shows that the effects of coupling between the resonators is negligible. It should be noted that by removing the walls, the distributed static capacitances between the resonators and ground are reduced. Strictly, the widths of the resonators should be redesigned such that the even-mode impedances of the resonators are equal to those in the distributed prototype. This idea comes from the pi-equivalent circuit of coupled open circuited transmission lines in a homogeneous medium and is discussed in more detail in chapter 5 when coupling between the resonators is considered. We find that the widths of the end and middle resonators should be increased by only 19.6% and 20.3% respectively. Clearly removal of the walls only produces a slight change in the impedances of the resonators, a result confirmed by the practical results.

The modified dimensions of the highpass are shown in Fig. 3.4.3.

3.5. Development, with practical results, of 4 GHz Highpass Filter

This filter was produced by simply scaling the lengths of the circuit elements of the 8 GHz highpass by a factor of two. It should be noted, however, that the fringing capacitances for each resonator in the 4 GHz

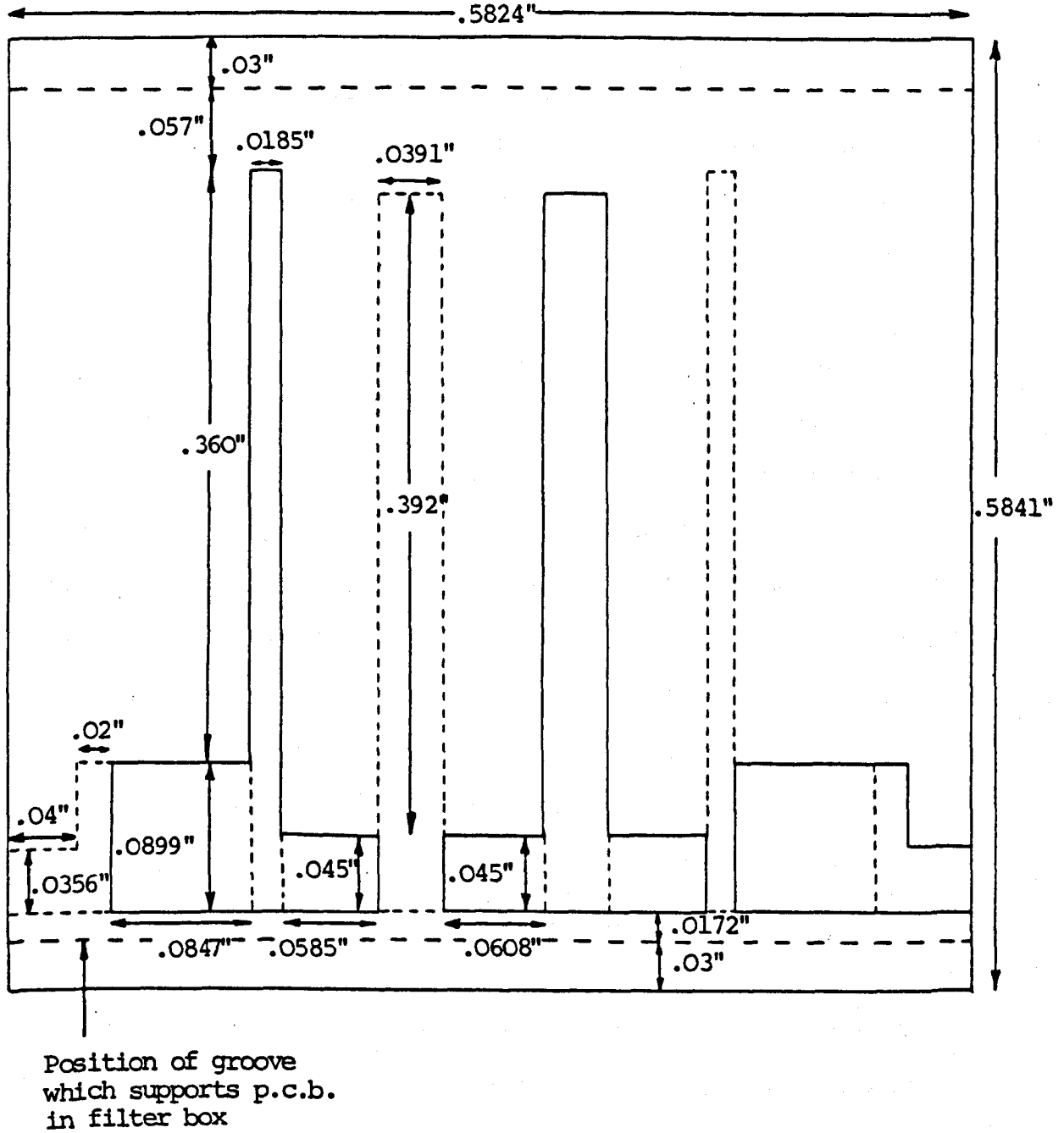

Fig. 3.4.3 Dimensions of printed circuit of 8 GHz highpass

highpass are far field components, so the widths of the resonators are the same as the corresponding 8 GHz lowpass resonators. In a correct design, account of the T-junction discontinuities both at 8 and 4 GHz should be considered. However, since little information was available on these, the 4 GHz highpass considered here was designed by simply scaling the overlapping lengths of the inhomogeneous sections and the physical lengths of the resonators (for the latter this means scaling ℓ'_{rH} in Fig. 3.2.2 by a factor of two). In chapter 5 some attention is given to the fringing capacitances at the ends of the inhomogeneous sections and it is proposed that these can be accounted for in terms of reference plane locations lying slightly inside each T junction (distance $\approx$ 0.005"). However, at 4 GHz it appears that neglecting the effects of the T junction discontinuities was justified since the electrical performance of the 4 GHz highpass was almost the correctly scaled version of that of the 8 GHz highpass. The main difference was that the nonresonator tuning screws only slightly improved the midband return loss, which is not surprising since the shunt capacitances produced by these screws were comparable to those in the 8 GHz highpass.

Several experiments on this filter finally led to a working device and the dimensions of the modified p.c.b. are given in Fig. 3.5.1. The main modifications were an increase in the length of the middle section, a

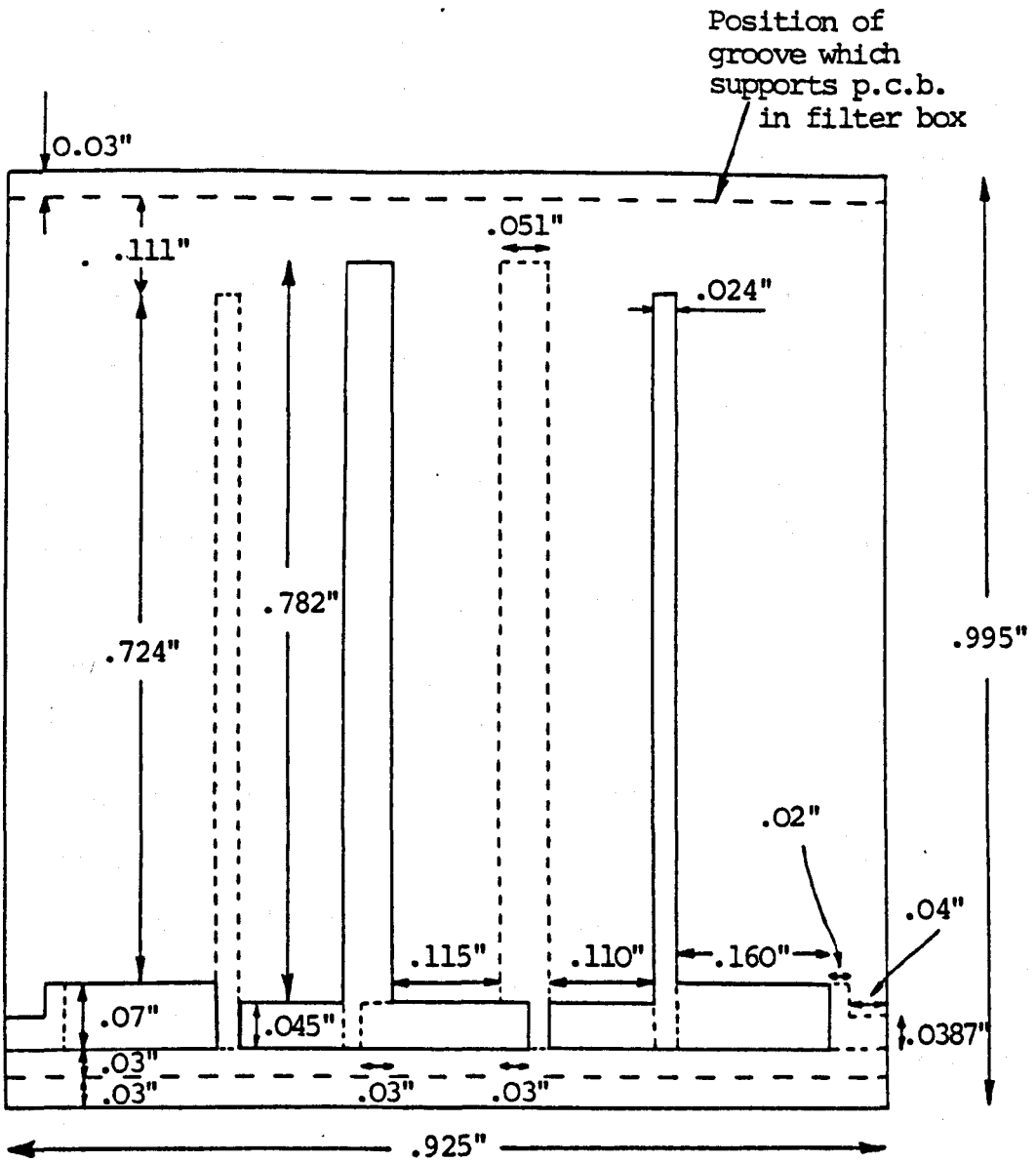

Fig. 3.5.1 Dimensions of modified printed circuit of 4 GHz highpass filter

reduction in the width of the end sections and an increase in the separation of the inhomogeneous sections from the side box wall from 0.0172" to 0.03". These modifications show that both the even and odd mode impedances and the lengths of the inhomogeneous sections are important and must be correctly designed. An analysis and improved design is given in chapter 5.

Tuned results for the modified filter are shown in Figs. 3.5.2 and 3.5.3. Measured minimum passband insertion loss for a plated device was 0.6 dB

The nonresonator tuning screws made little improvement on the tuned response - correct response has been achieved due to the modifications to the end sections themselves. Another point to note is that the minimum stopband level was improved from 34 dB to 40 dB as a result of these modifications, further showing that the series impedances produced by the inhomogeneous sections must now be almost correct. Finally, the box modes can be removed by placing thin inductive posts through the main housing in between the resonators; these posts do not interfere with the resonators.

3.6. Conclusion

This chapter has shown that a highly selective octave bandwidth highpass, meeting the requirements of the triplexer, can be produced in a suspended substrate realisation. Moreover due to the air realisation of the resonators, the filter should have good temperature

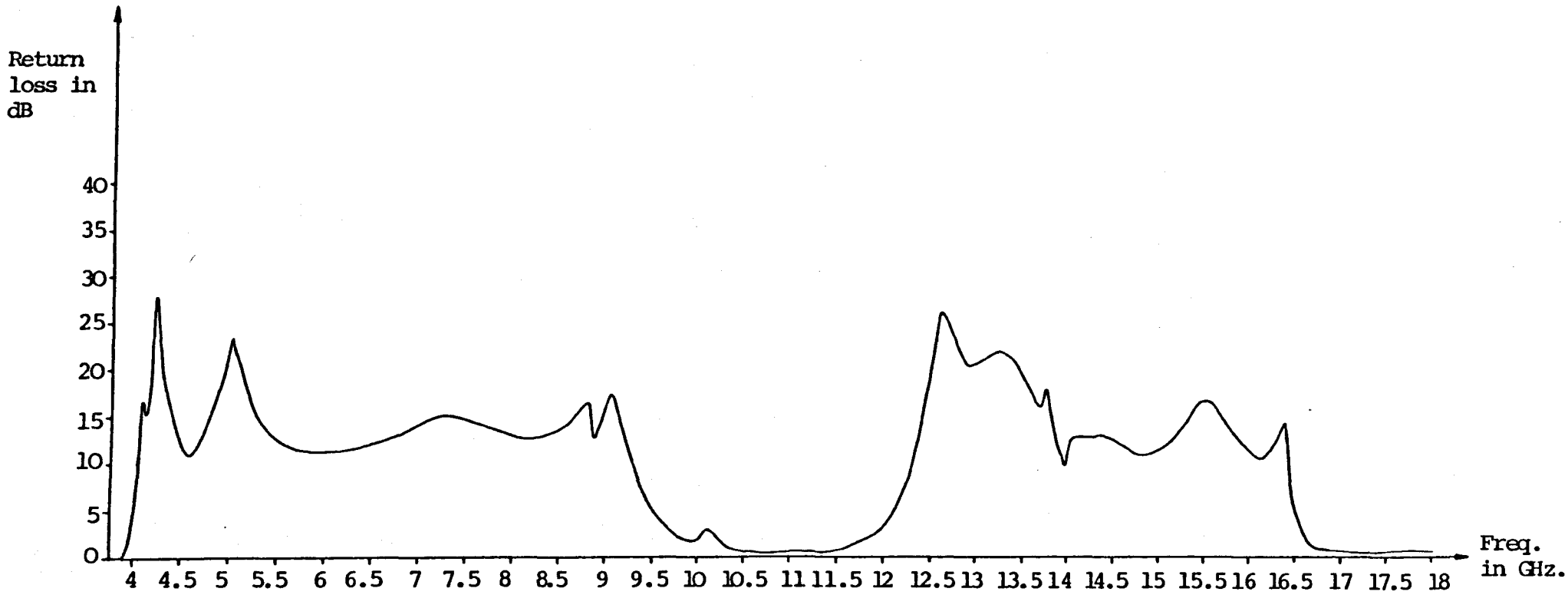

Fig. 3.5.2 Measured return loss of 4 GHz. highpass filter

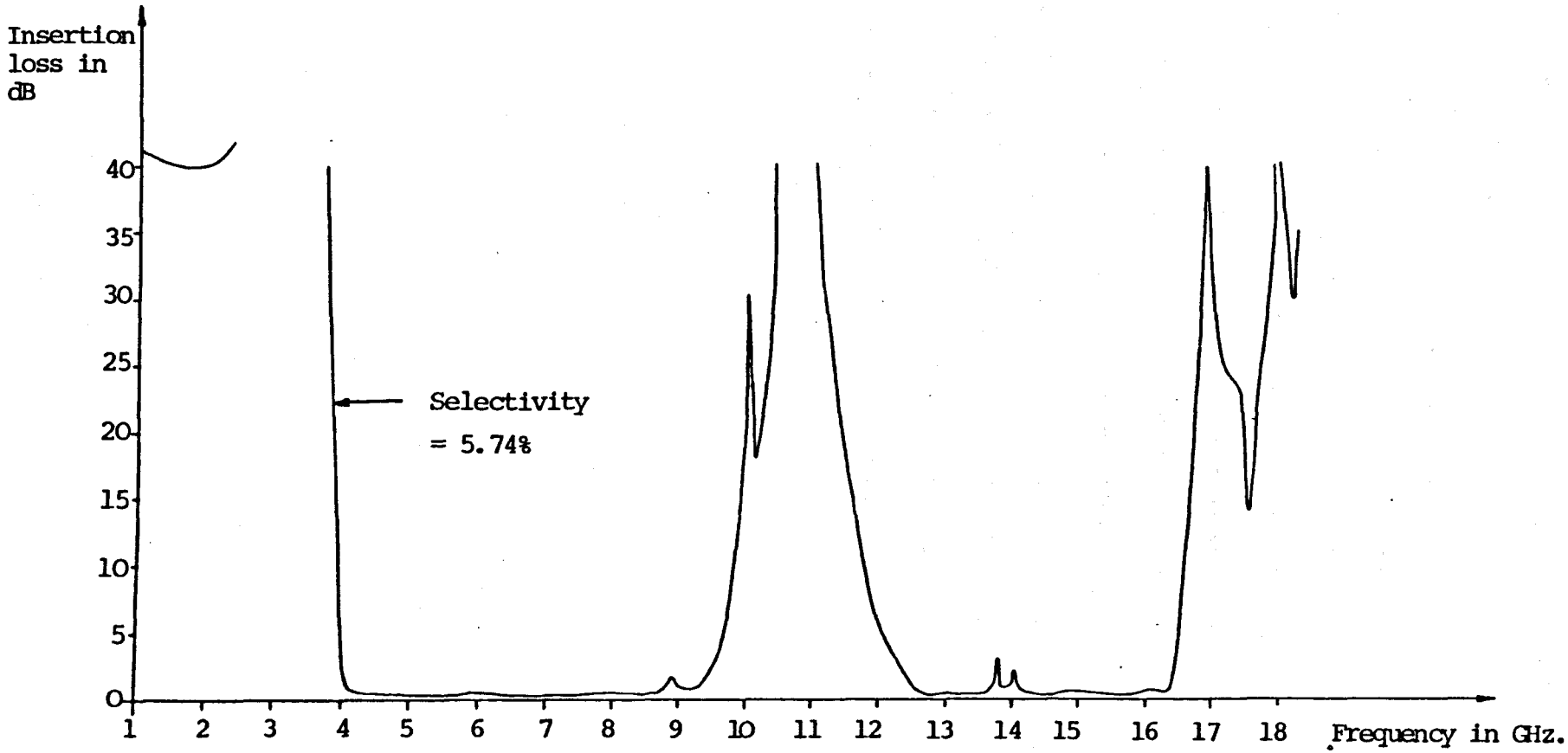

Fig. 3.5.3 Measured insertion loss of (plated) 4 GHz. highpass filter

properties. This observation was established by experiment where over a 100°C change in temperature, frequency shifts were less than ± 30 ppm/°C. This enables most military reqirements to be met. Also it should be noted that the first ordered sensitivity of the device due to movement of the suspended substrate is zero, enabling most vibrational requirements to be met. This latter requirement can be a problem in combline structures where critical capacitance gaps can change due to movement of the 'fingers' when the filter is subject to vibration. The above temperature and vibrational properties also apply to the lowpass, so the diplexer should have good tracking properties in most environmental situations.

4. DESIGN OF M.I.C. BROADBAND CONTIGUOUS DIPLEXERS AND MULTIPLEXERS

4.1. Theory of Broadband MIC Contiguous Diplexers

A factor which had to be considered when developing the MIC filters was that they had to be eventually diplexed. On a printed circuit a shunt connection is essential and since the filters commence with series inductive or capacitive elements this is possible.

Consider the lumped lowpass prototype (Fig. 2.2.1) scaled so that its 3dB point is at $\omega = 1$ and the complementary highpass prototype, also with its 3dB point at $\omega = 1$, formed by applying the transformation $\omega \rightarrow -1/\omega$ to this scaled lowpass prototype. By connecting these filters in shunt at the input port we produce a contiguous diplexer of the form required by the printed circuit. For a contiguous diplexer, a good input port return loss is required over both passbands and through the crossover region. Professor Rhodes has managed to produce a good match at the critical resonant frequencies of the scaled prototypes, by modifying the numerical values of the first series and first shunt elements of each prototype. These prototypes are then scaled by Richards transformation with the appropriate values a_H, α_H and a_L, α_L for each prototype. This forms a distributed prototype contiguous diplexer which can be physically realised using the previous design methods.

In the next chapter, a computer analysis of this theory is presented and results show that a good input port return loss is maintained over all passbands of the contiguous triplexer considered in the analysis. The return loss around the crossovers is reasonable but does fall to about 11 dB near the 8 GHz crossover. This result is expected because the theory is only a first ordered solution to the diplexing problem. Results can be improved by interaction with the computer (see next chapter) to produce a return loss of at least 14.2 dB over the complete bandwidth of the multiplexer.

The above design process inherently produces an enhanced stopband level over both channels at about 15 dB higher than that which would be achieved by an isolated filter. This improvement is due partly to the power split at the input which adds about 6 dB to a channel's isolation and partly to the change in the first two elements of the channel and the loading of the other channel, which effectively adds another 9 dB. Note that these effects also improve the selectivity of each channel when compared with the isolated filter's selectivity. It should be noted that results show that a complementary pair of singly terminated filters have about 15 dB greater stopband insertion loss per channel over the corresponding doubly terminated filters, when similar passband performances are required. However, since the distributed frequency transformation

is different for the low and highpass filters a normal complementary diplexer cannot be used directly, so a new approach has to be used.

The theory produced by Professor Rhodes is given in the Appendix, from which the equations for the first two element values of the prototypes in the lumped diplexer are:

$$L'_1 = \frac{\sqrt{(L_1^2 + 2)\omega_o^2 - 1}}{\omega_o} \qquad (4.1.1)$$

$$C'_2 = C_2 + \frac{(\omega_o^4 - 1)(L_1^2 - L_1 L'_1 + 1)}{\omega_o^2 L'_1 (\omega_o^2 + L_1^2)} \qquad (4.1.2)$$

(N.b. the quantities in these equations are found for a 3 dB frequency at $\omega = 1$).

Since only the first series and first shunt elements are modified, the two filters of the diplexer are asymmetrical. The physical dimensions of each filter in the distributed 8 GHz diplexer are designed using exactly the methods of the last two chapters and are calculated in the next section. The above equations mean that the modified elements become comparable to the middle elements, thereby easing the physical realisation of the diplexer.

4.2. Design of Physical Dimensions of 8 GHz Diplexer

The two filters designed in the last two chapters are integrated onto the same substrate and

suspended inside a box of ground plane spacing 0.07", as shown in photograph no. 3. Notice the inner box wall which separates the two channels. This wall prevents coupling between the channels and since it preserves the same cavity dimensions for each channel as those in the isolated filters, it should prevent any suprious modes from propagating from d.c. - 12 GHz. As discussed in the last section, the first series and first shunt elements of these filters must be modified for correct diplexing operation. Fig. 4.2.1 shows the diplexing junction and the dimensions to be calculated; all other dimensions have already been found in previous chapters. It should be noted that the following dimensions are calculated for walls between the highpass resonators. However, these are later removed without any significant change in electrical performance apart from box modes entering at 15.94 GHz and 17.95 GHz.

The design begins by using (4.1.1) and (4.1.2) to calculate the first two elements of the complementary prototypes of the lumped diplexer. The following elements are for a 3 dB frequency at $\omega = \omega_3$ (i.e. the 3 dB frequency of the original lowpass prototype) not $\omega = 1$:

$$L_1' = 1.20099 \quad H \qquad (4.2.1)$$

$$C_2' = 0.912758 \quad F \qquad (4.2.2)$$

The complementary prototypes are then scaled by Richards transformation with the appropriate values a_L, α_L and

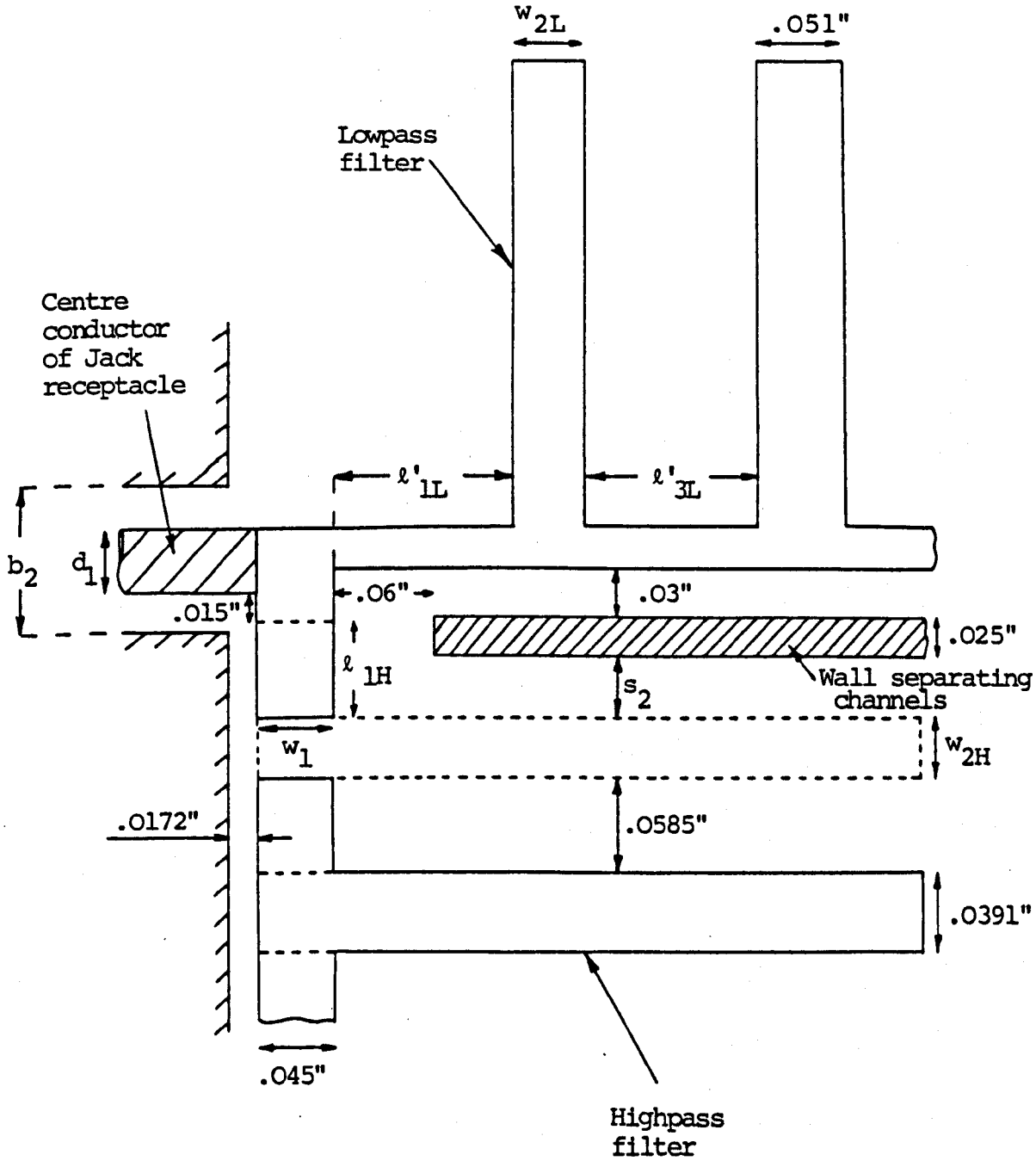

Fig. 4.2.1 Diplexing junction and dimensions to be calculated

(see also photograph no. 3)

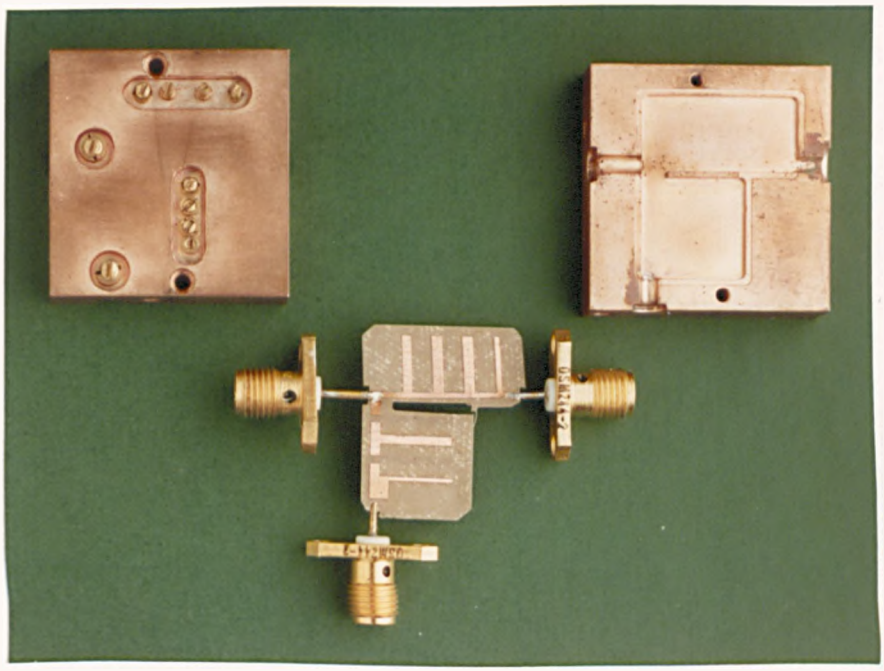

Photograph No. 3 Suspended substrate stripline 8 GHz diplexer

a_H, α_H for each prototype. This produces a distributed contiguous diplexer with a crossover at 8 GHz. The lowpass filter in this diplexer can then be physically realised using the methods of chapter 2. Thus the required length of its first u.e. is, using (2.4.17) with $L_1 = L'_1$,

$$\ell_{1L} = 0.1279" \qquad (4.2.3)$$

$$= \lambda_{12L}/7.69 \qquad (4.2.4)$$

where λ_{12L} is the wavelength in air at 12 GHz. Also, the width of the first lowpass resonator of the diplexer assuming far field fringing components is, using (2.4.7) with $Y_2 = C'_2\omega_o/2 = 0.563879$,

$$w_{2L} = 0.0433" \qquad (4.2.5)$$

Clearly $w_{2L} > 0.35(b-t)$ so the fringing fields of this resonator will not interact.

The reference plane locations assumed in this design are shown in Fig. (4.2.2). Recall that no known information exists, for frequencies from d.c. - 18 GHz, on the discontinuities of T junctions treated in terms of reference plane locations for the three arms and a shunt impedance in cascade with a transformer. Furthermore, the discontinuities at the diplexing junction are uncertain. However, in the next section possibly more accurate reference plane locations for the T junctions, given in Ref. [2.4], are considered. Using Fig. (4.2.2),

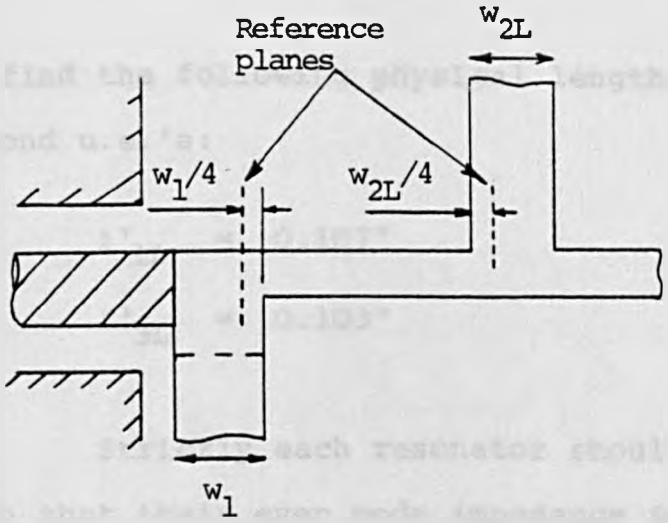

Fig. 4.2.2 Reference plane locations assumed for first unit element of 8 GHz diplexer

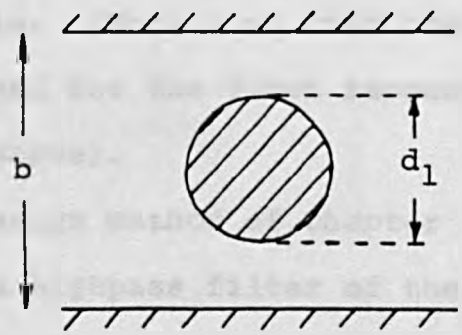

Fig. 4.2.3 Cross section of transmission line inside filter box formed by centre conductor of input Jack receptacle

we find the following physical lengths of the first and second u.e.'s:

$$\ell'_{1L} = 0.107" \qquad (4.2.6)$$

$$\ell'_{3L} = 0.103" \qquad (4.2.7)$$

Strictly each resonator should be designed such that their even mode impedance is equal to the impedance of the corresponding resonator in the distributed prototype diplexer. However, for the physical separations of the lowpass resonators designed here, referring to Getzinger's graphs [2.2] shows that the even mode fringing capacitances are equal to the far field component. Hence the assumption used above that the lowpass resonators can be considered in isolation was justifiable. (Note also that the left hand wall can be neglected for the first resonator, which was also assumed above).

The design method of chapter 3 is now applied exactly to the highpass filter of the distributed prototype diplexer. Firstly, the first series lumped capacitance required to produce a good match around the bandedge frequency of the highpass in the 8 GHz diplexer is, using (3.3.2) with $L_1 = L'_1$,

$$C_{1H} = 16.38 \text{ pF} \quad \text{(for 1 } \Omega \text{ terminations)} \qquad (4.2.8)$$

Following the design in chapter 3, the width of the first inhomogeneous section in the high channel of the

diplexer is,

$$w_1 = 0.045" \qquad (4.2.9)$$

Then using (3.3.8) with $L_1 = L'_1$, the length of this inhomogeneous section is,

$$\ell_{1H} = 0.0577" \qquad (4.2.10)$$

Using this length, the distance of the first highpass resonator from the wall separating the two channels of the diplexer is,

$$s_2 = 0.0314" \qquad (4.2.11)$$

Getzinger's graphs can now be used to find the distributed static fringing capacitance per unit length between the first highpass resonator and the wall separating the two channels. We find

$$C'_{fo}/\varepsilon_o = 0.50 \qquad (4.2.12)$$

Equation (3.3.26) is then solved to find the width of the first highpass resonator. In this equation we substitute $Y_2 = (C'_2\omega_o)/2 = 0.563879$ and use C'_{fo}/ε_o instead of C'_f/ε_o:

$$w_{2H} = 0.0361" \qquad (4.2.13)$$

The physical lengths of the first resonators of each channel are made:

$$\ell'_{2L} = 0.278" \qquad (4.2.14)$$

$$\ell'_{2H} = 0.292" \qquad (4.2.15)$$

These lengths are consistent with the other resonator lengths in the diplexer.

Finally, consideration must be given to the input feed to the diplexer. (The output feeds are as in the isolated filters). As shown in Fig. 4.2.1 a standard Jack receptacle is used with its centre conductor soldered directly onto the p.c.b. at the diplexing junction. The cross-section of the transmission line formed by this centre conductor inside the box is shown in Fig. 4.2.3 . The characteristic impedance of this line is [2.3]

$$Z = \frac{138}{\sqrt{\varepsilon_r}} \log_{10} \frac{4b}{\pi d_1} \qquad (4.2.16)$$

where ε_r = the dielectric constant of the medium containing the line = 1, in this case.

We require this line to be 50 Ω, so with b = 0.07",

$$d_1 = 0.0387" \qquad (4.2.17)$$

(2.4.21) is then solved for the side hole diameter to ensure that the coaxial transmission line formed by the centre conductor of the Jack receptacle in this hole is 50 Ω . We find,

$$b_2 = 0.0891" \qquad (4.2.18)$$

It should be noted that the distance from this centre conductor to the bottom strip of the first inhomogeneous section is chosen to be 0.015", thereby preventing unwanted coupling between these conductors.

4.3. Practical Results and Modifications to P.c.b. of 8 GHz Diplexer

Recall that the highpass filter had a low 3 dB frequency of 7.55 GHz and so it was necessary to scale this frequency to around 8 GHz by shortening the resonators. Following this modification a good diplexing performance was achieved by fine tuning of the resonators. This tuning process was relatively simple and took no longer than a few minutes. Furthermore, the crossover frequency could easily be shifted by about 200 MHz so that a crossover exactly at 8 GHz was readily achieved. For a plated device, the insertion loss at crossover was about 4.8 dB with a corresponding common port return loss of at least 15 dB. The stopband levels of each channel were certainly much better than in the individual filters, in particular the insertion loss of the low channel was at least 40 dB up to 12.93 GHz instead of 11.63 GHz. Also, the channel selectivities were improved by diplexing with the low channel's improved to 5.25%.

The input port return loss was at least 10 dB from d.c. - 12 GHz and the passband insertion loss in each channel was less than 1 dB. It should be noted, however, that this level of input port return loss could only be achieved over the highpass passband by use of the nonresonator screws. Furthermore, these screws tended to deteriorate the input port return loss at lower frequencies, producing a 'see-saw' effect.

Now the input port return loss around 6.5 GHz was only 12½ dB without nonresonator tuning and must be improved to prevent a bad mismatch in the 4 - 8 GHz channel of the triplexer, when this diplexer is cascaded with the 4 GHz highpass filter.

The comparatively low input port return loss around 6.5 GHz was due to incorrect reference plane locations used for the unit elements of the lowpass, especially for the first u.e. By performing several experiments on the widths of these u.e.'s, a much improved performance was finally achieved. Infact, the widths of the u.e.'s had to be increased, meaning that reference plane locations too far away from the centre of each lowpass T junction had been originally assumed for the u.e.'s. Due to the change in the input impedance of the lowpass, the width of the first inhomogeneous section in the highpass had to be very slightly reduced before a good input port return loss was achieved through crossover and over the passband of the highpass. Indeed, experiments have shown that the input port return loss is quite sensitive to a few percent change in the first series elements of each channel. These elements must be realised to within 1% for a good input port return loss. The modified dimensions of the diplexer are shown in Fig. 4.3.1.

A complete set of results on the modified diplexer are shown in Figs. (4.3.2) and (4.3.3). These results satisfy the requirements for the 8 GHz diplexer in the triplexer and note especially the improvement

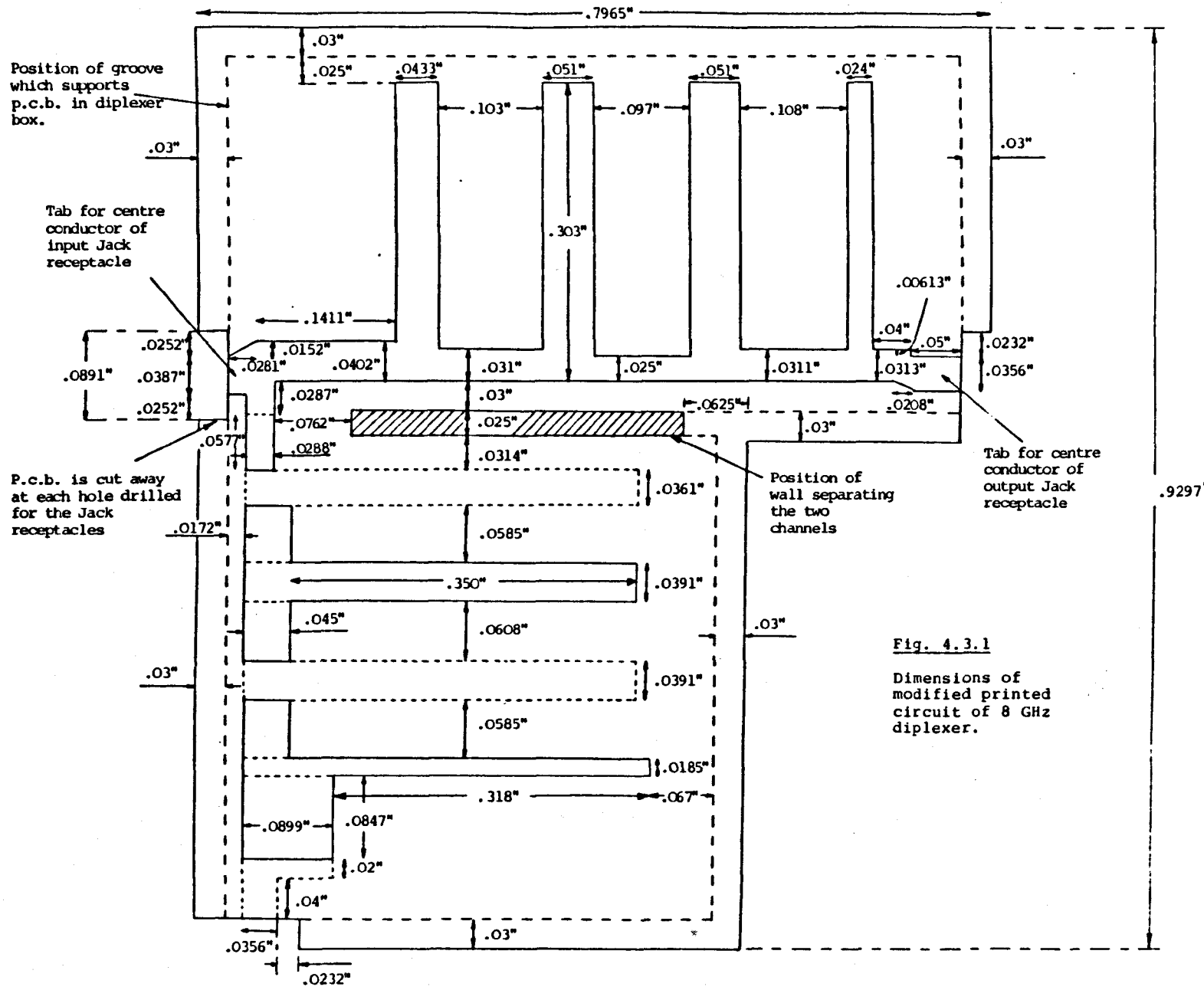

Fig. 4.3.1

Dimensions of modified printed circuit of 8 GHz diplexer.

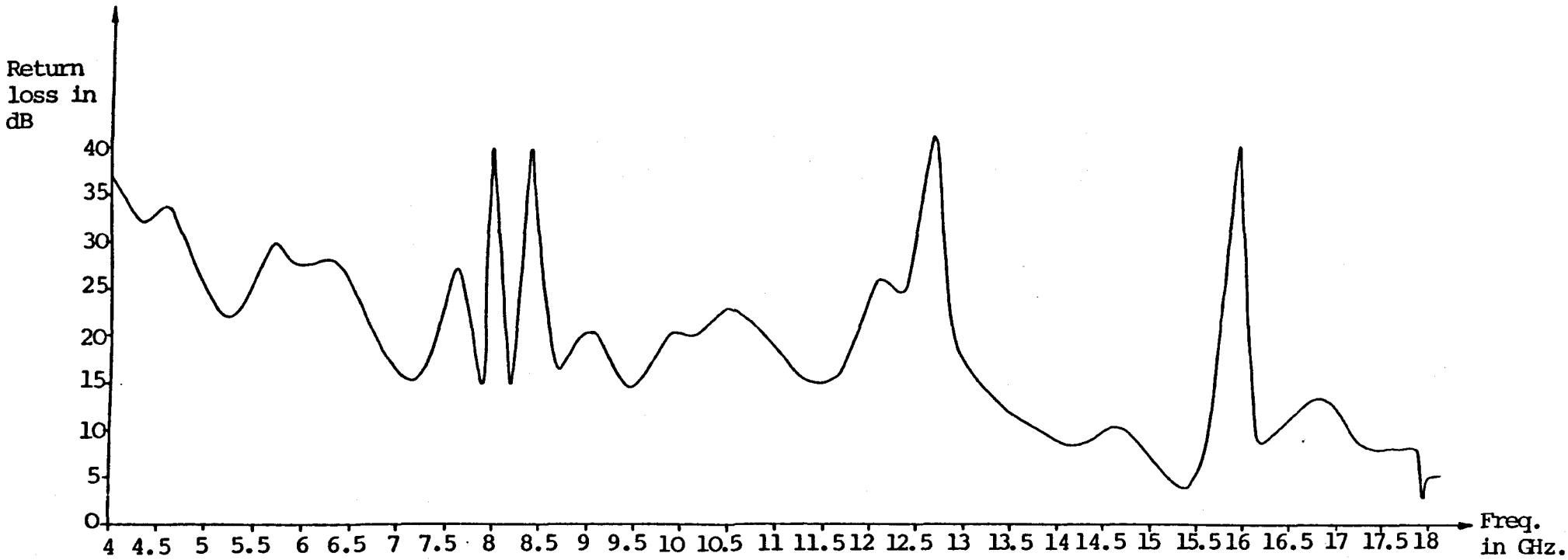

Fig. 4.3.2 Measured input port return loss of tuned 8 GHz. diplexer

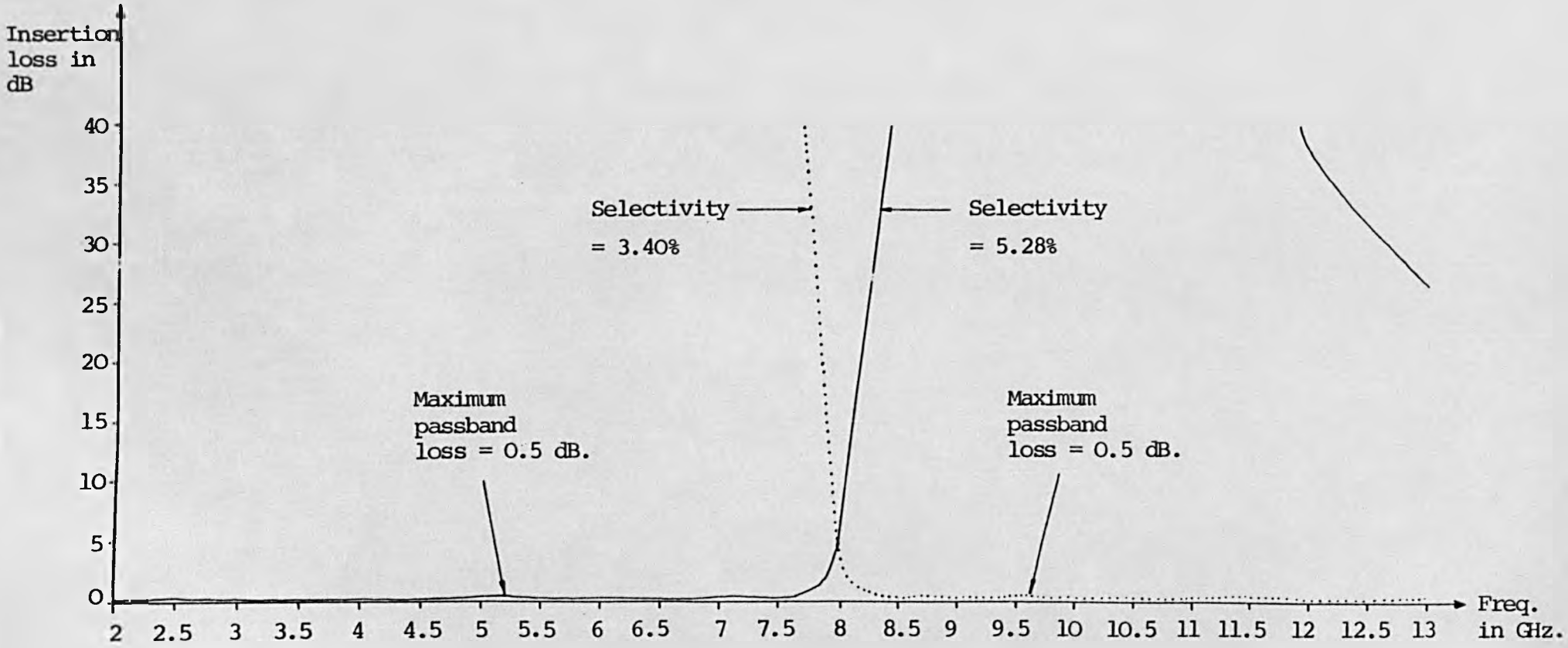

Fig. 4.3.3 Measured insertion loss of the two channels of tuned (plated) 8 GHz diplexer

in return loss around 6.5 GHz. Besides resonator tuning, the only other tuning was done using the non-resonator screw at the output of the high channel. The other nonresonator screw deteriorated the high channel response because the first inhomogeneous section is now almost correct - a fact which is confirmed by computer analysis in the next chapter. Also the input port return loss over the highpass passband has been improved from 10 to 15 dB mainly because of the modification to the first inhomogeneous section. Some other points to note about the tuned results are firstly that the 1 dB frequencies of the low and high channels are within 3.68% and 3.93% of crossover, respectively, thereby easily meeting the 5% requirement of the triplexer; note also the low passband insertion losses of each channel. Finally, the stopband insertion loss of each channel over d.c. - 11.92 GHz is greater than 40 dB apart from within about 5% of the crossover frequency.

It should be noted that due to the modifications to the u.e.'s, the frequency where the low channel insertion loss falls below 40 dB has been reduced from 12.93 GHz to 11.92 GHz. However, this new 40 dB frequency agrees better with the computer analysis given in chapter 5. This analysis shows that the stopband insertion loss of the isolated 8 GHz lowpass, having the same u.e. widths as in the lowpass of the modified diplexer, falls to 25 dB at 12.08 GHz. Since this loss

will be increased to about 40 dB when the lowpass is diplexed with the highpass, the theory and practical results are in good agreement. The analysis also shows that the stopband insertion loss of the lowpass increases slightly as the impedance of the u.e.'s decreases. Hence the modified diplexer could be re-designed with narrower u.e.'s, and correct reference plane locations for the T junctions, to increase the lowpass loss around 12 GHz.

To conclude this section, we consider in more detail the reference plane locations for the u.e.'s at the T-junctions. Reference [2.4] gives graphs for these reference planes based on experiments on various T-junctions. Using these graphs, the reference plane locations for each T junction in the lowpass of the modified diplexer are as shown in Fig. 4.3.4. Note that although the T-junctions in the modified lowpass are slightly asymmetrical, it is assumed that the required reference planes are those obtained for the mean of the left arm and right arm impedances of each T. Using these reference planes, we can calculate the actual lengths of the u.e.'s (except the first) in the modified diplexer and then compare them with the required designed values calculated using (2.4.17) and the impedances of the u.e.'s in the modified diplexer. We find that the errors in the actual lengths of the u.e.'s for the second to fifth u.e.'s are respectively, +0.3%, +4.8%, -2.2% and -0.8%. Now if the above

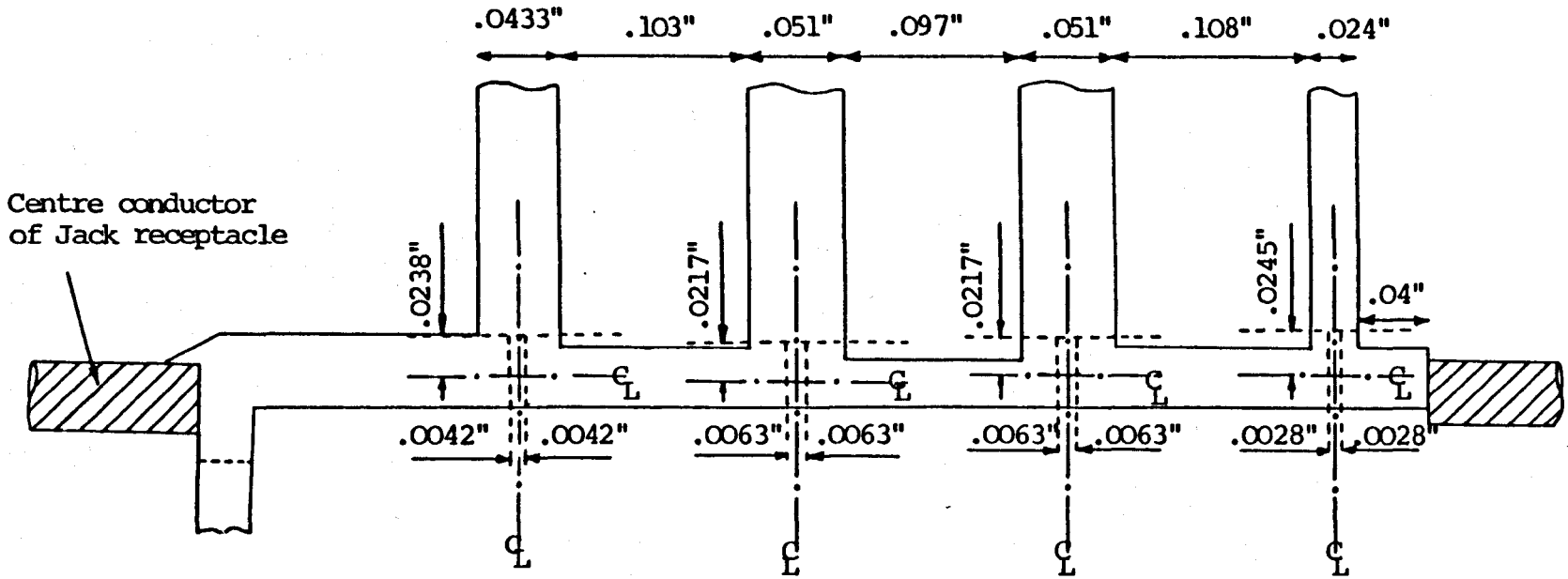

Key:

———·———·——— Centre line of resonator or right hand arm of each T

---------- Reference plane locations for resonators or unit elements.

N.B. The reference planes for the resonators do not take account of the fringing capacitances at the ends of the resonators

Fig. 4.3.4 Reference plane locations for the T junction discontinuities of the low channel of the modified 8 GHz diplexer using the graphs in Ref. [2.4]

process is repeated for the unmodified diplexer, then the errors become +9.7%, +4.8%, +7.4% and 8.3% (N.b. For these latter errors, the designed lengths are the ones calculated in chapter 2). Note also that the first u.e. of the unmodified diplexer will be in significant error - this point will be discussed in the next paragraph. It appears therefore that the reference plane locations given in Ref. [2.4] are more accurate than the ones used in previous designs. However, it must be emphasised that the graphs given in Ref. [2.4] are only based on experimental data and take no account of frequency or coupling between the resonators.

Finally, an estimation of the reference plane location for the first u.e. at the diplexing junction of the modified diplexer can be made. This is based on the assumption that the length of this u.e. is correct. However, this is justified since the input port return loss over the low channel is close to the theoretically predicted value. The required (correct) length of the first u.e. in the modified diplexer is found using (2.4.17) with $L_1 = L'_1 = 1.20099$ and with Z_L equal to the impedance of the modified first u.e. By accounting for the reference plane at the first T junction, using Ref. [2.4], the reference plane location for the first u.e. at the diplexing junction is as shown in Fig. 4.3.5. Clearly, the original reference plane assumed at the diplexing junction (see

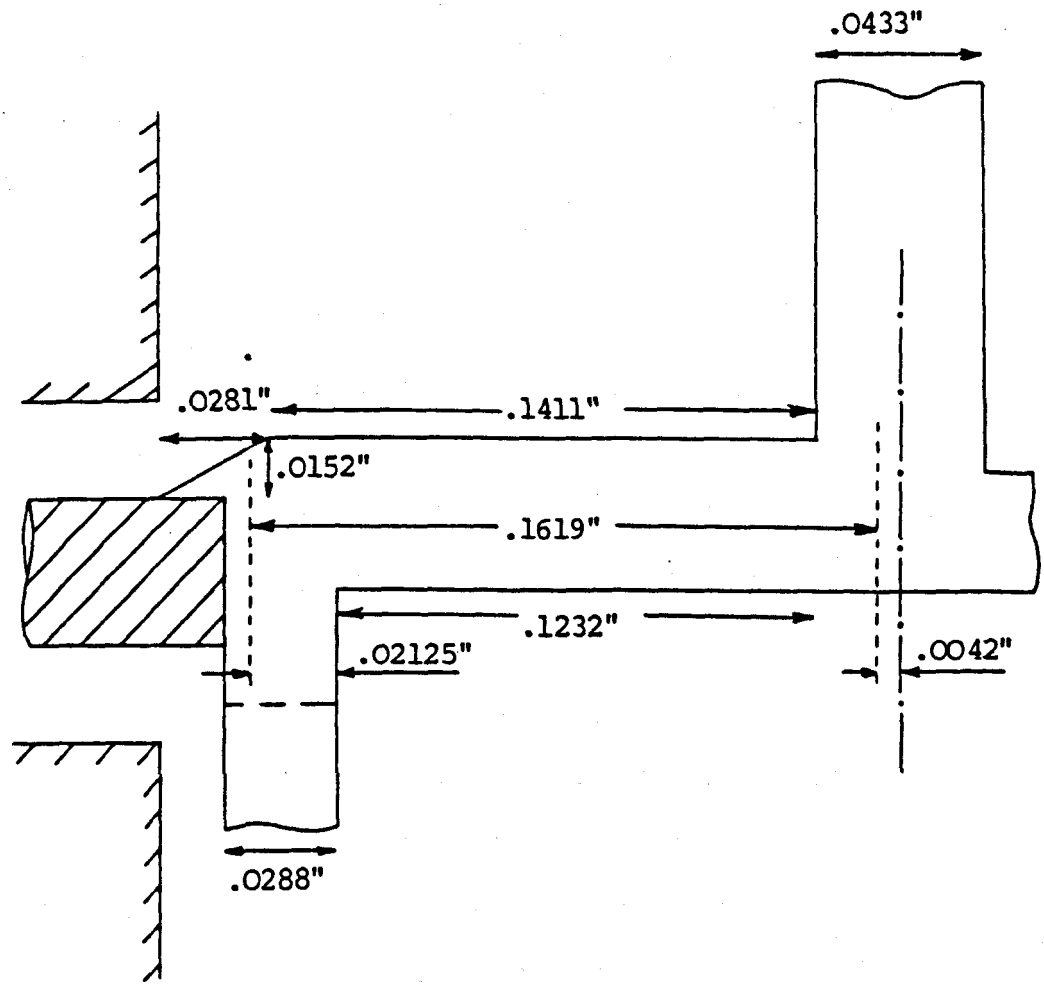

Key:

--------- Reference plane locations for first u.e.

N.B. The required length of the first u.e. = .1619"

Fig. 4.3.5 Probable reference plane locations for the first u.e. in the modified 8 GHz diplexer

Fig. 4.2.2) was incorrect and effectively led to an error of 20% in the characteristic impedance of the first u.e.

4.4. Design and Practical Results of 12 GHz Diplexer

This diplexer was designed by scaling the length of every element of the first working 8 GHz diplexer, that is, the diplexer before the modifications to its unit elements. Note that for the inhomogeneous sections, only their overlapping lengths were scaled and for the resonators, only their physical lengths from the T-junctions were scaled. Also, reference plane locations similar to those in the 8 GHz lowpass design were assumed for the u.e.'s. Each shunt resonator was designed assuming far field components, however this was justified since the widths of all resonators are only increased by a few percent when even mode fringing fields are considered instead. Practical results showed an input port return loss of only 2.6 dB around 13 GHz and a minimum level of 10 dB over the low channel, occurring around 8 GHz.

Several experiments were performed to improve these results and these led to the circuit shown in Fig. 4.4.1, with its results in Figs. 4.4.2 and 4.4.3. The modifications were firstly an increase in the widths of the first to fifth unit elements from 0.025" throughout to 0.0528", .0414", .0389", .0399" and .0406"

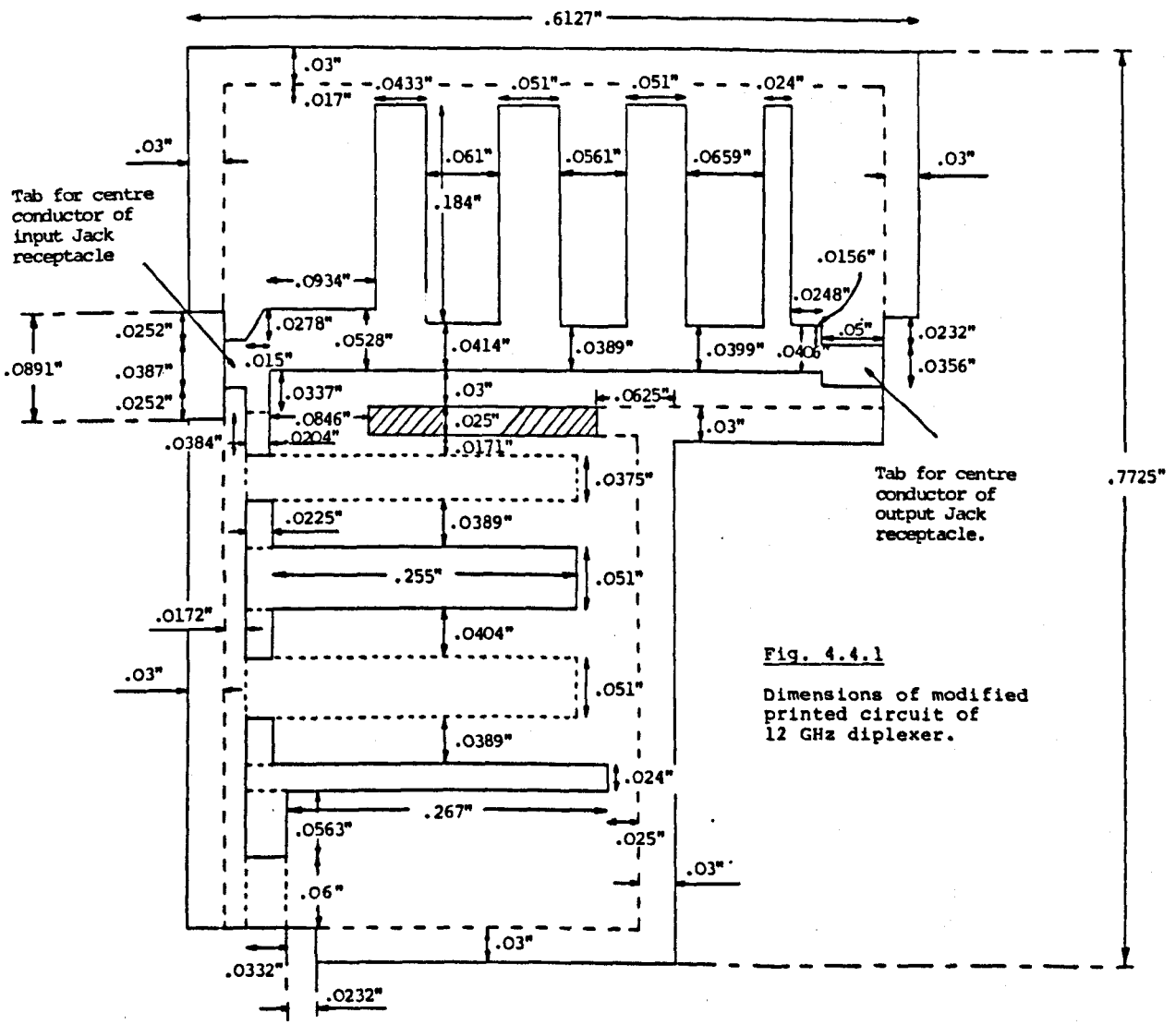

Fig. 4.4.1

Dimensions of modified printed circuit of 12 GHz diplexer.

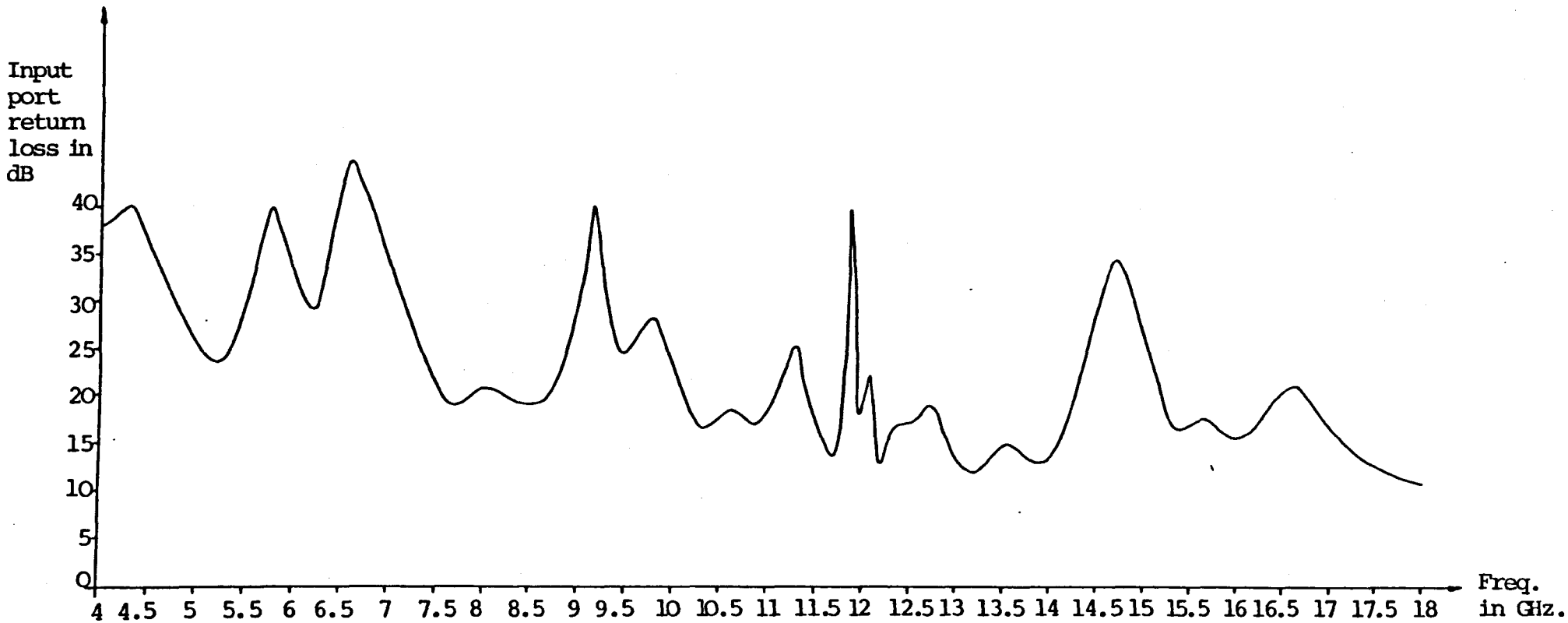

Fig. 4.4.2 Measured input port return loss of tuned 12 GHz. diplexer

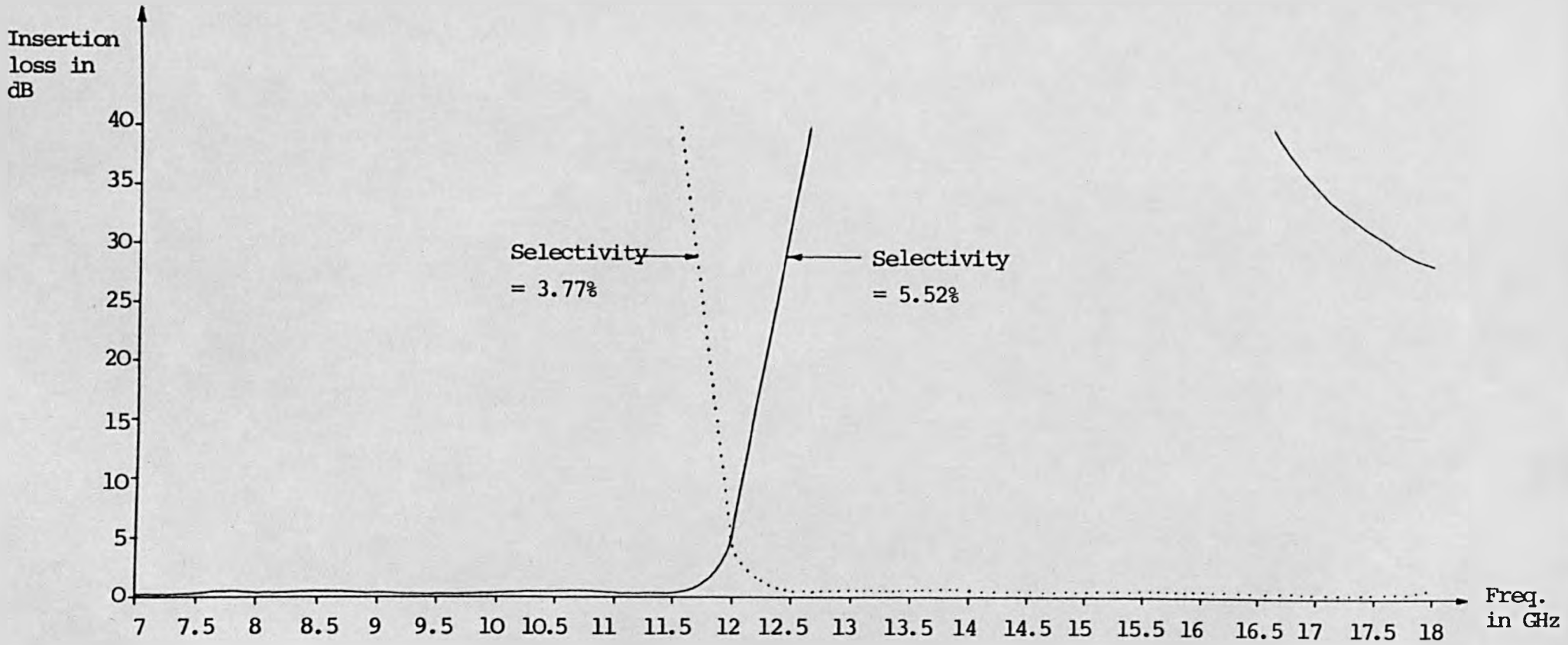

Fig. 4.4.3 Measured insertion loss of the two channels of (unplated) tuned 12 GHz. diplexer

respectively. Secondly, the lengths of the lowpass resonators were increased from .209" to .224" (these lengths include the widths of the u.e.'s). Finally, the widths of the first to fifth inhomogeneous sections were reduced from 0.045" (first four) and 0.0899" (last section) to 0.0198", .0225", .0225", .0225" and 0.0332" respectively. Clearly, the percentage errors in the original dimensions were significant for this relatively small diplexer, but the new highpass dimensions agree better with theory (see next chapter). The practical results show a considerably improved input port return loss especially around 8 GHz, through crossover and over the high channel. The falling stopband insertion loss of the low channel between 17 and 18 GHz agrees with theory (see next chapter) and this causes the insertion loss of the 8 - 12 GHz channel of the triplexer to fall to 32 dB in this frequency region.

4.5. Design and Practical Results of Single Substrate Triplexer

The modified 12 GHz and 8 GHz diplexers and 4 GHz highpass filter were cascaded together to form a triplexer and results were very encouraging with an input port return loss of at least 10.7 dB from 4.05 - 18 GHz. Following this, a single suspended substrate triplexer was designed and constructed, a breakdown of which is shown in photograph no. 4. The modified units are integrated directly onto the same substrate and

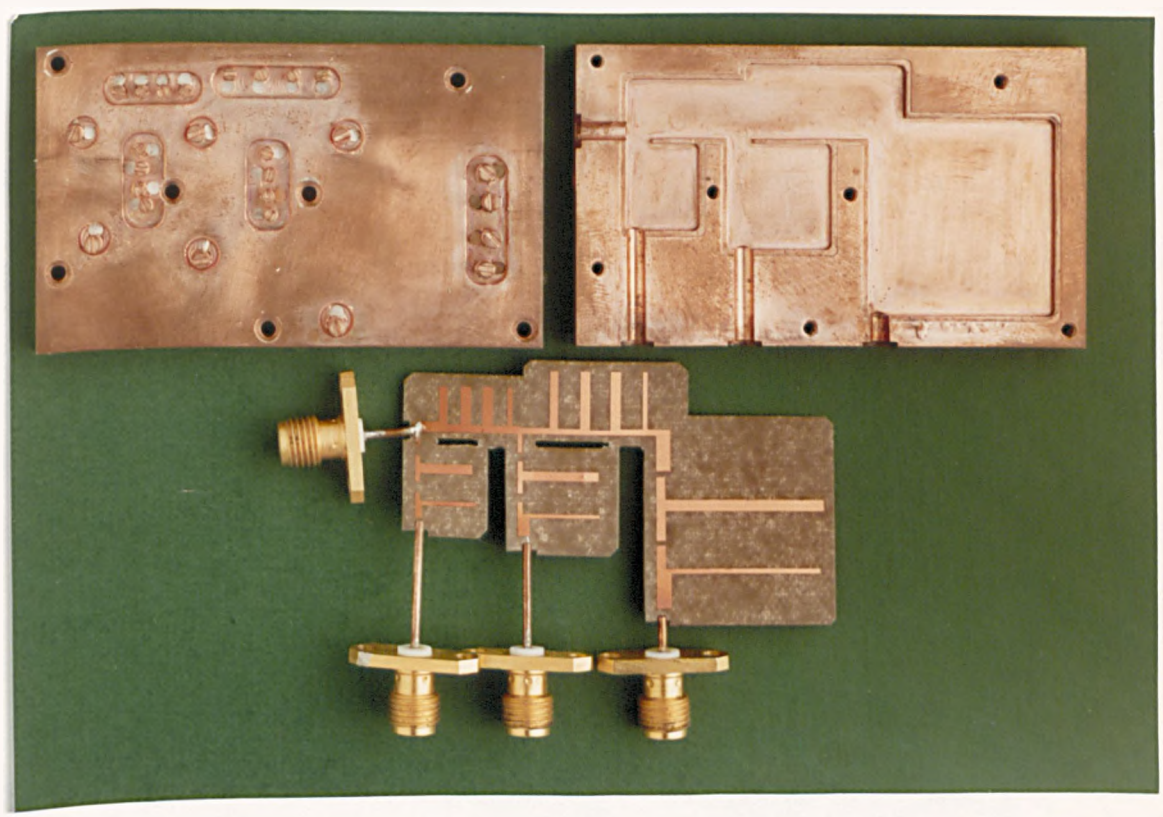

Photograph No. 4 Triplexer covering the bands 4 → 8, 8 → 12 and 12 → 18 GHz, printed on a single suspended substrate

the only new problems concern the junctions of the 12 GHz and 8 GHz diplexers and the 8 GHz diplexer and the 4 GHz highpass. A practical point to note is that nylon plugs are used with the tuning screws instead of locking nuts. A shallow hole is drilled besides each tuning screw hole and a small nylon plug (about 0.05" high) is inserted in it. This plug overlaps the tuning screw by the thickness of its thread thereby gripping the screw. This tightens the screw as it is turned allowing very fine tuning. Moreover, the screw remains in its tuned position and can easily be glued in position using the small recess around the tuning screws (see photograph no. 4).

To produce good transitions between the units of the triplexer, the units were connected directly together on the substrate without any 50 Ω connecting lines etc., to form the junctions shown in Fig. (4.5.1). It is assumed that the uncertain effects of the transitions to the 50 Ω coaxial lines in the individual units and the transition to the complex right angle bend on the triplexer substrate at the input of the 4 GHz highpass, can be neglected. All other dimensions for the triplexer are found from those of the individual 12 GHz and 8 GHz diplexers and the individual 4 GHz highpass.

The following points should be carefully noted. The first design of this single substrate triplexer used 50 Ω striplines at the outputs of the 12 - 18 and 8 - 12 GHz channels, instead of 50 Ω coaxial lines. These striplines were printed onto the substrate and

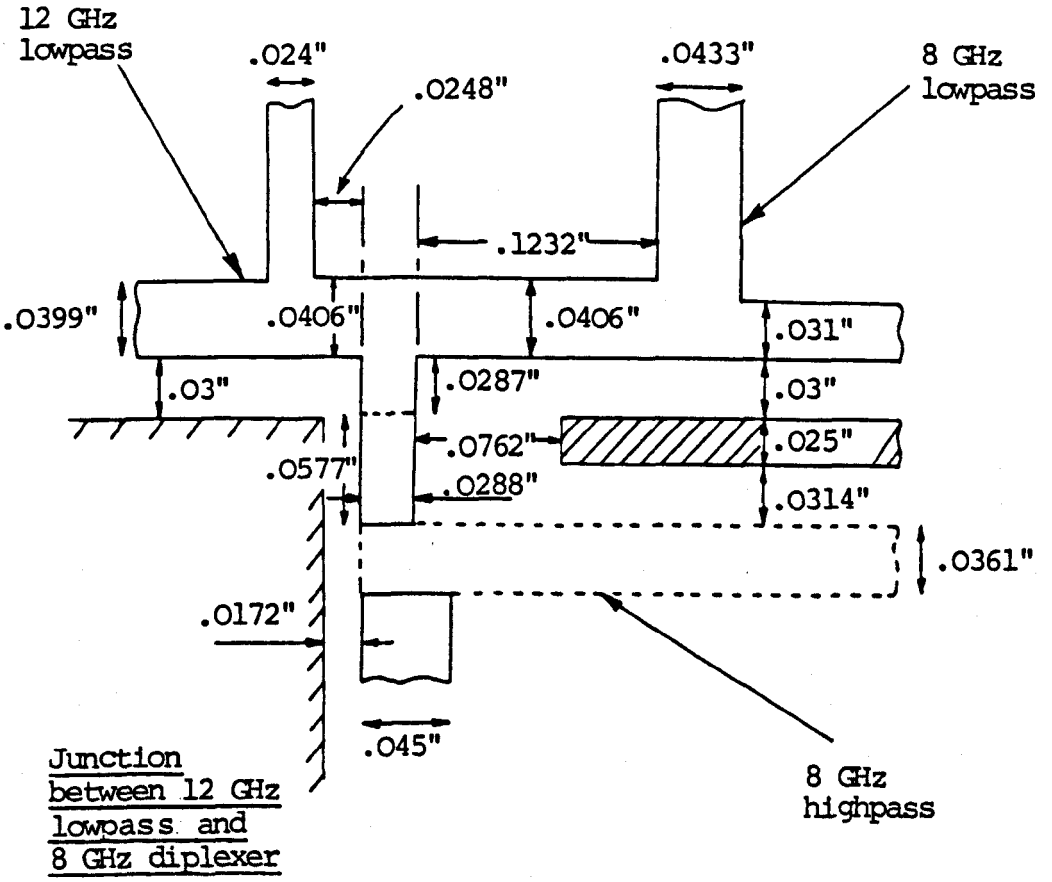

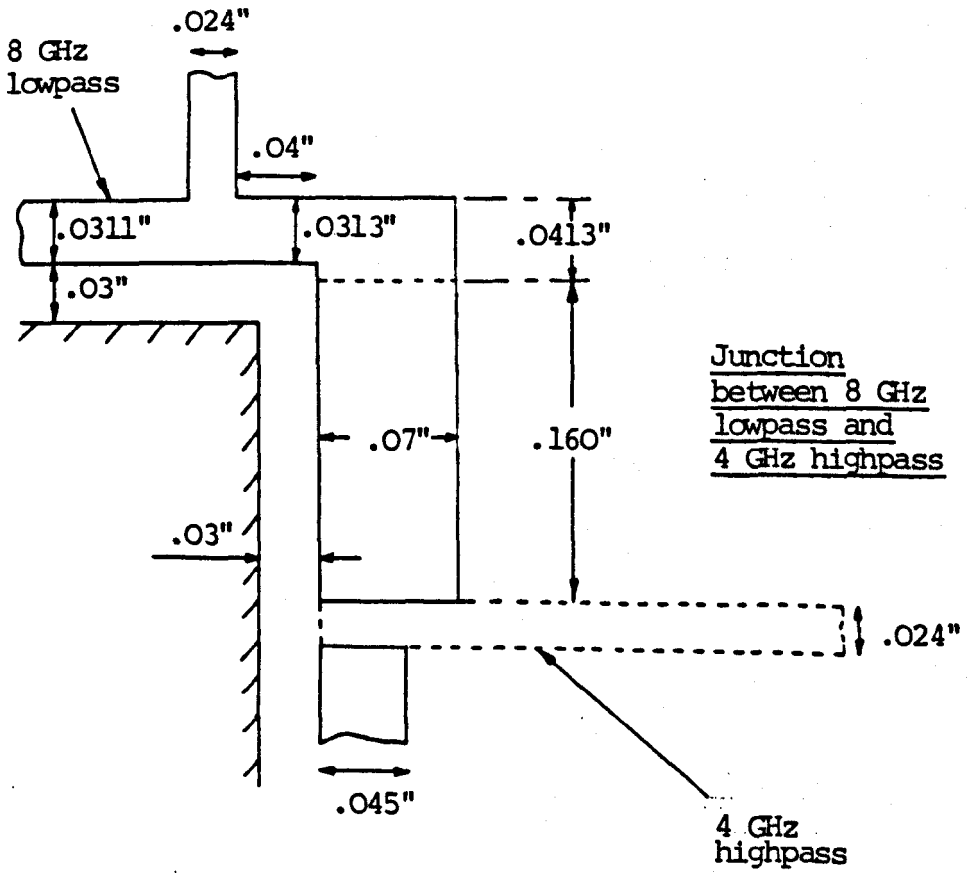

Fig. 4.5.1 Details of triplexer junctions

the idea was to avoid the use of long coaxial lines. It was first thought that these latter lines had to be turned from brass rods - a process which is impossible for the lengths and diameters involved. However, it was later realised that copper wire, 0.035" in diameter, would easily suffice. Now due to the extra mismatches introduced by these striplines, together with the particular lengths of the striplines, there was much difficulty in producing good 12 - 18 and 8 - 12 GHz channels, especially the latter. Only through the following modifications was a satisfactory operation achieved for the 8 - 12 GHz channel. Firstly, the width of the first u.e. in the 8 GHz lowpass was reduced from .0406" to .0335". Finally, the widths of the first to last inhomogeneous sections in the 8 - 12 GHz channel were reduced from 0.0295", .045" (second to fourth) and .0899" to 0.0258", .029" (second to fourth) and .0612" respectively. The 50 Ω striplines also meant that the width of the cavity inside the triplexer was greater than that in either the individual 12 GHz or 8 GHz diplexers; note also in this first design, the cavity size of the 4 - 8 GHz channel was larger than in the individual 4 GHz highpass. These larger cavities allowed a serious box mode to appear at the 8 - 12 GHz output at about 17.5 GHz and allowed another mode to interfere with the 8 GHz crossover, either appearing at the 4 - 8 GHz or 8 - 12 GHz outputs depending on the exact crossover frequency. Therefore it was necessary

to return to the cavity sizes of the individual units, yielding the triplexer structure shown in photograph no. 4 with the modifications shown in Fig. 4.5.2. Overall dimensions of the substrate are only 2.085" x 1.263", so the box size is only about 2.4" long x 1.45" wide x .38" deep. The 50 Ω striplines are replaced by 50 Ω coaxial lines thereby preserving the same output junctions as in the individual units. Note that the above modifications to the printed circuit are still used, although even without them it is likely the triplexer would work satisfactorily since we are now using coax outputs. The modified dimensions are, however, close to the theoretical values. (see next chapter).

Initial sealing problems were eliminated by slightly increasing the box thickness to 0.5" and, moreover, by milling a groove 0.007" deep in only one half of the box to support the substrate. The original 0.005" groove when plated tended to prevent a good seal. These problems were not accounted in the previous, physically smaller, devices designed in this work. The increased box thickness also allows the use of the more robust square flanged receptacles.

Tuned results are shown in Figs. 4.5.3 and 4.5.4. Very little tuning is done using the non-resonator screws because the end sections of the high-pass filters in the triplexer are now almost correct. By tuning the resonators, crossover frequencies exactly at 8 GHz and 12 GHz can be readily achieved and one diplexer can be aligned without affecting the other.

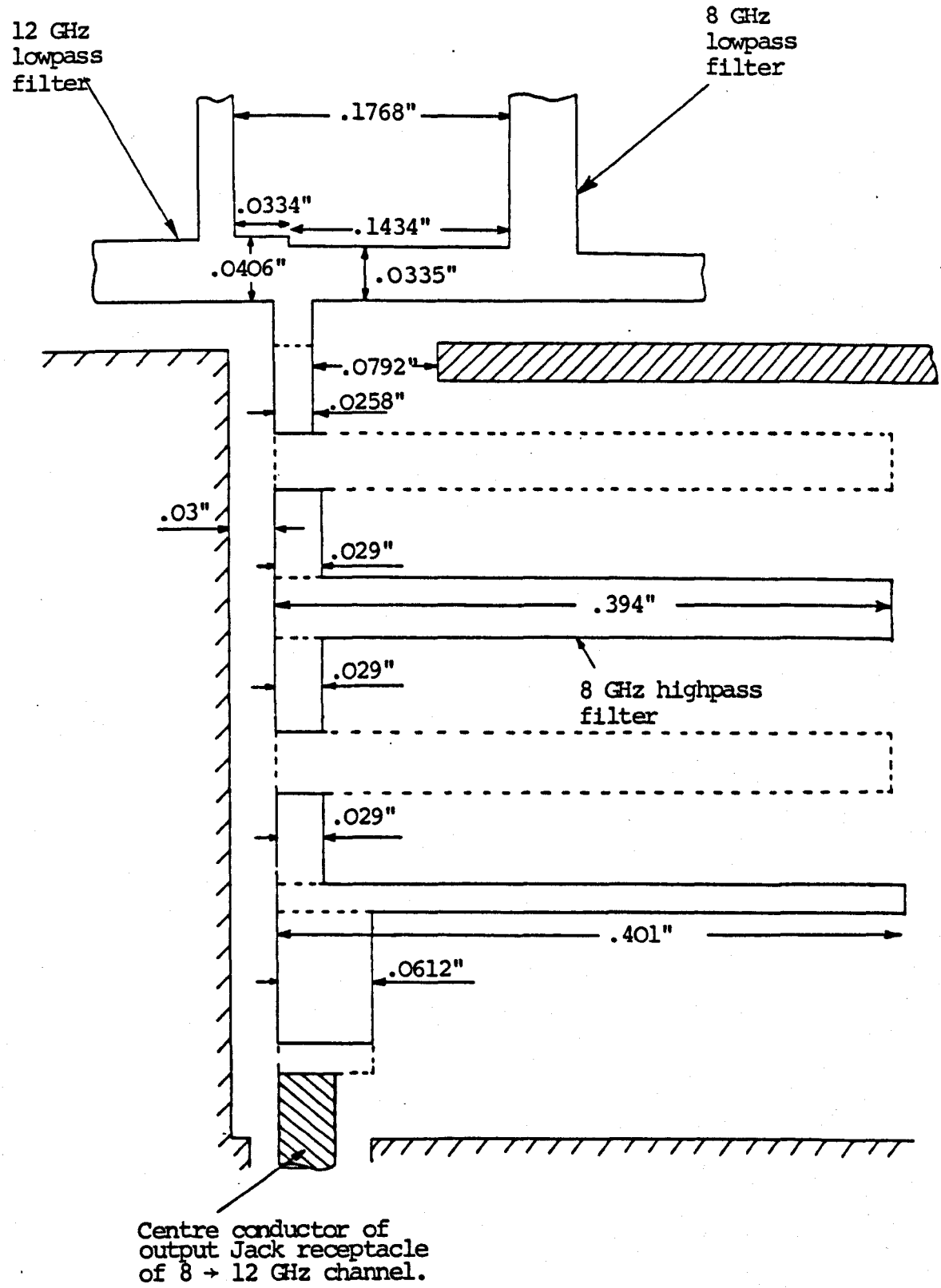

Fig. 4.5.2 Modifications to single substrate triplexer

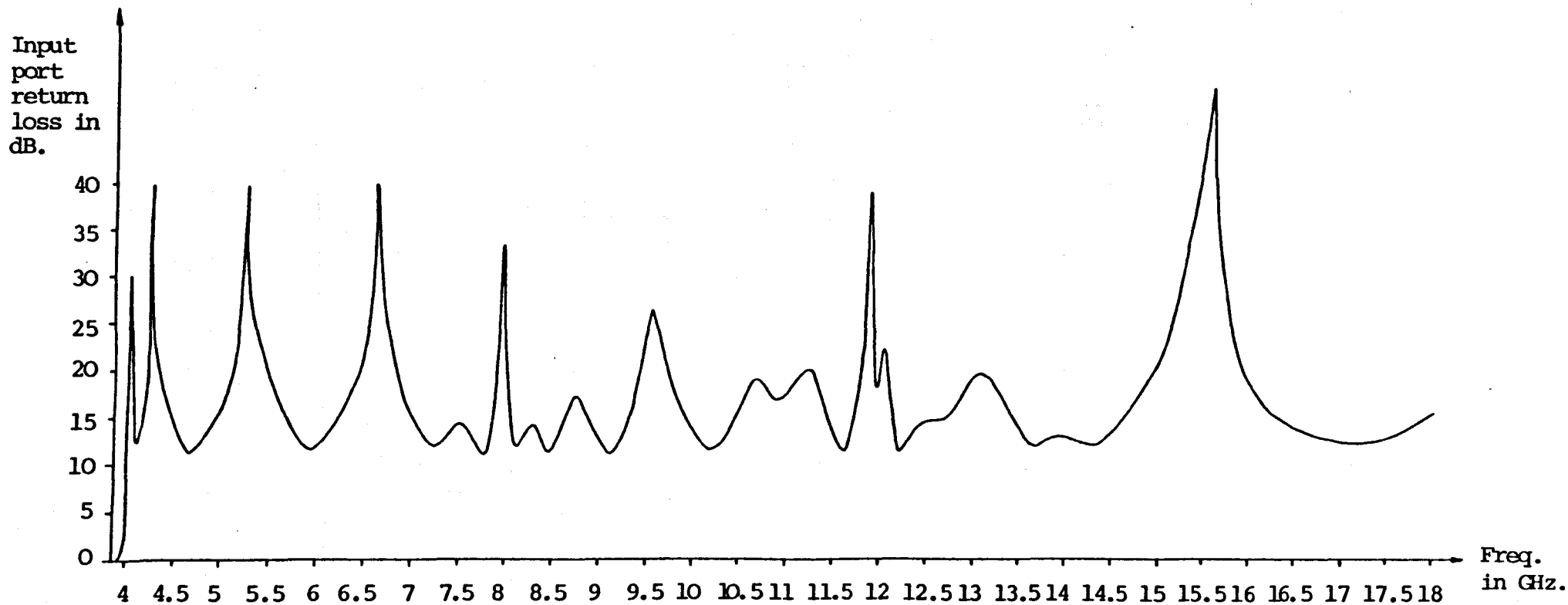

Fig. 4.5.3 Measured input port return loss of tuned triplexer covering the bands 4 → 8, 8 → 12 and 12 → 18 GHz.

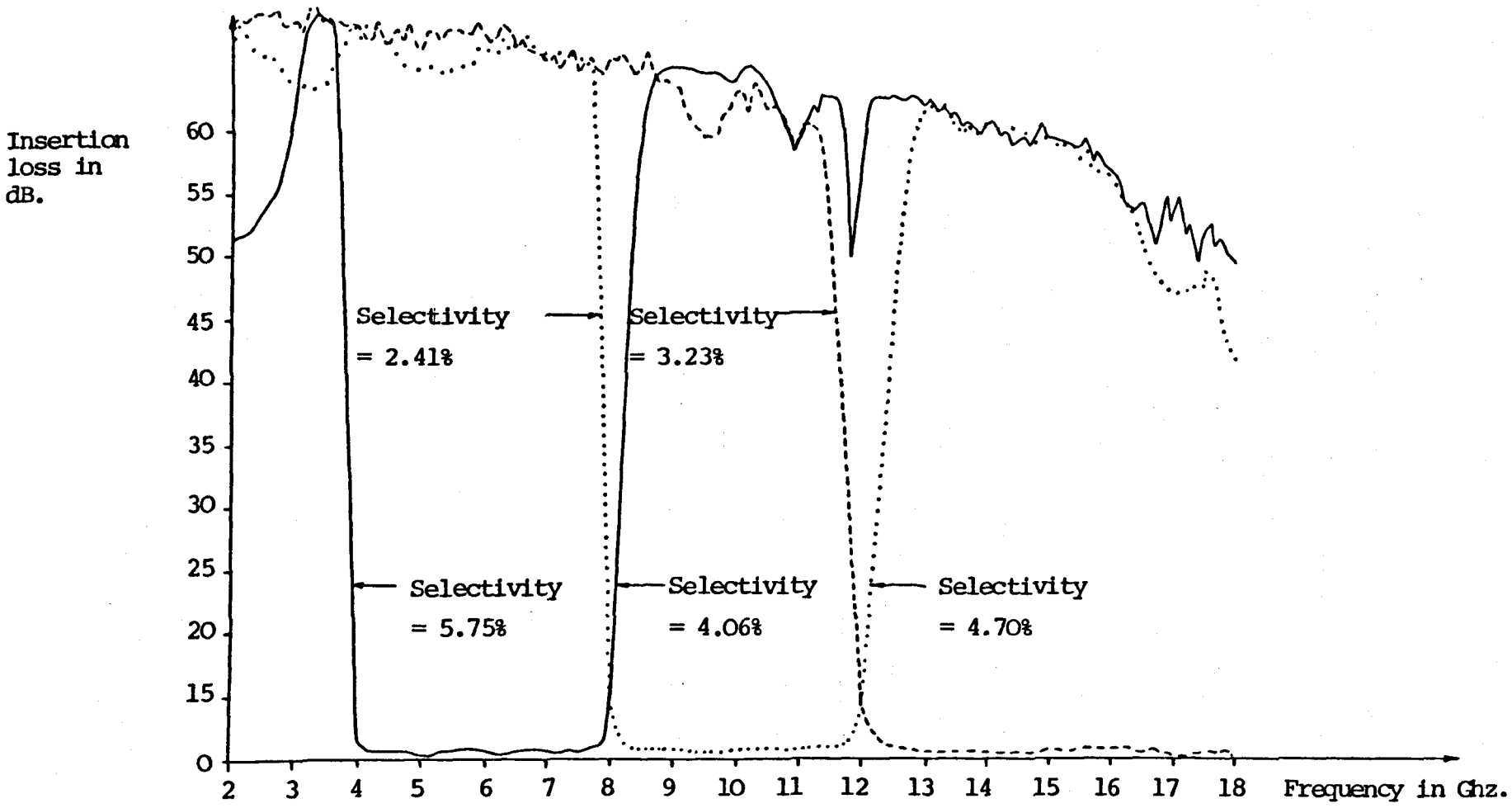

Fig. 4.5.4 Measured insertion loss of the three channels of (plated) tuned 4 → 18 GHz triplexer.

The maximum passband loss in each channel, for a plated device, is about 0.9 dB and the crossover levels are about 5 dB. Also the bandedge frequencies (i.e. the 1 dB points) of any channel are within 5 % of crossover. The minimum stopband loss in the 4 - 8 GHz channel, i.e. 40 dB near the 12 GHz crossover, is due to the insertion loss of the 8 GHz lowpass falling to around 40 dB in this region. This could be improved by slightly increasing the crossover frequency of the 8 GHz diplexer.

The experimental results show that the triplexer essentially meets the required specification given in Fig.1.3.3, chapter 1. The results are in close agreement with the computer analysis presented in the next chapter. Several triplexers have been to the same specification and first results suggest that a very high degree of population tracking will be achieved for both amplitude and phase.

5. FILTER AND MULTIPLEXER ANALYSIS

5.1. Introduction

This chapter contains a detailed computer analysis, using the LEVEL 2 BASIC programming language, of the filters, diplexers and triplexer designed in the previous chapters. The results of the analysis are in good agreement with the practical results. The basic ideas and equations behind the computer programs are presented. The analysis of the highpass leads to a much improved design for this filter, whilst the analysis of the lowpass shows that the present design of this filter is clearly acceptable.

5.2. Analysis of the Lowpass Filter

5.2.1. Distributed lowpass prototype

The first computer program calculates the insertion and return losses, at a number of frequencies, for the distributed lowpass prototype having its 3 dB frequency at 8 GHz. At each frequency, the program first calculates the overall transfer matrix of the prototype between the terminations. If this matrix is $\begin{bmatrix} A & jB \\ jC & D \end{bmatrix}$ then the insertion and return losses can be respectively found from [5.1]:

$$L_A = 10 \log_{10} [1 + \tfrac{1}{4}(B-C)^2 + \tfrac{1}{4}(A-D)^2] \qquad (5.2.1)$$

$$L_R = 10 \log_{10} [\frac{(A+D)^2 + (B+C)^2}{(A-D)^2 + (B-C)^2}] \qquad (5.2.2)$$

The results given in Figs. 5.2.1 and 5.2.2 show an equiripple passband return loss of minimum value 20 dB and a minimum stopband insertion loss of 40 dB.

5.2.2. Lumped inductor approximation of the series stubs of the distributed lowpass prototype

The next program calculates the frequency response when the series short circuited stubs of the distributed prototype are replaced by lumped inductors. The program uses the above transfer matrix approach to evaluate the frequency response. The series inductances are calculated in the program and are found by equating, at the bandedge frequency, the impedance of each lumped inductor to that of the corresponding series stub in the distributed prototype. The results shown in Figs. 5.2.3 and 5.2.4 show that this pure lumped inductor simulation of the required series impedance is inadequate, since it produces a return loss of 15.25 dB at 2.54 GHz. This level is caused by the impedances of the inductors decreasing too slowly with frequency and would cause a poor input match to the triplexer where the lowpass filters are in cascade.

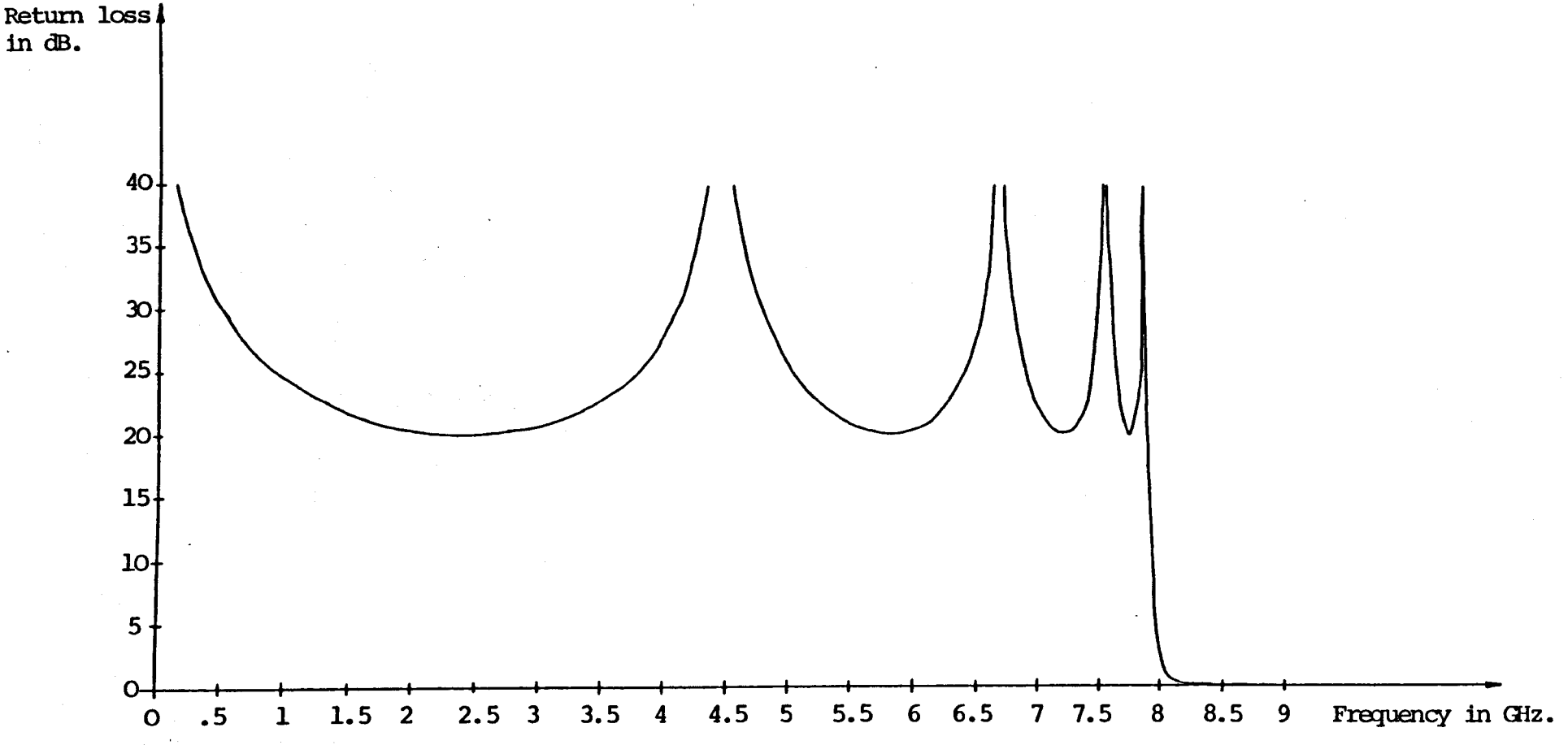

Fig. 5.2.1 Return loss of distributed quasi lowpass prototype filter with 3 dB. frequency at 8 GHz (Degree nine)

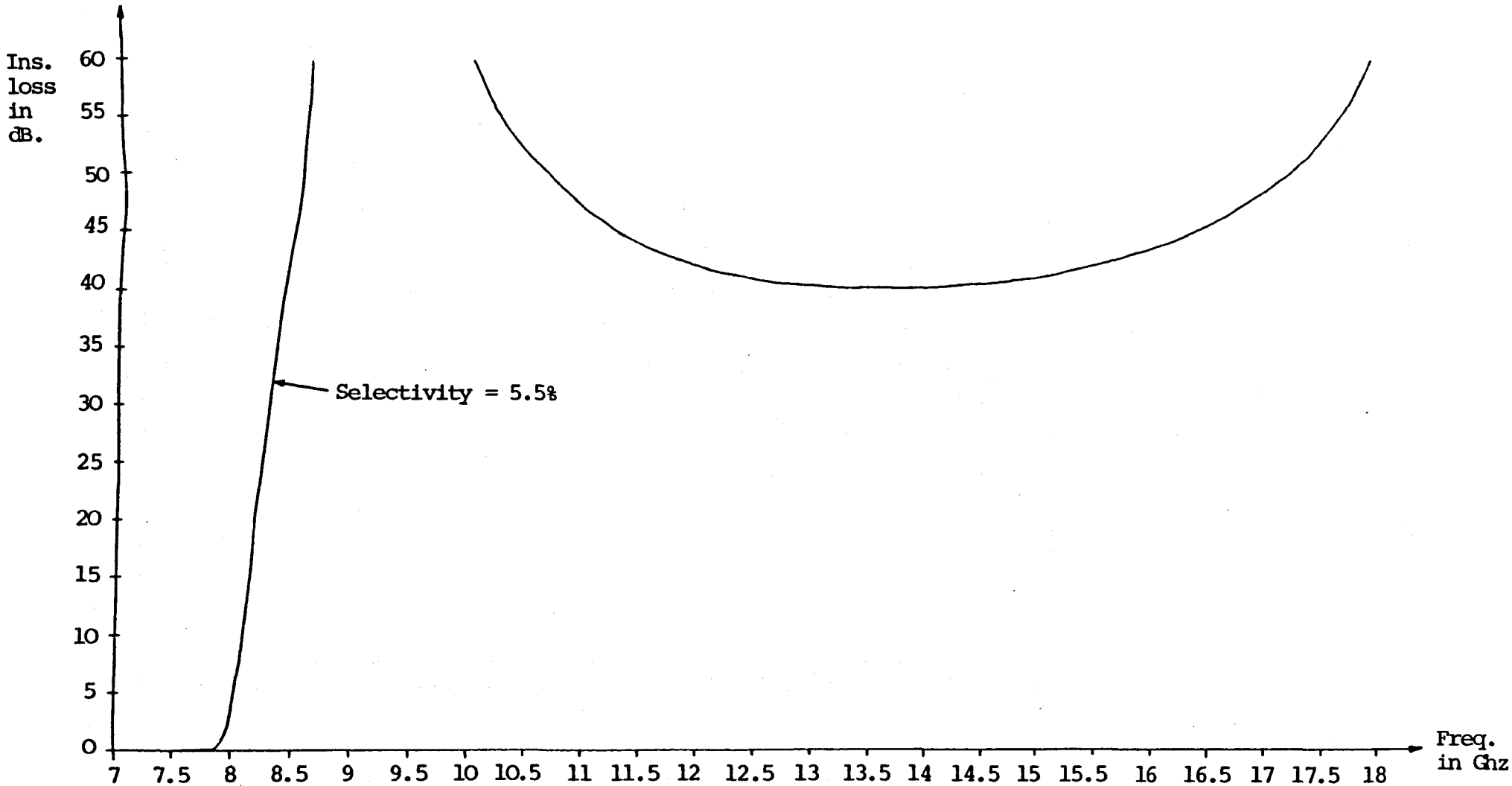

Fig. 5.2.2 Insertion loss of distributed quasi lowpass prototype filter with 3 dB. frequency at 8 Ghz. (Degree nine)

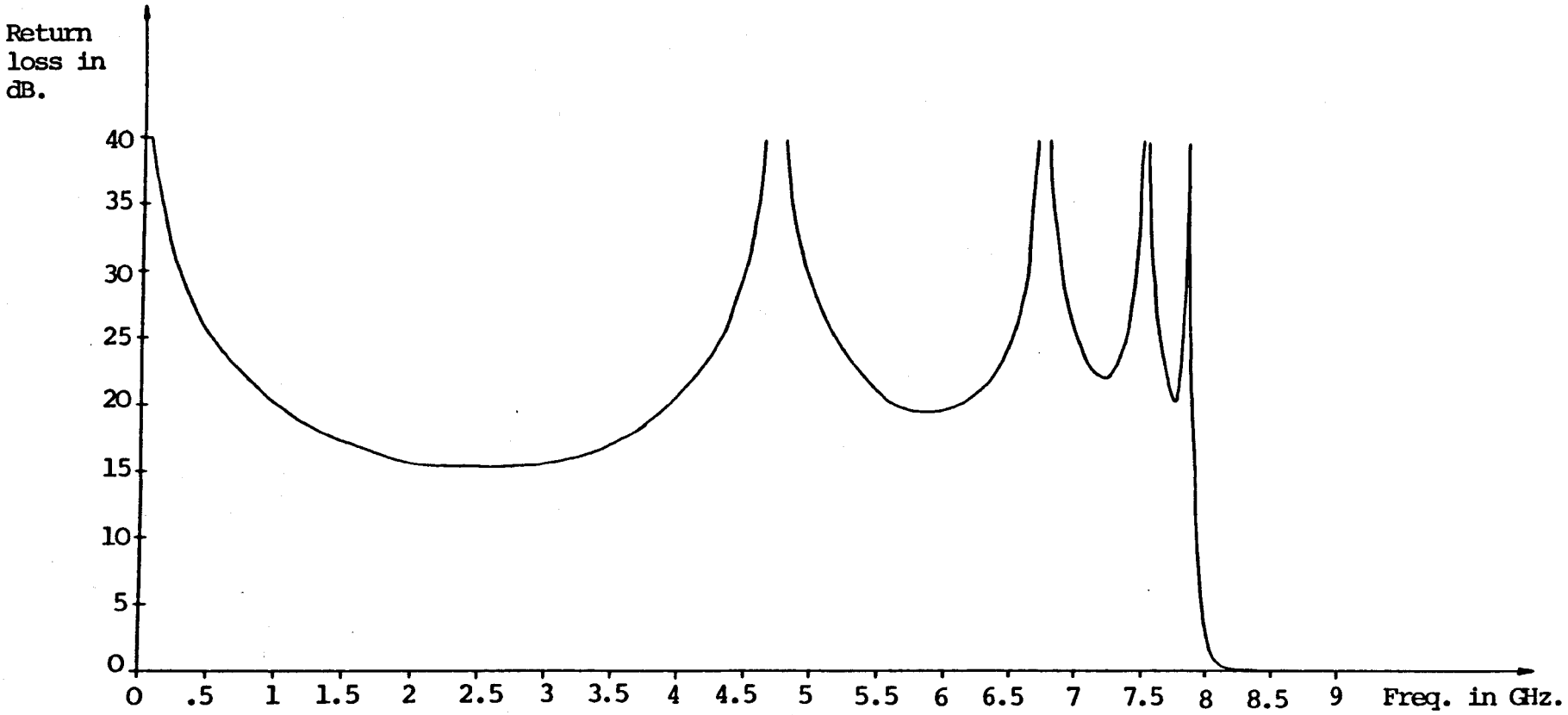

Fig. 5.2.3 Return loss when the series s/c stubs of the distributed lowpass prototype are replaced by lumped inductors

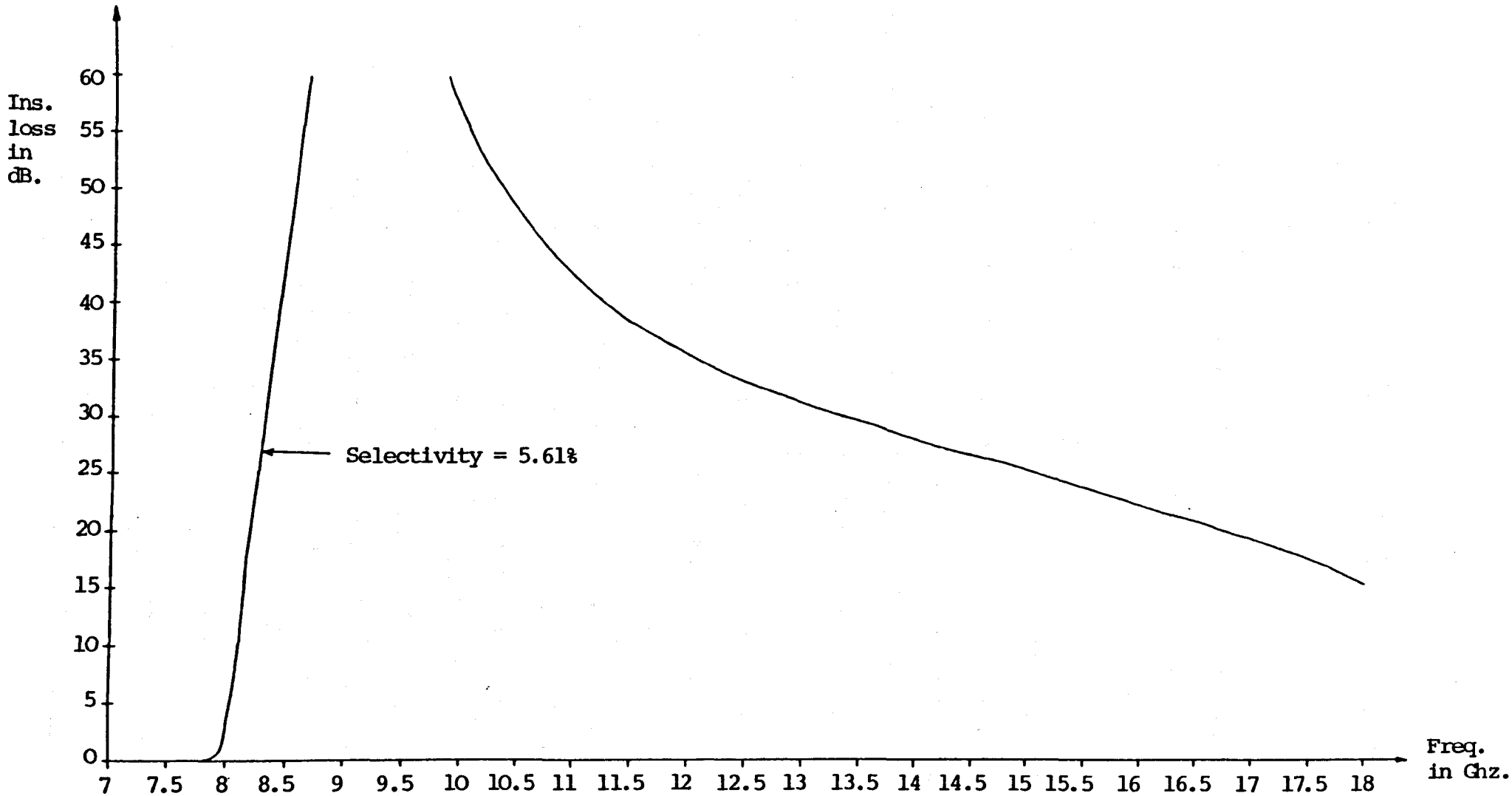

Fig. 5.2.4 Insertion loss when the series s/c stubs of the distributed lowpass prototype are replaced by lumped inductors

5.2.3. Unit element approximation of the series stubs of the distributed lowpass prototype

The third program analyses the practical lowpass circuit in which unit elements are used to approximate the series impedances of the distributed prototype. In this program the widths of the u.e.'s are input to the computer via an INPUT statement instead of a DATA statement. This allows an easy investigation of the effect of the widths on the frequency response. The program finds the characteristic impedance of each u.e. using (2.4.6) and (2.4.23) and then calculates its length using (2.4.17), where for a 8 GHz lowpass f_{bL} = 7.888 GHz and for a 12 GHz lowpass, f_{bL} = 3 x 7.888/2 = 11.832 GHz. Again the overall transfer matrix of the filter is found to determine the insertion and return losses.

When designing the 8 GHz lowpass, a width of 0.025" was chosen for all the u.e.'s and Figs. 5.2.5 and 5.2.6 show the frequency response for this choice. Note that these results agree well with the practical results given in Figs. 2.5.1 and 2.5.2. In particular note the very good return loss over the lower frequency region of the passband, necessary for the triplexer, and the falling stopband insertion loss above 9.8 GHz. The insertion loss of 25 dB at 12.30 GHz would be improved to about 40 dB in the 8 GHz diplexer due to the change in the first series element of the lowpass in the diplexer and the effect of the highpass, as

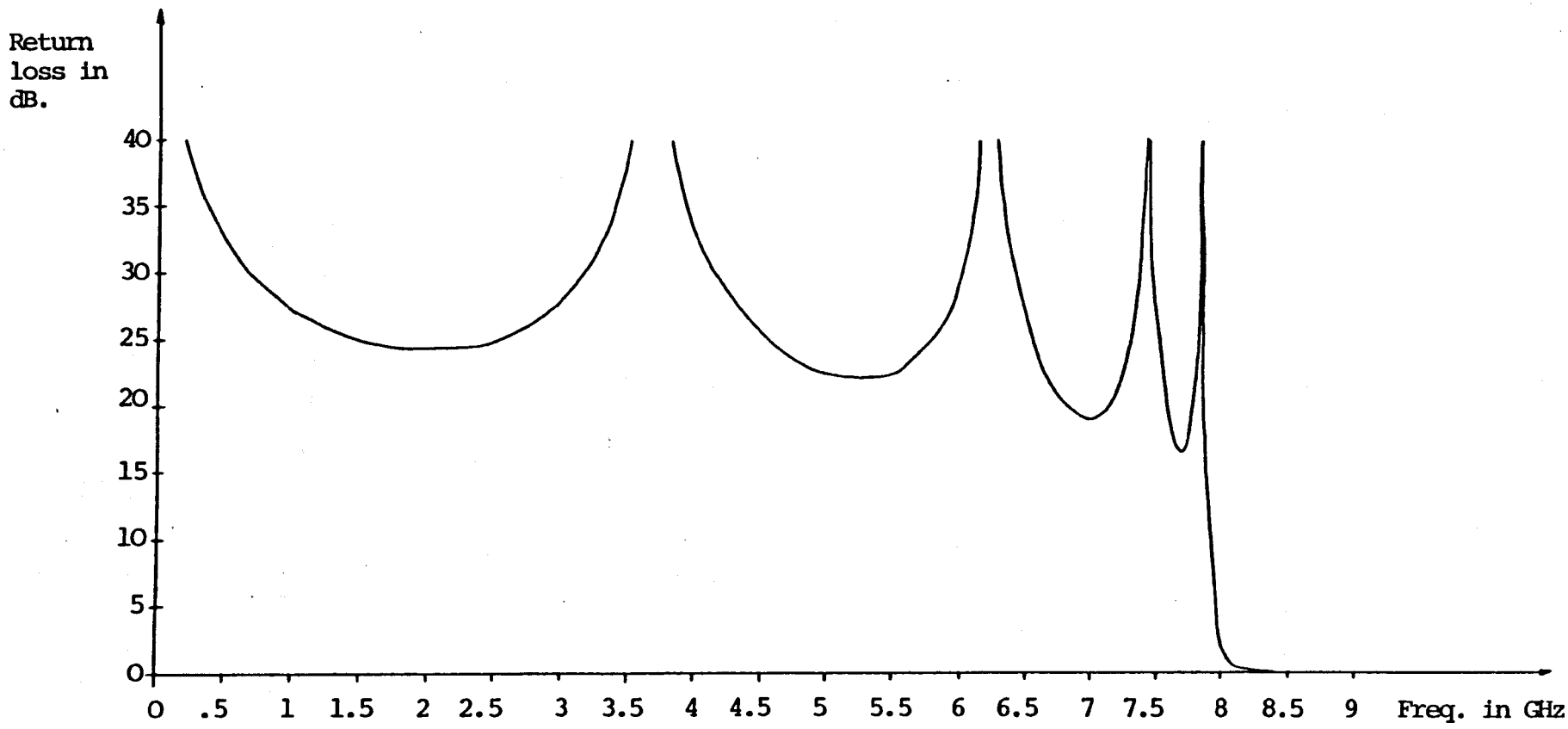

Fig. 5.2.5 Return loss of 8 GHz distributed lowpass filter with unit elements as the coupling elements. (Widths of u.e.'s = 0.025" throughout).

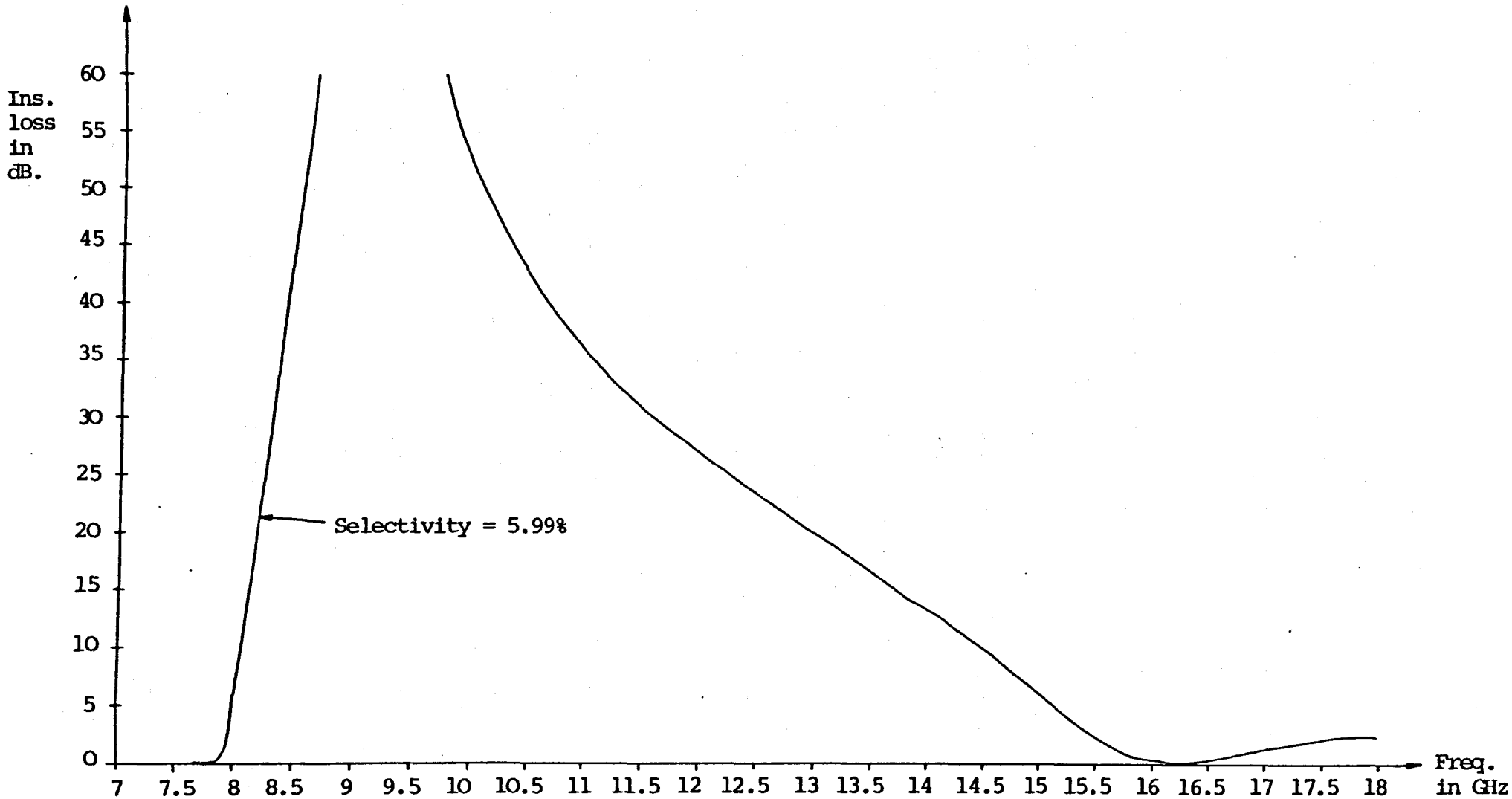

Fig. 5.2.6 Insertion loss of 8 GHz distributed lowpass filter with unit elements as the coupling elements. (Widths of u.e.'s = 0.025" throughout).

discussed in the last chapter. Hence this lowpass effectively has the half-octave 40 dB stopband bandwidth required for the triplexer.

The next two pairs of graphs Figs. 5.2.7 - 5.2.10 show the responses of the isolated lowpass filters formed by using the modified widths of the low channels of the 8 and 12 GHz diplexers. Note that for these isolated filters, the width of the first and last u.e.'s must be equal. The computer results are in good agreement with the performances of the low channels in the practical 8 and 12 GHz diplexers when the following points are noted. Firstly, the main passband return loss of the isolated filters will change little when used in the diplexers. Secondly, the frequencies for these filters where the stopband insertion loss is maintained up to 40 dB will be increased to about 12.08 GHz and 17.44 GHz in the 8 and 12 GHz diplexers respectively (for the latter, the insertion loss will be about 35 dB at 18 GHz). These frequencies are slightly higher than measured in practice, but it should be noted that the measured values depend critically on the crossover frequencies of the diplexers. Indeed, if these crossovers were tuned to slightly higher frequencies, then the upper 40 dB frequencies of the low channels would increase to the theoretically predicted values.

The unit element approximation of the series elements of the distributed prototype produces good

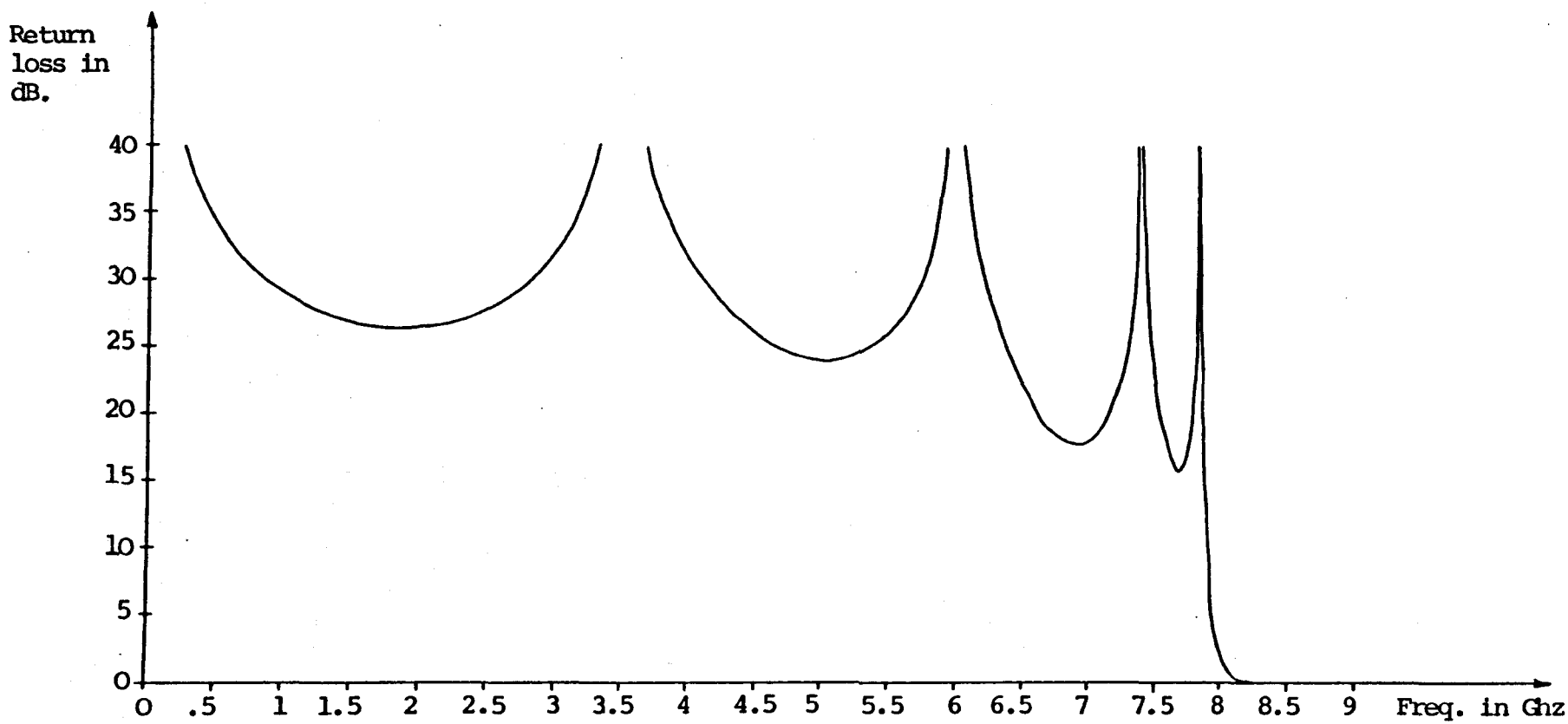

Fig. 5.2.7 Return loss of 8 GHz distributed lowpass filter with unit elements as the coupling elements. (Widths of first to fifth u.e.'s = .0313", .031", .025", .031" and .0313" respectively)

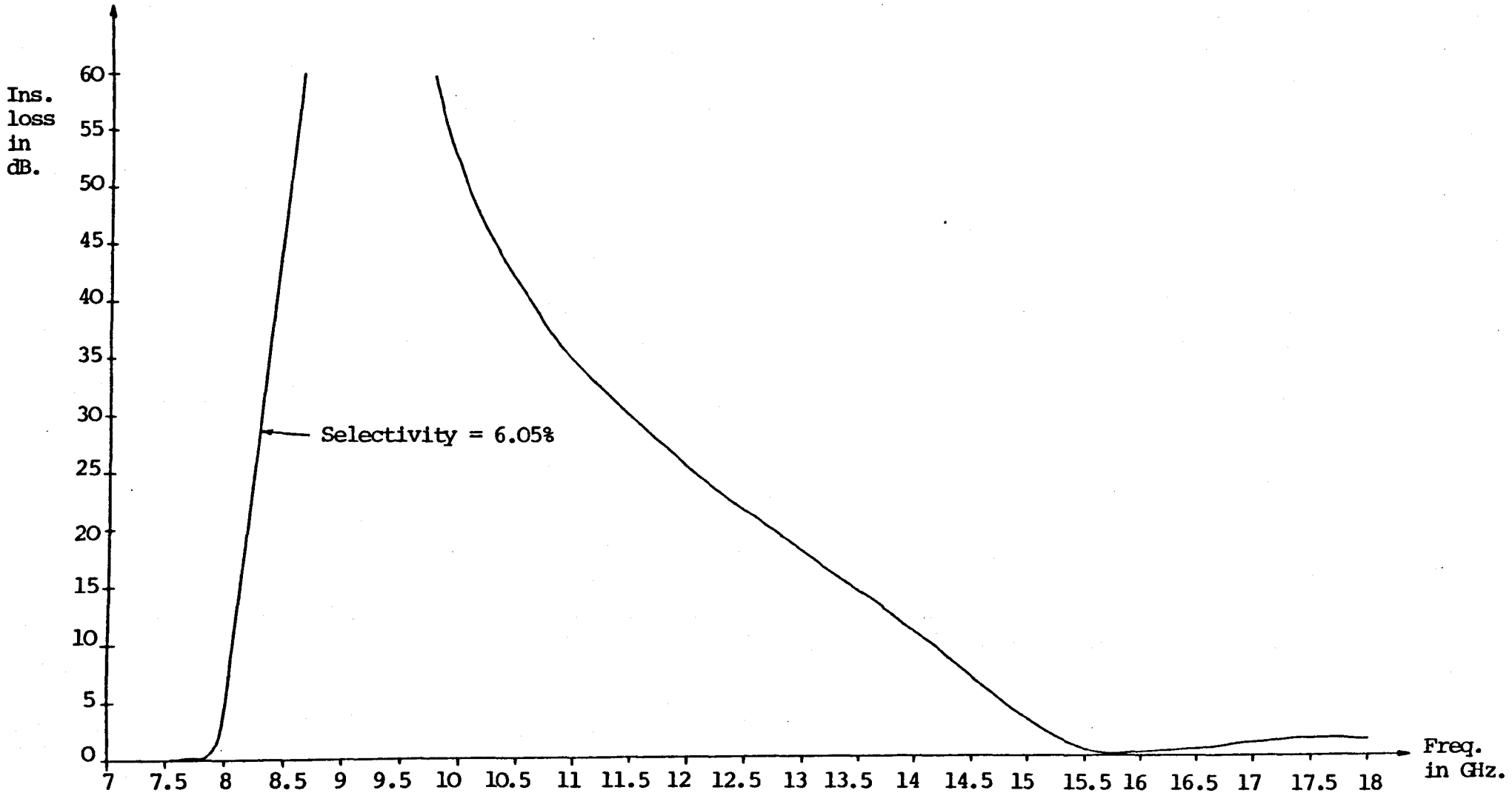

Fig. 5.2.8 Insertion loss of 8 GHz distributed lowpass filter with unit elements as the coupling elements. (Widths of first to fifth u.e.'s = .0313", .031", .025", .031" and .0313" respectively).

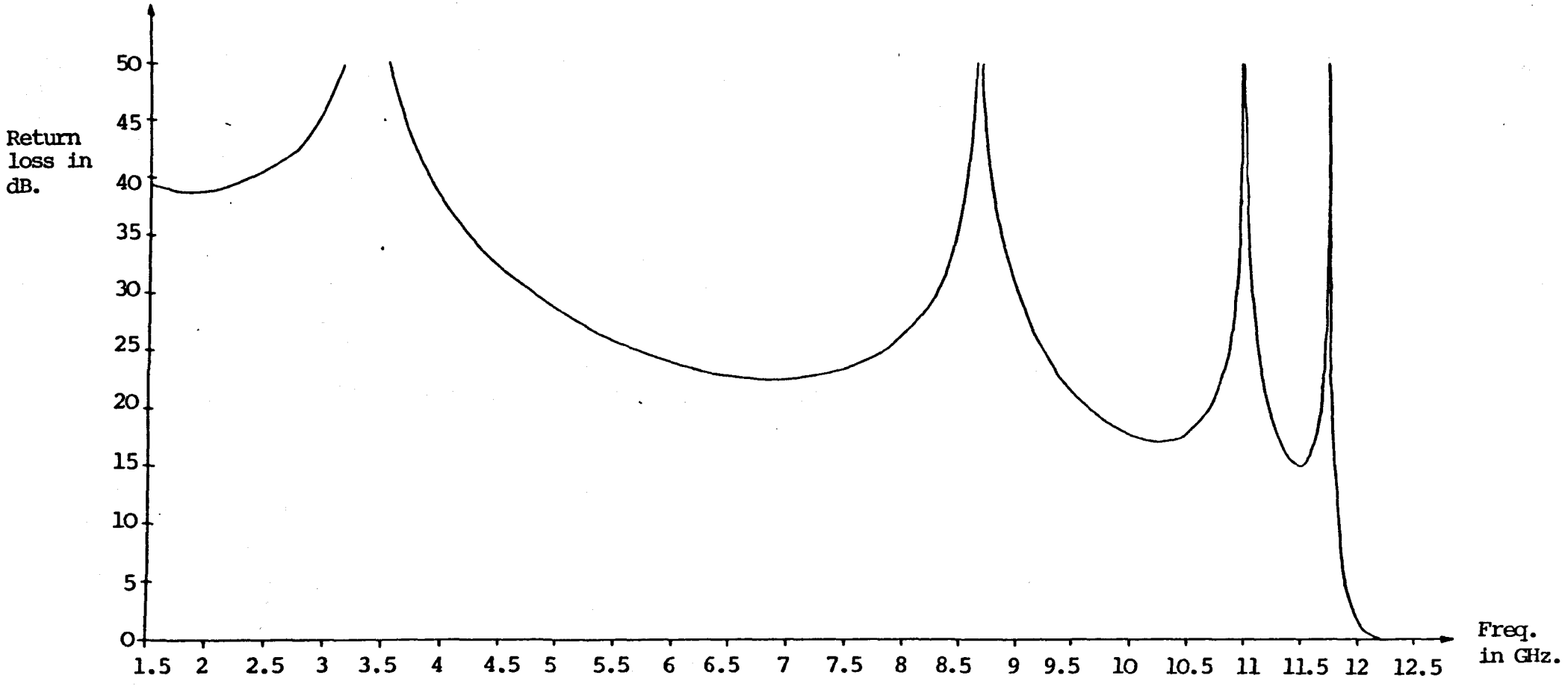

Fig. 5.2.9 Return loss of 12 GHz distributed lowpass filter with unit elements as the coupling elements. (Widths of first to fifth u.e.'s = .0406", .0414", .0389", .0414" and .0406" respectively)

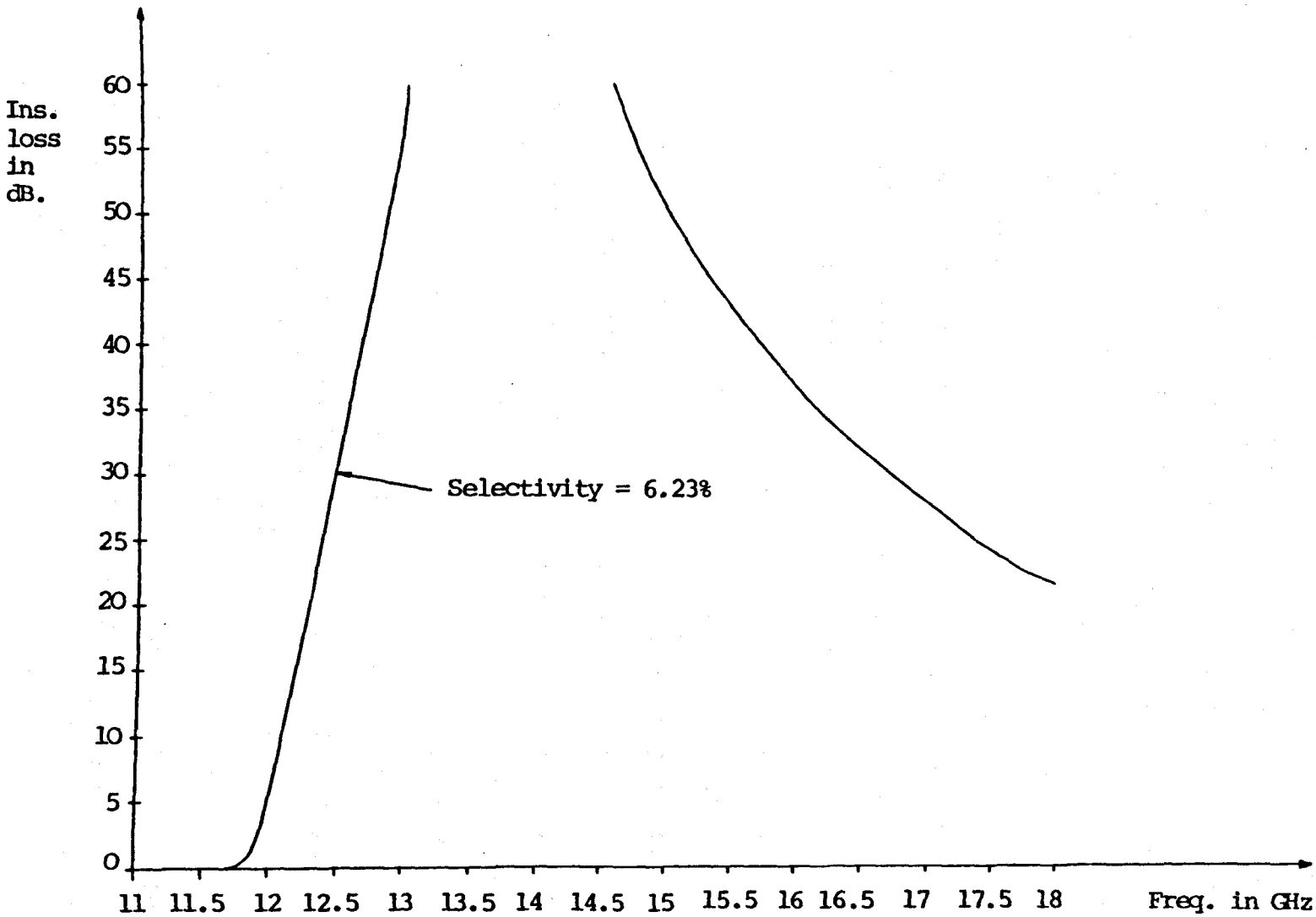

Fig. 5.2.10 Insertion loss of 12 GHz distributed lowpass filter with unit elements as the coupling elements. (Widths of first to fifth u.e.'s = .0406", .0414", .0389", .0414" and .0406" respectively).

passband return loss ripples near bandedge. This is because we approximate the series impedance of the equivalent pi-circuit of each u.e. (see Fig. 5.2.11 and Ref. [2.1]) to the corresponding series impedance of the distributed prototype, at the bandedge frequency. However, the two passband ripples nearest bandedge and the selectivity of the transition curve are somewhat poorer than for the pure lumped inductor approximation of the series elements; on the other hand, the return loss ripples away from bandedge are much better. Also these differences are slightly enhanced as the widths of the u.e.'s are increased - compare the last three pairs of graphs. These differences are due to the shunt admittances of the pi-circuit of the unit elements adding to the admittances of the shunt resonators and the resultants interacting with the series impedances. This can be proved by analysing the lowpass circuit where only the series impedance of the pi circuit of each u.e. is considered, together with the shunt resonators. Indeed, such an analysis for the lowpass with 0.025" wide unit elements, shows that the first minimum of return loss falls from 24.16 dB to 15.36 dB, the second minimum drops to 19.12 dB, the two ripples near bandedge improve especially the nearest one and the selectivity improves from 5.99% to 5.29%. The very good return loss over the lower frequency region of the passband is also expected from physical considerations, since in this region the lowpass approachs a simple d.c. path between the source

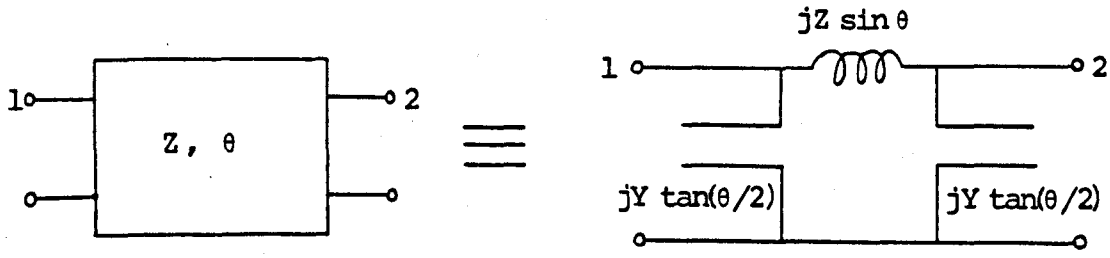

Legend:

$Z = 1/Y$: Characteristic impedance of u.e.

θ : Electrical length of u.e.

N.B. For the pi-network, the expressions given are impedance for the series element and admittance for the shunt elements.

Fig. 5.2.11 Pi-network of a unit element (u.e.)

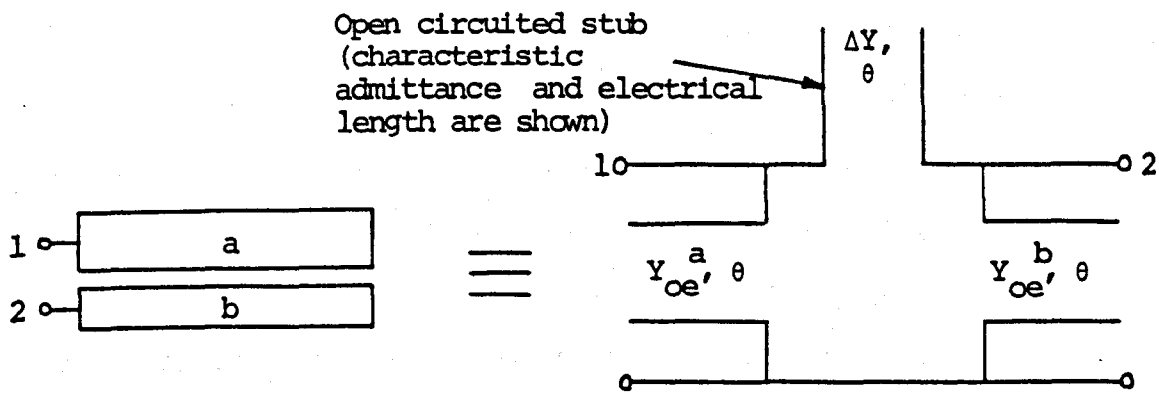

Legend:

Y_{oe}^{a}, Y_{oe}^{b} : Even mode characteristic admittances of lines a and b respectively

Y_{oo}^{a}, Y_{oo}^{b} : Odd mode characteristic admittances of lines a and b respectively

ΔY : $\Delta Y = (Y_{oo}^{a} - Y_{oe}^{a})/2$ i.e. coupling admittance

θ : Electrical length

Fig. 5.2.12 Unsymmetrical comb line section in a homogeneous medium

and load. The two ripples nearest bandedge can be improved by tuning, whilst only slightly deteriorating the two lower frequency return loss ripples, to produce the two minima nearest bandedge of about 17 dB for all the u.e. widths considered here.

5.2.4. Effect of the distributed coupling between the resonators

The last program in this section analyses the effect of the distributed electromagnetic coupling between the resonators, which was neglected in the previous designs. The exact equivalent circuit for a pair of coupled open circuited transmission lines operating in the TEM mode is shown in Fig. 5.2.12. The coupling is represented by a series open circuited stub and in the lowpass this will be in parallel with the series element produced by the u.e. joining the pair of resonators. In other words, the series impedance between the resonators is changed by the coupling. However, as discussed below, analysis shows that for the physical separations between the resonators for all the lowpass filters in the triplexer, the effect of the coupling is very slight.

Firstly, for the isolated 8 GHz lowpass, having the modified widths of the lowpass u.e.'s in the 8 GHz diplexer, the passband ripples hardly change, except the minimum nearest bandedge improves from 15.28 dB to 16.5 dB. Also, the 3 dB frequency is only reduced by 0.13%. Secondly, for the isolated modified 12 GHz low-

pass, the minima of passband return loss change from 38.9, 22.3, 16.96 and 14.93 dB to 38.66, 23.02, 17.66 and 17.15 dB respectively. Also, the 3 dB frequency is reduced by the coupling by 0.96%. The selectivity of the skirt response deteriorates from 6.23% to 6.44% and the bandedge frequency (i.e. 0.0432 dB frequency or 20 dB return loss frequency) changes from within 1.45% to within 1.62% of the 3 dB frequency, with a consequent slight 'rounding' of the insertion loss characteristic between these frequencies. Clearly, the above effects of the coupling between the resonators are slight and so it was justifiable to neglect the coupling when designing the series elements. The shift in the 3 dB frequency can be accounted for by simply rescaling the designed filter. Finally, the total admittance produced by each coupling element between the resonators and the series element of the u.e. joining the resonators, has a zero just above bandedge. Thus the circuit has extra transmission zeros at frequencies just less than that of the multiple ordered zero produced by the resonators. However, these extra zeros do not improve the filter's selectivity.

5.3. Analysis of the Highpass Filter

5.3.1. Distributed highpass prototype and the lumped capacitor approximation to its series stubs

The return and insertion losses for the distributed highpass prototype with 3 dB frequency at 8 GHz

are shown in Figs. 5.3.1 and 5.3.2. Figs. 5.3.3 and 5.3.4 show the frequency response for the lumped capacitor approximation to the series open circuited stubs of this prototype. The admittance of each lumped capacitor is made equal to the admittance of the corresponding series stub in the distributed prototype, at the bandedge frequency. The results show that this approximation is inadequate for octave passbands and is caused by the reactances of the lumped capacitors not falling to zero quickly enough away from bandedge. This means the reactances do not resonate at some frequency close to bandcentre and then increase positively, which are requirements for an octave passband.

5.3.2. Highpass with inhomogeneous coupled lines

The next program analyses the practical highpass filter where inhomogeneous open circuited digital sections are used to approximate the series open circuited stubs of the distributed highpass prototype. Considerable work has been done on these and related inhomogeneous sections. Firstly, Speciale [5.2] has proved that propagation along a pair of nonsymmetrical inhomogeneous coupled lines can be considered in terms of an even mode voltage wave and an odd mode current wave, provided the so-called 'congruence condition' is satisfied. This condition means that the ratio of the per-unit-length conductor-to-ground capacitances of the two lines must be the same when the dielectric is present and when

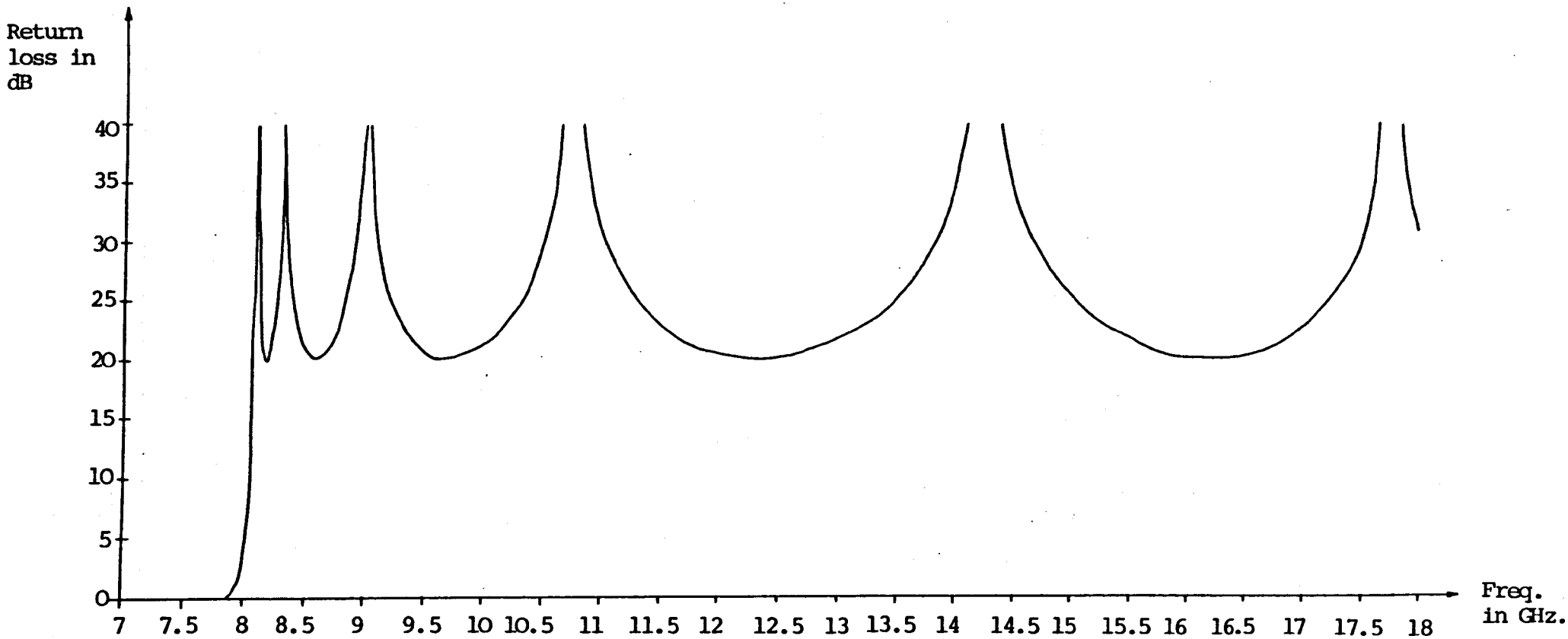

Fig. 5.3.1 Return loss of distributed quasi highpass prototype filter with 3 dB frequency at 8 GHz.

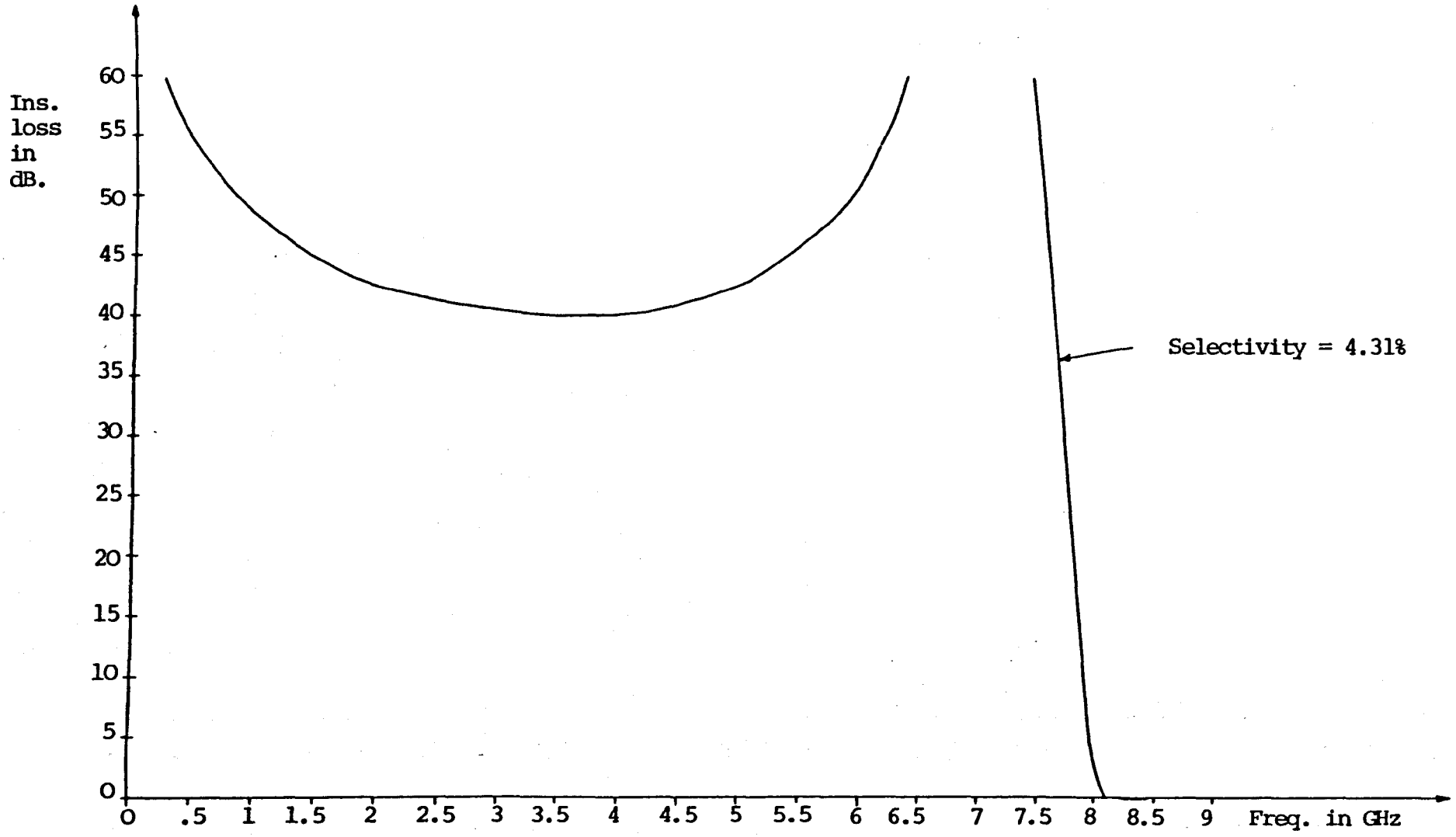

Fig. 5.3.2 Insertion loss of distributed quasi highpass prototype filter with 3 dB. frequency at 8 GHz.

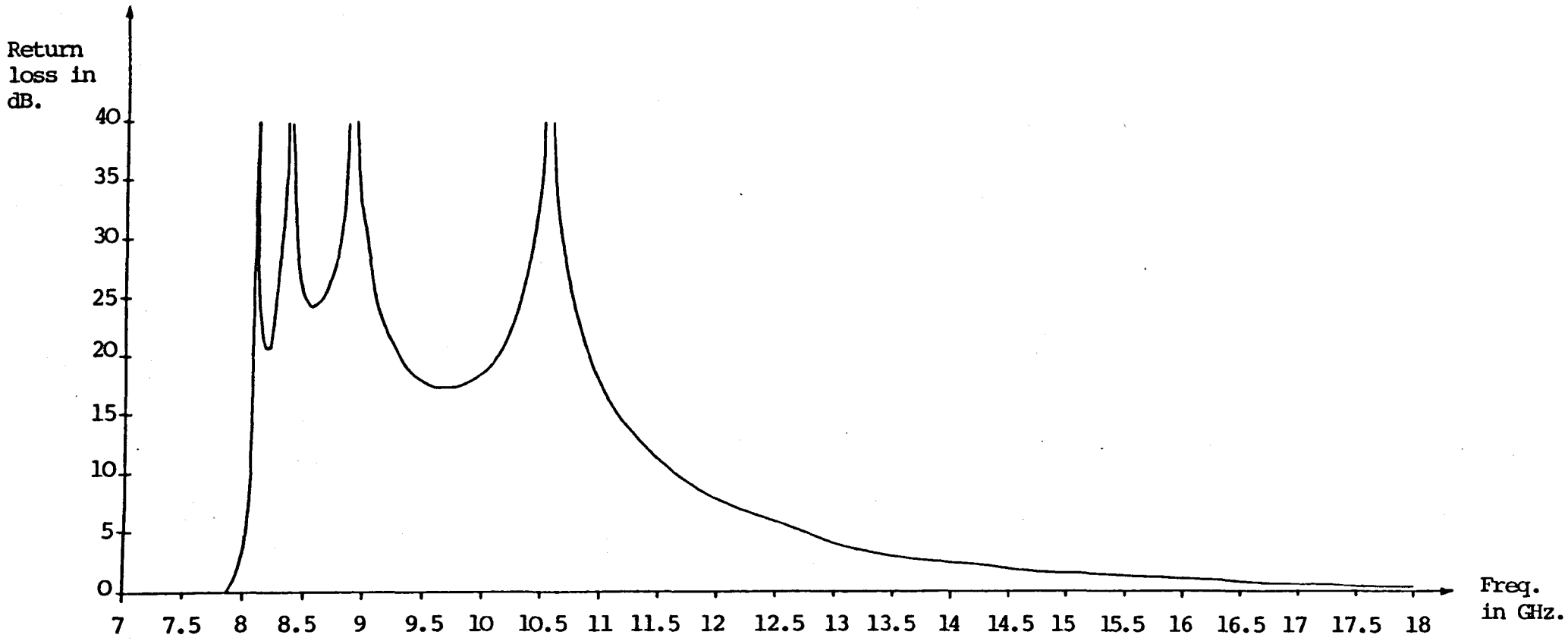

Fig. 5.3.3 Return loss when the series o/c stubs of the distributed highpass prototype are replaced by lumped capacitors

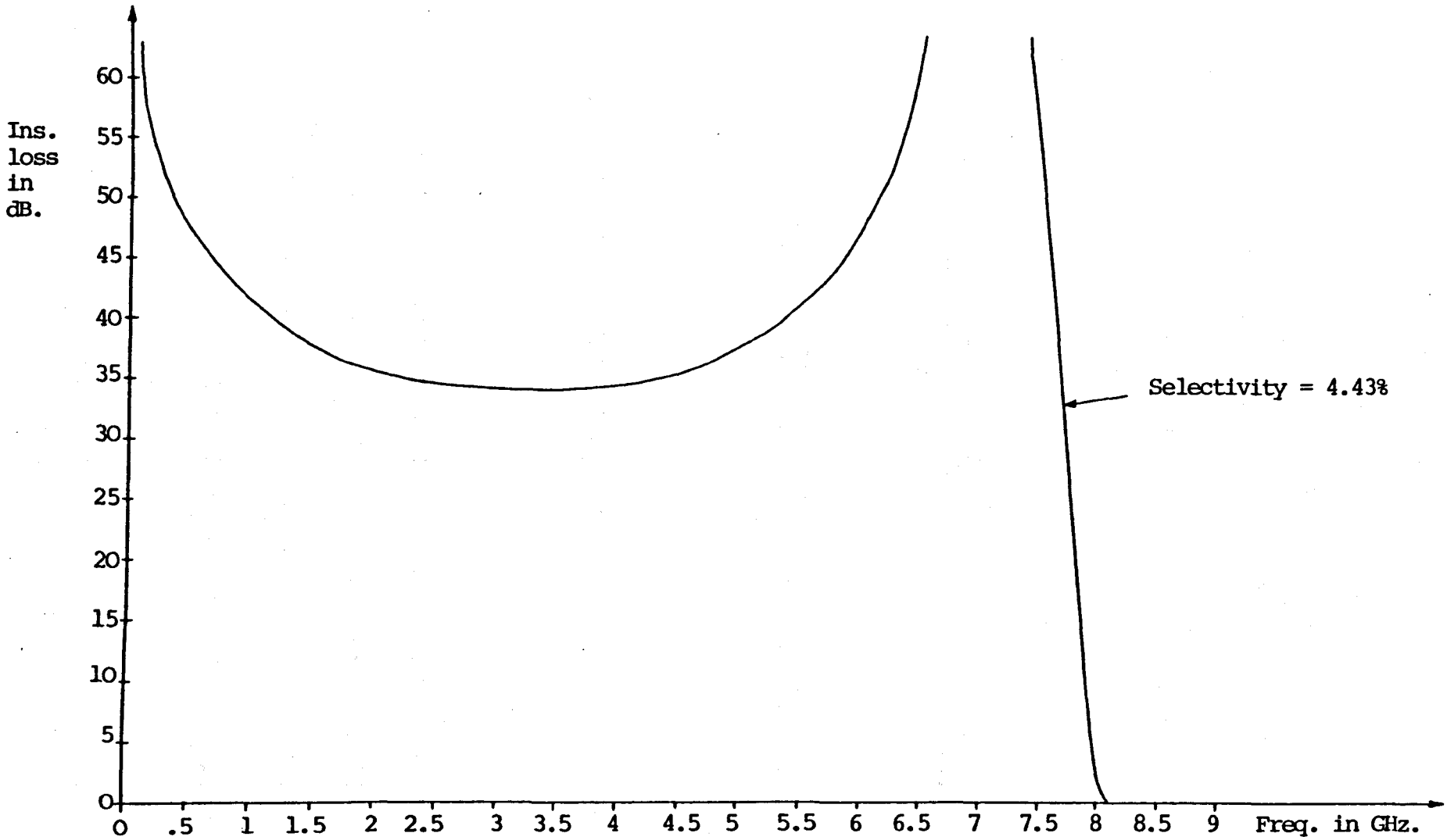

Fig. 5.3.4 Insertion loss when the series o/c stubs of the distributed highpass prototype are replaced by lumped capacitors

it is removed. For the simpler case of symmetrical inhomogeneous coupled lines, the propagation degenerates to the sum of an even and an odd mode voltage wave. Using these TEM modes, Zysman and Johnson [5.3] have developed equivalent circuits for symmetrical inhomogeneous coupled lines having various terminations and the equivalent circuit for the open circuited digital section is shown in Fig. 5.3.5. The ABCD parameters for this two port are:

$$A_r = \frac{Z_{oer} \cot \theta_{er} + Z_{oor} \cot \theta_{or}}{Z_{oer} \csc \theta_{er} - Z_{oor} \csc \theta_{or}} = D_r \qquad (5.3.1)$$

$$B_r = \frac{j}{2} \frac{Z^2_{oer} + Z^2_{oor} - 2 Z_{oor} Z_{oer} (\cot \theta_{er} \cot \theta_{or} + \csc \theta_{er} \csc \theta_{or})}{Z_{oer} \csc \theta_{er} - Z_{oor} \csc \theta_{or}} \qquad (5.3.2)$$

$$C_r = \frac{2j}{Z_{oer} \csc \theta_{er} - Z_{oor} \csc \theta_{or}} \qquad (5.3.3)$$

where,

Z_{oer} = even mode characteristic impedance of each line

Z_{oor} = odd mode characteristic impedance of each line

$\theta_{er} = \frac{\omega \ell}{u_{er}}$ = even mode electrical length of each line

$\theta_{or} = \frac{\omega \ell}{u_{or}}$ = odd mode electrical length of each line

u_{er} = even mode phase velocity

u_{or} = odd mode phase velocity.

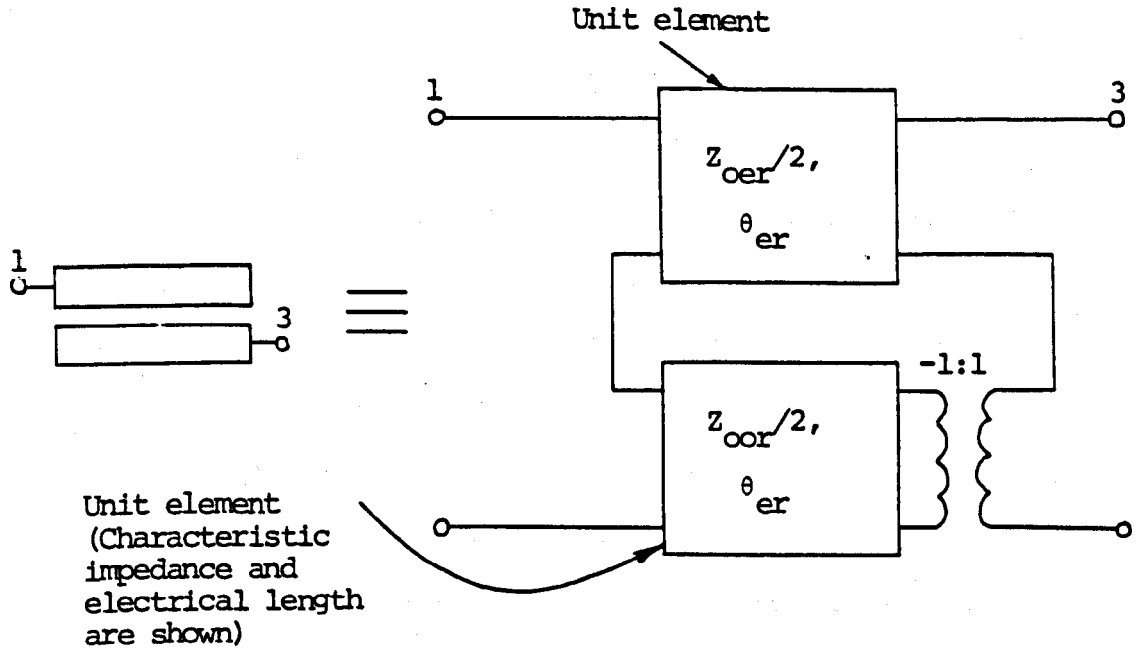

Fig. 5.3.5 Open circuited digital section in an inhomogeneous medium

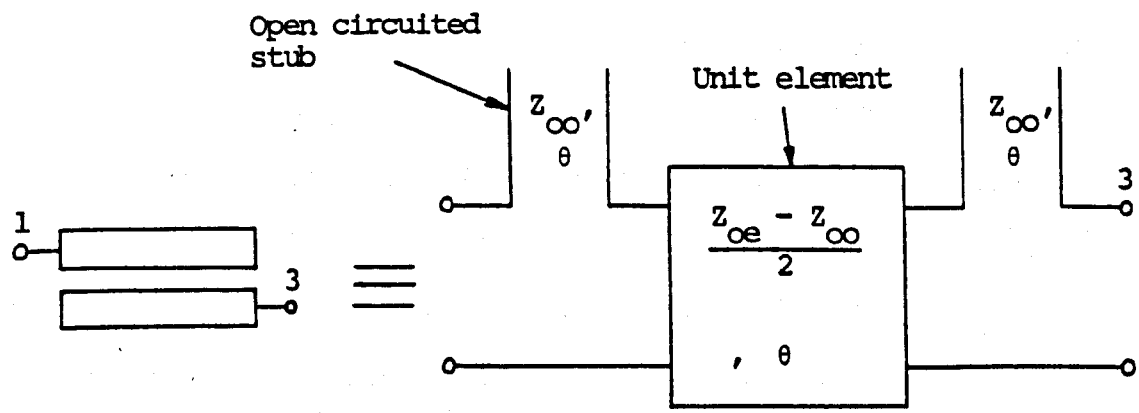

Legend for each coupled line

Z_{oe} : Even mode characteristic impedance

Z_{oo} : Odd mode characteristic impedance

θ : Electrical length

Fig. 5.3.6 Open circuited digital section in a homogeneous medium

The suffix r takes the values 1, 3,...,9 and is used to denote the different sections of the highpass filter. It should be noted that the circuit in Fig. 5.3.5 is different and much more complex than the one for the homogeneous open circuited digital section, which for comparison is given in Fig. 5.3.6.

In the computer program, the width and length of each inhomogeneous section are supplied using an INPUT statement, enabling the effects of different inhomogeneous sections on the frequency response of the filter to be easily analysed. Using another INPUT statement, the bandedge frequency is supplied to the computer. This scales the shunt resonator lengths and so by varying this input, the capacitive tuning at the ends of the resonators can be simulated. From the physical dimensions, the computer calculates and prints out the even and odd mode characteristic impedances and the effective relative dielectric constant, ε_{er}, for the odd mode, for each pair of inhomogeneous coupled lines in the highpass. Equation (3.3.11) gives the odd mode characteristic impedance and (3.3.12) yields the effective relative dielectric constant for the odd mode. Dispersion is neglected which, as discussed in chapter 3, is certainly justified up to 18 GHz. The even mode phase velocity is assumed to be the velocity of light in free space, u, and the even mode characteristic impedance of each coupled line is found from the following equation:

$$Z_{oer} = \frac{7.534}{\frac{1}{2}[w_r/(b-h-2t)] + C'_f + C'_{fo}} \qquad (5.3.4)$$

$$= \frac{7.534}{(w_r/0.03165) + 1.08} \quad , (r=1,3 \ldots 9) \qquad (5.3.5)$$

where w_r is the width of the coupled lines. The equation is derived by using the relationship between the characteristic impedance of a transmission line operating in the TEM mode and the static distributed capacitance between conductors of the line (see equation (2.4.6)). The components of the static capacitance are shown in Fig. 5.3.7. and it is assumed here that the fringing capacitances can be found using Getzinger's graphs [2.2].

The program then finds the overall transfer matrix of the filter using the ABCD parameters of the inhomogeneous sections given in (5.3.1) - (5.3.3). Note that $u_{er}=u$ and $u_{or} = u/\sqrt{\varepsilon_{er}}$ for r = 1,3 ...9. From this matrix, the insertion and return losses are then calculated using (5.2.1) and (5.2.2).

The first analysis considers the isolated 8 GHz highpass formed by using the modified widths of the inhomogeneous sections of the 8 GHz highpass in the single substrate triplexer. Note that for this isolated filter, the widths of the first and last inhomogeneous sections must be equal. When just the overlapping lengths of the inhomogeneous sections are considered (i.e. .0847",

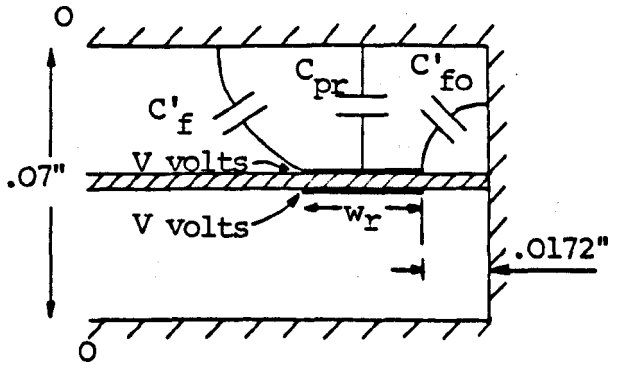

Fig. 5.3.7 Per-unit-length capacitance-to-ground of each inhomogeneous coupled line for even mode excitation

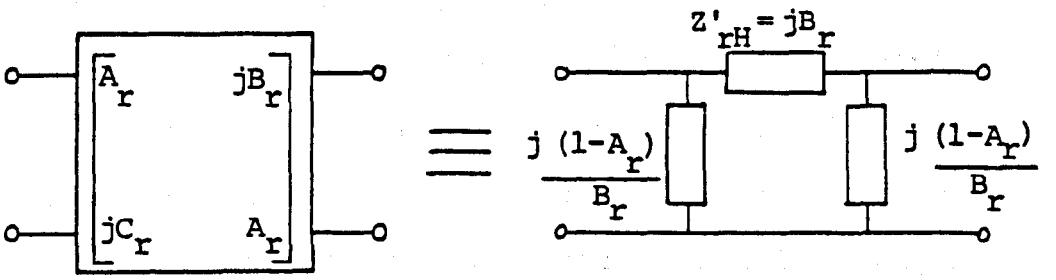

N.B. For the pi-network the expressions given are <u>impedance</u> for the series element, and <u>admittance</u> for the shunt elements.

Fig. 5.4.1 Pi-network of rth inhomogeneous section of highpass filter (r = 1,3,...,9)

.0585" and .0608"), the minima of passband return loss are only 8.89, 3.53, 2.17 and 4.30 dB. However, by varying the lengths of these sections the response can be improved. Figs. (5.3.8) and (5.3.9) show that by increasing the lengths of the two end and middle three sections to .0905" and .0716" respectively, a passband return loss of at least 16.56 dB is maintained up to nearly 2½ times the 3 dB frequency. Clearly the effective lengths of the inhomogeneous sections of the 8 GHz highpass in the practical triplexer must be close to these increased lengths (except for the first section, of course). That is, it appears that the fringing capacitances at the ends of each inhomogeneous section can be accounted for by a slight increase in the overlapping length of the inhomogeneous section. There must be some reference plane locations for the lengths of each inhomogeneous section lying slightly inside each T junction - the above results suggest that this extension into the T is only about 0.005".

Finally, it should be noted that the bandedge frequency input to the computer for the working analysis was 8.24 GHz, not 8.088 GHz. Consequently, the selectivity of the skirt response is better than for the distributed highpass prototype, which agrees with the practical results. Each inhomogeneous section can be replaced by its equivalent pi-network and the improvement in selectivity is due to the shunt admittances of this network adding to the admittances of the shunt resonators. This will be discussed later in section 5.4.

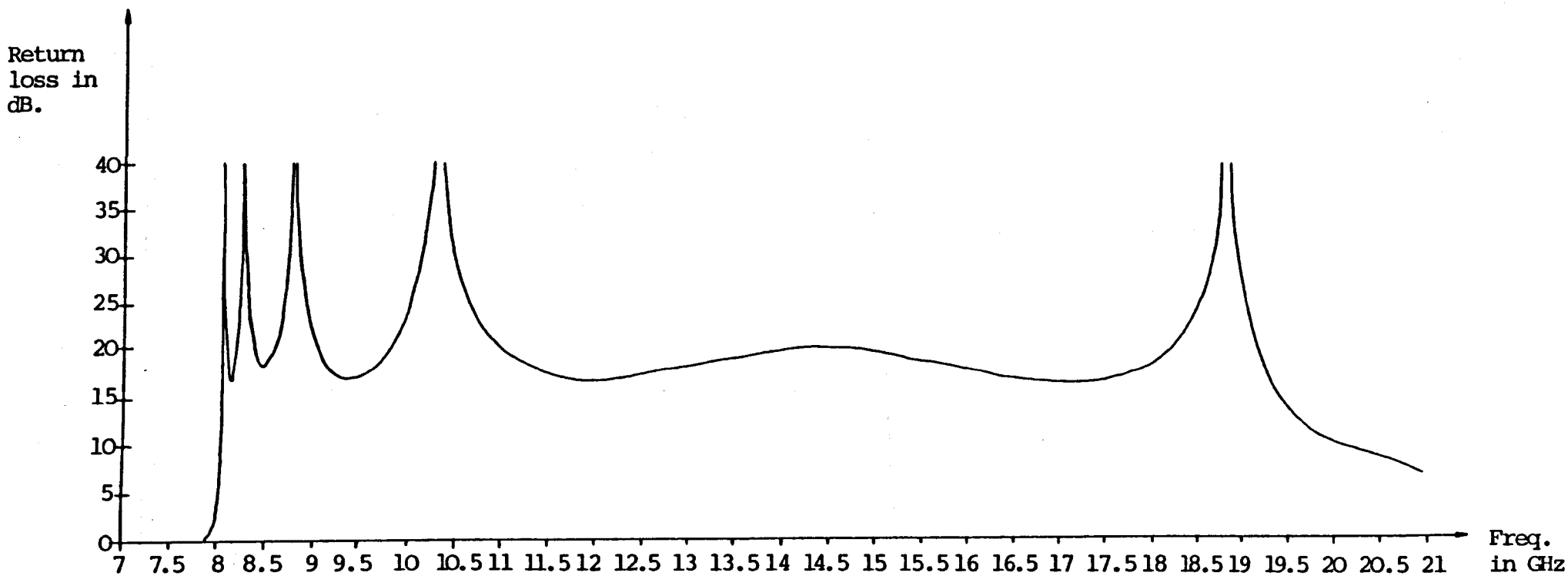

Fig. 5.3.8 Return loss of the distributed 8 GHz highpass having complex inhomogeneous sections as coupling elements. These sections are based on the modified sections of the 8 GHz highpass in the single substrate triplexer

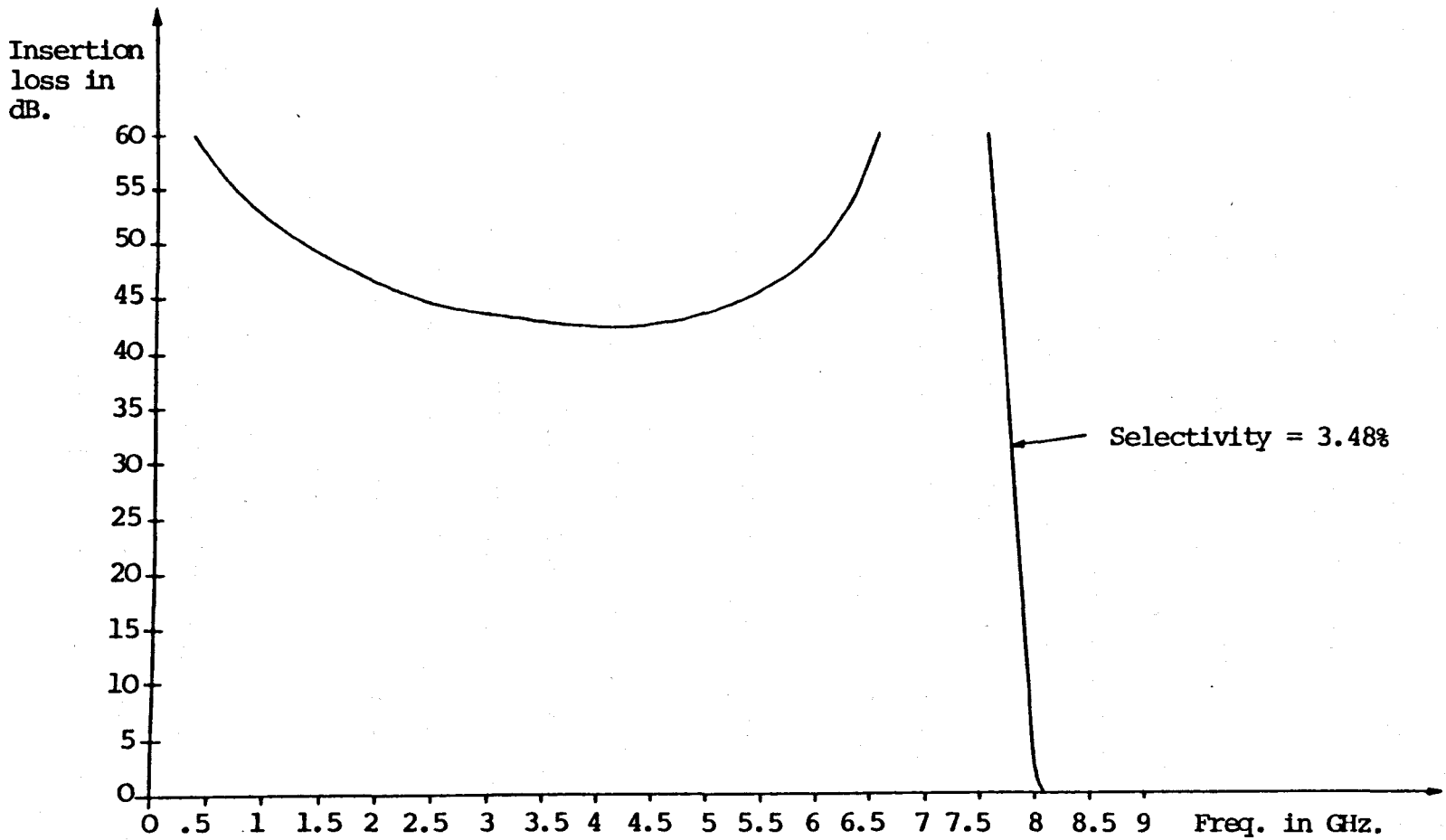

Fig. 5.3.9 Insertion loss of the distributed 8 GHz highpass having complex inhomogeneous sections as the coupling elements. These sections are based on the modified sections in the single substrate triplexer

The next analysis considers the isolated 12 GHz highpass formed by using the modified widths of the 12 GHz highpass in the practical triplexer. When just the overlapping lengths of the inhomogeneous sections are considered (i.e. .0563", .0389" and .0404"), the first two minima of passband return loss are 5.20 dB at 13.36 GHz and 2.22 dB at 18.42 GHz. However, by increasing the lengths of the two end and middle three sections to .0636" and .0520" respectively, the much improved response from 12 - 18 GHz, shown in Figs. (5.3.10) and (5.3.11), is achieved. Again the effective lengths of the inhomogeneous sections of the 12 GHz highpass in the practical triplexer must be close to these increased lengths. Note that the bandedge frequency input to the computer was 12.275 GHz.

5.3.3. Effect of the distributed coupling between the resonators

The next two programs analyse the effects of the electromagnetic coupling between the resonators. As discussed in the lowpass analysis, this coupling affects the series impedance between the resonators. The first program considers the working isolated 8 GHz highpass studied in the last but one paragraph. For the separations of the resonators in this highpass, the coupling admittance between neighbouring resonators are found using Getzinger's graphs [2.2]. The information from these graphs is stored in DATA statements in the

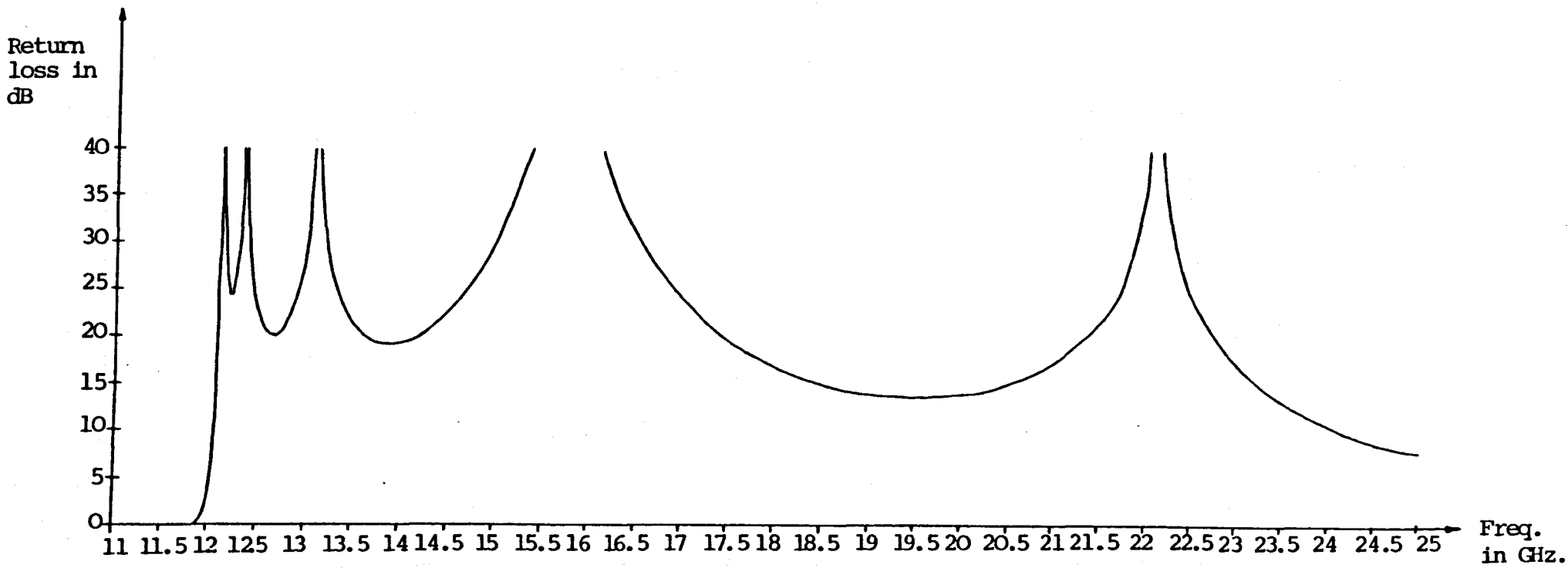

Fig. 5.3.10 Return loss of the distributed 12 GHz highpass having complex inhomogeneous sections as coupling elements. These sections are based on those of the 12 GHz highpass in the single substrate triplexer

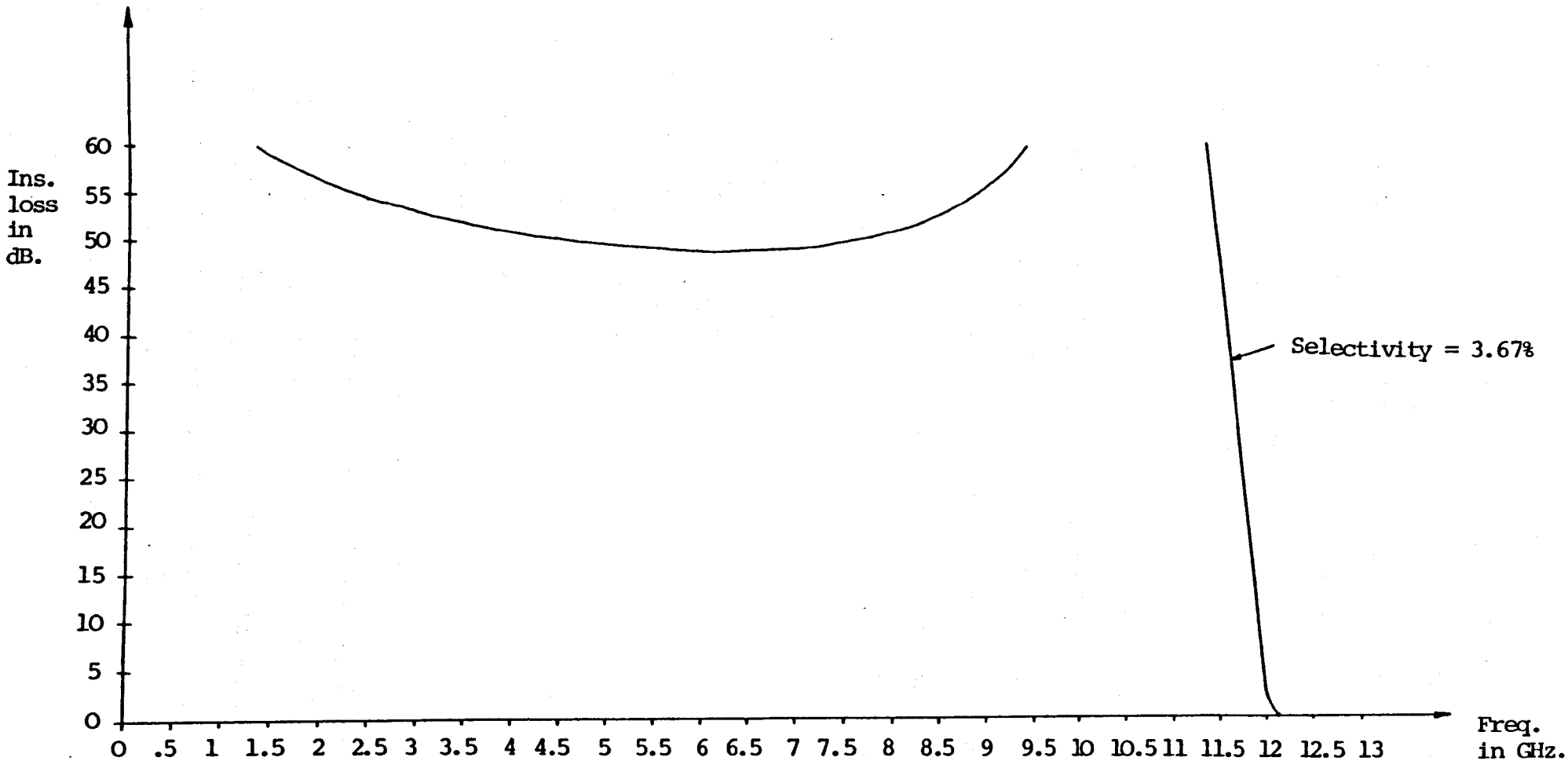

Fig. 5.3.11 Insertion loss of the distributed 12 GHz highpass having complex inhomogeneous sections as coupling elements. These sections are based on those of the 12 GHz highpass in the single substrate triplexer

program, from which the resultant transfer matrix of each u.e. and the coupling open circuited stub produced by neighbouring resonators is found. The overall transfer matrix of the filter is then calculated, from which the insertion and return losses are calculated and printed out. (N.b. the lowpass program with resonator coupling was developed in the same way).

Results for the 8 GHz highpass show that the first three minima of passband return loss slightly improve to 17.45, 21.94 and 17.48 dB; the next two ripples hardly change. The 3 dB frequency is increased by 0.60%, the selectivity is unchanged and the bandedge frequency changes from within 0.79% to within 0.82% of the 3 dB frequency.

The second program considers the effect of coupling in the working isolated 12 GHz highpass. Results again show that the main passband return loss is only slightly changed and a minimum of 16.9 dB is still achieved up to 19 GHz. The 3 dB frequency is increased by 1.57%, the selectivity is practically unchanged and the bandedge frequency changes from within 0.97% to within 1.07% of the 3 dB frequency.

The above results show that it was justifiable to neglect coupling between the resonators when designing the series elements. It should be noted that the small changes in the ripples close to bandedge are really equivalent to the effects of tuning the resonators, so they are not significant. Also the shift in the 3 dB

frequency of each filter can be accounted for by simply rescaling the designed filter. Finally, the coupling between the resonators introduces extra transmission zeros at frequencies just above the frequency of the multiple-ordered zero produced by the resonators. However, these extra zeros do not improve either filters selectivity.

5.4. Further Analysis Leading to an Improved Design of Highpass

This section describes the analysis steps that were taken which led to suitable design equations for the inhomogeneous sections of the highpass. These equations must be satisfied if a good match over at least an octave bandwidth is to be achieved.

Firstly, each inhomogeneous section of the highpass can be replaced by its equivalent pi-network as shown in Fig. 5.4.1. Now a computer program was written which calculates and prints out the series reactance and shunt susceptance of this network at a number of frequencies. The program also calculates the susceptance of the first shunt resonator in the highpass. The width and length of the inhomogeneous section are supplied to the computer via an INPUT statement, for easy analysis. From these dimensions, the computer calculates the ABCD parameters of the section, using the same equations as in the program used to analyse the 8 GHz highpass in the last section. The required immittances are then found using the relationships shown in Fig. 5.4.1.

Recall from (3.3.1) that the impedance of each series open circuited stub of the distributed highpass prototype, at the bandedge frequency, is given by

$$Z_{rH} = -jL_r \qquad (r=1,3...9) \qquad (5.4.1)$$

Substituting for L_r, the required impedances at bandedge are,

$$\left.\begin{aligned} Z_{1H} = Z_{9H} &= -j.418398 \qquad (5.4.2)\\ Z_{3H} = Z_{7H} &= -j\ 1.18012 \qquad (5.4.3)\\ \text{and } Z_{5H} &= -j\ 1.20707 \qquad (5.4.4)\end{aligned}\right\} \text{ at bandedge}$$

Also recall from (3.1.9) that,

$$Z_{rH} = 0 \text{ at } 14.27 \text{ GHz} \qquad (r=1,3...9) \qquad (5.4.5)$$

The series impedances in the pi-networks of the inhomogeneous sections of the working 8 GHz highpass (i.e. the highpass of Figs. 5.3.8 and 5.3.9) are now compared with those in the distributed prototype. Using the pi-network analysis program, the series impedances produced by the inhomogeneous sections, at the same bandedge frequency are,

$$\left.\begin{aligned} Z'_{1H} = Z'_{9H} &= -j\ .136773 \qquad (5.4.6)\\ Z'_{3H} = Z'_{7H} &= -j\ 1.02444 \qquad (5.4.7)\\ \text{and } Z'_{5H} &= -j\ 1.02444 \qquad (5.4.8)\end{aligned}\right\} \text{ at bandedge}$$

The resonant frequencies of these impedances are found to be,

$$Z'_{1H} \text{ or } Z'_{9H} = 0 \text{ at } 9.08 \text{ GHz} \qquad (5.4.9)$$

$$Z'_{3H} \text{ or } Z'_{7H} = 0 \text{ at } 12.98 \text{ GHz} \qquad (5.4.10)$$

$$Z'_{5H} = 0 \text{ at } 12.98 \text{ GHz} \qquad (5.4.11)$$

If a suitable design were based on producing the correct series impedances, then it would appear that the middle sections are almost correct but the end sections are in error. Now, by varying the dimensions of the inhomogeneous section input to the pi-network analysis program, it is found that the dimensions of the inhomogeneous sections which produce exactly the bandedge impedances of the distributed prototype and resonate at band centre are,

$$w_{1H} = 0.115" \; ; \; \ell_{1H} = 0.054" \qquad (5.4.12)$$

$$w_{3H} = 0.032" \; ; \; \ell_{3H} = 0.0637" \qquad (5.4.13)$$

$$w_{5H} = 0.031" \; ; \; \ell_{5H} = 0.064" \qquad (5.4.14)$$

We would possibly expect these sections to produce a good highpass response. However, when the highpass formed by these sections is analysed, the minima of passband return loss are only 12.72, 8.32, 3.01, 4.76 and 2.90 dB! In other words, we have shown that for a good broadband match, it is not sufficient when designing the inhomogeneous sections, just to produce the correct series impedances in the equivalent pi-networks. The reason is that the shunt impedance produced by these sections must be taken into consideration. Also, special attention must be given to the end sections.

The next step was to write a computer program which compares the terminating impedances produced by the two end inhomogeneous sections of the working 8 GHz highpass, with those produced by the two end stubs of the distributed prototype. The two impedances are shown in Fig. 5.4.2. It is possible these impedances are similar and would account for the shunt impedances of the two end inhomogeneous sections. The computer results show that at the bandedge frequency of the distributed prototype,

$$Z_{in} = 1 - j.418398 \qquad (5.4.15)$$

$$\text{and } Z'_{in} = .867478 - j.409453 \qquad (5.4.16)$$

(Z_{in} and Z'_{in} are defined in Fig. 5.4.2)

As the frequency increases beyond bandedge, the reactive components approach zero and we have

$$Z_{in} = 1 \text{ at } 14.27 \text{ GHz} \qquad (5.4.17)$$

$$\text{and } Z'_{in} = 1 \text{ at } 14.02 \text{ GHz} \qquad (5.4.18)$$

(N.b. $\mathrm{Re}Z'_{in} \to 1$ as $f \to 14.02$ GHz)

The impedances Z_{in} and Z'_{in} are in good agreement, so possible design equations could be

$$\mathrm{Im}\, Z'_{in} = \mathrm{Im}\, Z_{in} \text{ , at bandedge frequency} \qquad (5.4.19)$$

$$Z'_{in} = 0 \text{ , at bandcentre} \qquad (5.4.20)$$

and,

$$Z'_{rH} = Z_{rH} \text{ , at bandedge frequency} \qquad (5.4.21)$$

$$Z'_{rH} = 0 \text{ , at bandcentre} \qquad (5.4.22)$$

(r = 3,5 and 7)

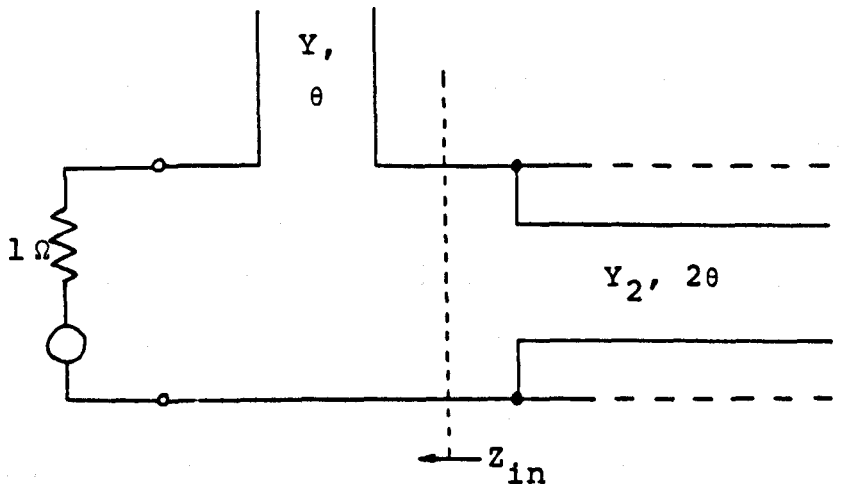

$$Z_{in} = 1 + \frac{1}{jY\tan\theta}$$

$$= 1 - j\frac{L_1\alpha_H}{\tan(a_H\omega)}$$

Terminating impedance, Z_{in}, produced by first series stub of distributed highpass prototype

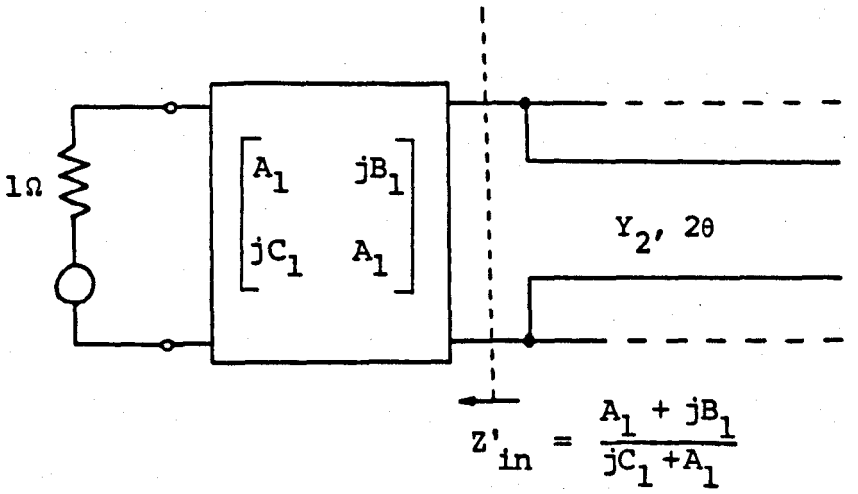

Terminating impedance, Z'_{in}, produced by first inhomogeneous section of suspended substrate highpass filter

Fig. 5.4.2 Terminating impedances produced by end elements of practical and theoretical highpass filters.

Note that this design assumes that the shunt impedances produced by the middle three inhomogeneous sections can be neglected.

From the above analysis, (5.4.19) and (5.4.20) are approximately satisfied by the two end sections of the working 8 GHz highpass, and the middle three sections which satisfy (5.4.21) and (5.4.22) are given by (5.4.13) and (5.4.14). Analysis of the highpass formed by these sections and the shunt resonators, shows that the first four minima of passband return loss are: 25.09 dB at 8.227 GHz, 19.63 dB at 9.12 GHz, 7.78 dB at 12.65 GHz and 7.70 dB at 17.01 GHz.

Clearly, the design equations (5.4.19) - (5.4.22) are not quite correct. The good match near bandedge is due to the correct series impedances produced by the inhomogeneous sections around this region. Further, the shunt admittances around bandedge produced by the middle three inhomogeneous sections can be neglected in comparison with the admittances of the shunt resonators. However, as the above analysis shows, these shunt admittances cannot be neglected from 11 GHz onwards. Indeed, their frequency behaviour is approximately that of a lumped capacitor, so they become significant when compared with the admittances of the shunt resonators for frequencies from 11 GHz onwards. For the above design, the mismatch around bandcentre is caused by the total shunt admittance produced by each resonator and neighbouring (middle) inhomogeneous

sections not becoming zero at the same frequency as the series reactances become zero. This results in interactions occurring between the series and shunt elements of the filter and therefore causes the poor mismatch at 12.65 GHz. This fact is confirmed when we study the working 8 GHz highpass. Here the series impedances produced by the middle sections become zero at 12.975 GHz and the total shunt admittances become zero at almost the same frequency viz. 12.835 GHz and 12.425 GHz. The terminating reactances produced by the end sections become zero at 14.02 GHz.

5.4.1. New design equations

We can now write down new design equations for the inhomogeneous section highpass. That is,

$$\left.\begin{aligned} \text{Im } Z'_{in} &= \text{Im } Z_{in} \\ Z'_{rH} &= Z_{rH} \end{aligned}\right\} \text{ at bandedge frequency} \qquad (5.4.23),\ (5.4.24)$$

$$\left.\begin{aligned} \text{Im } Z'_{in} &= 0 \\ Z'_{rH} &= 0 \end{aligned}\right\} \text{ at } f_c < f_{cH} \qquad (5.4.25),\ (5.4.26)$$

where r = 3,5 and 7

and f_c is the solution of both

$$j\,Y_2 \tan(4\pi a_H f) + Y'_3(f) = 0 \qquad (5.4.27)$$

and $$j\,Y_4 \tan(4\pi a_H f) + Y'_3(f) + Y'_5(f) = 0 \qquad (5.4.28)$$

where Y'_3 and Y'_5 are the shunt admittances produced by the second and third inhomogeneous sections respectively.

Equations (5.4.23) and (5.4.24) ensure a good match around bandedge. The concept behind the other equations is that we make the series impedances produced by the inhomogeneous sections resonate at the same frequency as that when the total shunt admittances in the highpass become zero. This will ensure a good match at this frequency and hence at frequencies beyond it. Notice that the resultant immittances in the circuit will all increase positively above this frequency (N.b. we even make the terminating reactive component zero at this frequency - see (5.4.25)).

It should be noted that the working 8 GHz highpass (Fig. 5.3.8) almost satisfies the new design equations, which accounts for its good passband. In practice the exact solution to these equations would be difficult, but considerable simplification can be achieved by making the middle three sections equal. Equation (5.2.24) is then solved for the second section only, but the error in the series impedance produced by the third section will be negligible. The simplification also means that (5.4.27) and (5.4.28) cannot be satisfied by the same frequency, however their solutions are close and it is sufficient to satisfy only (5.4.27). In physical terms, this means that there will be a small shunt admittance when the series reactances are zero. However, this can be altered by scaling the shunt resonator lengths to produce an optimal performance (see next but one paragraph).

Equations (5.4.23) - (5.4.27) could be simply solved, for example, by numerical techniques. However, using the last two programs and varying the dimensions of the inhomogeneous section in these programs, we find that accurate solutions to the equations are given by the following inhomogeneous sections:

$$w_{1H} = w_{9H} = 0.0539" \; ; \; \ell_{1H} = \ell_{9H} = 0.0910" \qquad (5.4.29)$$

and

$$\left.\begin{aligned} w_{3H} = w_{5H} = w_{7H} &= .0227" \\ \ell_{3H} = \ell_{5H} = \ell_{7H} &= .0757" \end{aligned}\right\} \qquad (5.4.30)$$

These sections mean that the solutions to (5.4.27) and (5.4.28) are 12.885 GHz and 12.490 GHz respectively, which are clearly close together. Also, the error in the bandedge impedance of the third section is only 2.23%.

Analysis of the highpass formed by these sections shows a minimum passband return loss of 14.85 dB was achieved up to 19 GHz. Although the shunt resonators were resonant at the correct frequency for an 8 GHz highpass, the 3 dB frequency was 7.973 GHz not 8 GHz. By scaling the lengths of these resonators by 8.088/8.3, the very good response shown in Figs. 5.4.3 and 5.4.4 was achieved. These results show a minimum passband return loss of at least 17 dB up to nearly 2½ times the 3 dB frequency (> 18.82 dB over the first octave) and there is the correct number of passband ripples. Clearly, scaling of the resonators can account for the

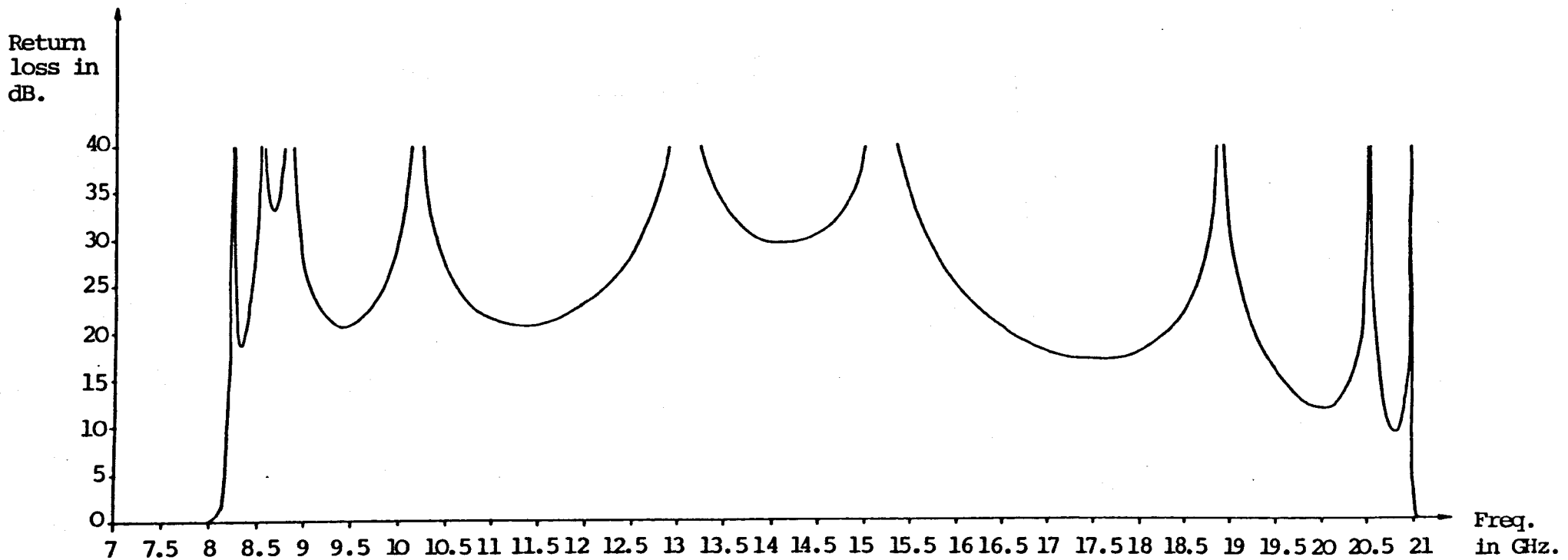

Fig. 5.4.3 Return loss of the 8 GHz highpass filter, where the complex inhomogeneous coupling elements are designed using equations (5.4.23) - (5.4.26)

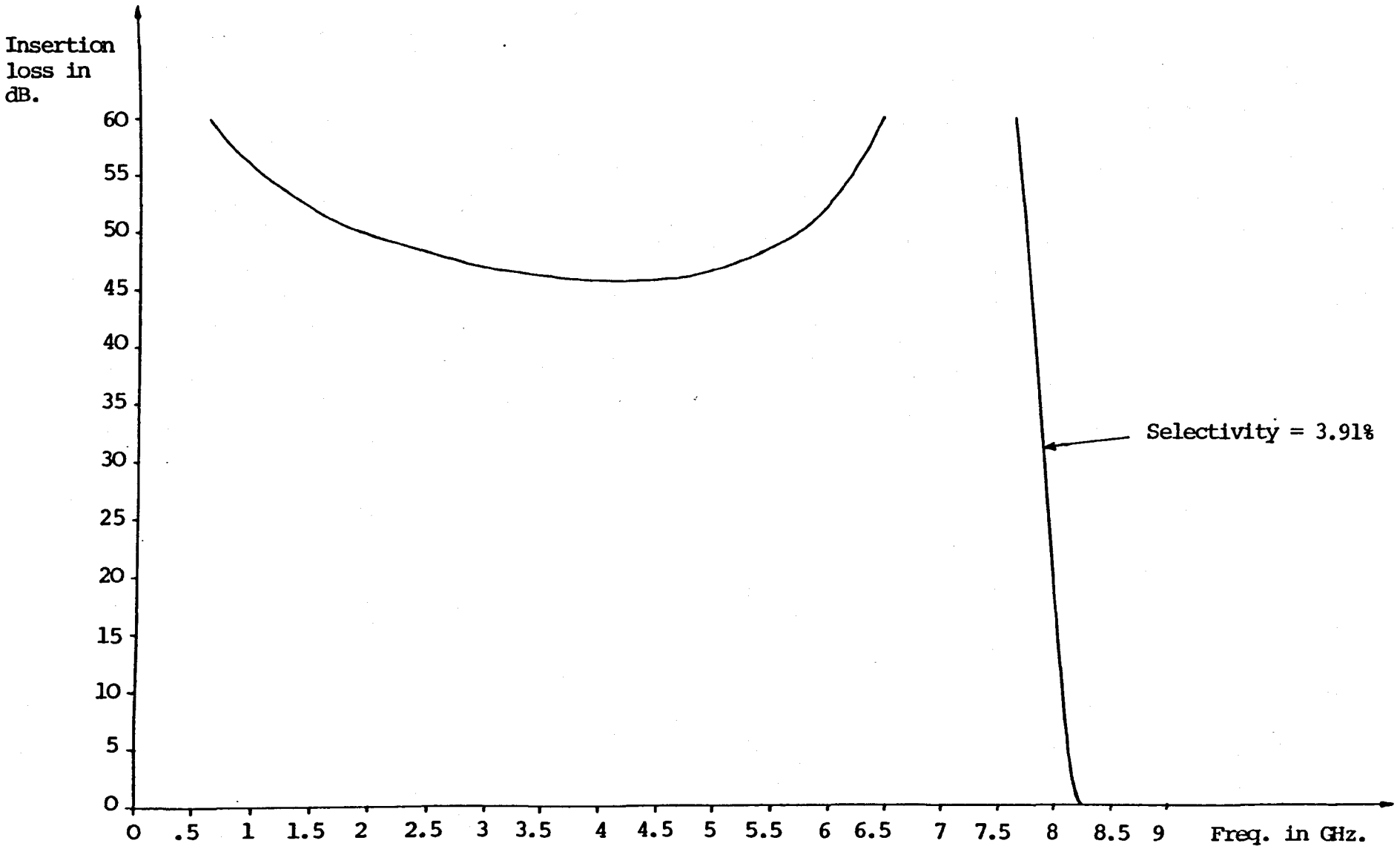

Fig. 5.4.4 Insertion loss of the 8 GHz highpass filter, where the complex inhomogeneous coupling elements are designed using equations (5.4.23) - (5.4.26)

non zero middle shunt admittances which occur when the other immittances are zero. This produces a more optimum response by producing a trade-off between the minima at 11.32 GHz and 17.55 GHz with the two minima near bandedge, especially the nearest (before this scaling, the ripple nearest bandedge was 21.04 dB). The 3 dB frequency is increased to 8.141 GHz, but the length of every element can be rescaled by 8.141/8 to produce a 3 dB frequency at 8 GHz. Another advantage of this design is that the minimum stopband insertion loss is greater than that for the distributed highpass prototype. This is because by making the series impedances resonate below bandcentre, they have a higher reactance in the stopband than the series impedances of the distributed prototype.

Finally, the design of a high degree (say degree 15) highpass must be considered. Firstly, it must be realised that for any degree, n, of the generalised Chebyshev prototype, the series elements except the first and last are very similar. The same is true for the shunt resonators. Hence little error in the series impedances would be introduced by making all the inhomogeneous sections the same, except the two end ones. A suitable design would then be to solve (5.4.23) - (5.4.26), where (5.4.24) is only solved exactly for two inhomogeneous sections symmetrically positioned about the centre of the filter. We shall choose the two sections closest to the centre of the filter, so that f_c is now the solution of:

$$Y_{(n-1)/2} \tan (4\pi a_H f) + 2Y'(f) = 0 , \quad \text{for m even} \qquad (5.4.31)$$

$$\text{or} \quad Y_{(n-3)/2} \tan (4\pi a_H f) + 2Y'(f) = 0, \quad \text{for m odd} \qquad (5.4.32)$$

where

m = (n-1)/2 = number of shunt resonators in the filter. $Y_{(n-1)/2}$ or $Y_{(n-3)/2}$ are the characteristic admittances of the two identical shunt resonators symmetrically positioned about, and closest to, the centre of the filter

and $Y'(f)$ is the shunt admittance produced by each middle inhomogeneous section.

Owing to the variation in the admittance of the resonators through the filter, the resultant shunt admittances will not all be zero exactly at the same frequency. However since the impedance variation is slight, the zero frequencies will be very close. In any case, this can be accounted for by scaling the shunt resonator lengths, as in the 8 GHz highpass designed in this section.

We now have a novel design technique for the broadband generalised Chebyshev highpass using inhomogeneous coupled lines. It should be noted that the Elliptic Function prototype would not be suitable for this design owing to the large impedance variation in the prototype.

5.5. Multiplexer Analysis

5.5.1. Explanation of the multiplexer analysis computer programs

The first program analyses the theory of generalised Chebyshev contiguous diplexers developed by Professor Rhodes (see Appendix for theory). The program considers the distributed 4 - 18 GHz triplexer 'prototype' and the cascade arrangement of it is shown in Fig. 5.5.1. The term 'prototype' is used because the triplexer consists of two distributed diplexer prototypes, scaled to 12 and 8 GHz, and a 4 GHz distributed highpass prototype. By a distributed diplexer prototype, we mean that lumped diplexer prototype considered in the theory by Rhodes, scaled by Richard's frequency transformation (with the appropriate constants α_L, a_L and α_H, a_H for the lowpass and highpass filters respectively). This means that the series elements of the filters in the triplexer are the ideal short or open circuited stubs which result from application of Richards transformation. In the practical triplexer analysis program, these stubs are replaced by unit elements or inhomogeneous coupled lines. The basic structure of the multiplexer analysis programs will now be explained.

The first stage is to calculate and store, using array variables, the ABCD parameters of the transfer matrix of every filter in the triplexer, at some

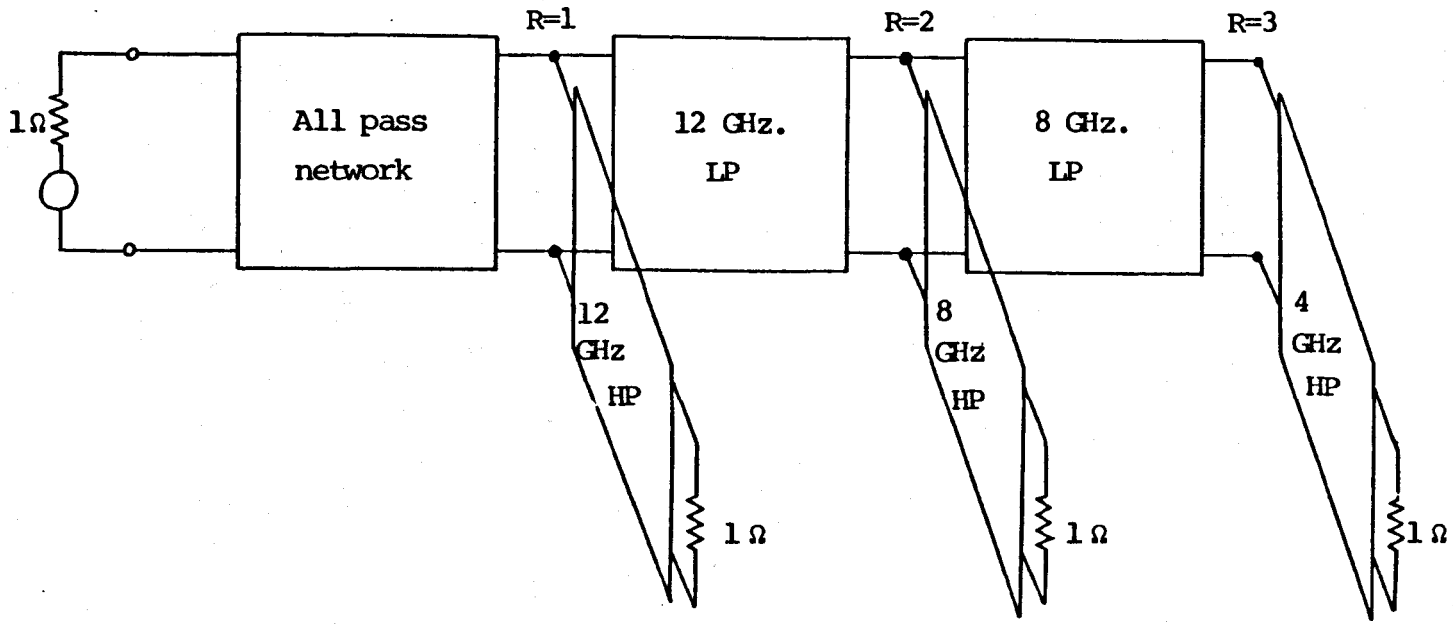

Key

F GHz. HP : Distributed highpass prototype with 3 dB frequency at F GHz

F GHz. LP : Distrubuted lowpass prototype with 3 dB frequency at F GHz.

N.B. The first series and first shunt elements of the prototypes forming each diplexer are suitably modified for correct operation (see Appendix)

Fig. 5.5.1 Distributed triplexer 'prototype' covering the bands 4 → 8, 8 → 12 and 12 → 18 GHz.

frequency. Let the transfer matrices of the lowpass filters be given by

$$(T)_{LR} = \begin{bmatrix} A1(R-1) & j\,B1(R-1) \\ jC1(R-1) & D1(R-1) \end{bmatrix} \qquad (5.5.1)$$

where R = 1,2 or 3

Note that for R=1, this is made the unity matrix and corresponds to the redundant all-pass network inserted between the source and the 12 GHz highpass, as shown in Fig. 5.5.1. This network is inserted to make the form of the analysis for the 12 - 18 GHz channel, the same as for the other channels. The transfer matrices of the 12 and 8 GHz lowpass filters are given by R = 2 and R = 3 respectively. Let the transfer matrices of the 12, 8 and 4 GHz highpass filters be given by

$$(T)_{HR} = \begin{bmatrix} A(R) & j\,B(R) \\ jC(R) & D(R) \end{bmatrix} \qquad (5.5.2)$$

for R = 1,2 and 3 respectively.

Fig. 5.5.2 shows the complete program used to analyse the practical triplexer, but the basic form of this program is the same as the one used to analyse the prototype triplexer. Lines 10-520 calculate and store, in the form discussed above, the transfer matrix of every filter in the triplexer. The multiplexer analysis section of the program is contained in lines 620 - 990.

Consider now the junction of the Rth highpass filter with the main line of the triplexer (see Fig.

Fig. 5.5.2 Computer program which analyses suspended substrate triplexer

```
10 PRINT "PRACTICAL MULTIPLEXER RESPONSE":PRINT
20 DATA .418398,0,2.49996,.182736,2.10855,.0905
30 DATA 1.18012,.661355,3.77404,.350661,2.03442,.0716
40 DATA 1.20707,.970846,3.77404,.350661,2.03442,.0716
50 DIM L(5),CP(5),ZE(5),ZO(5),EF(5),LN(5),Z(2)
60 Z(1)=1.75098:Z(2)=2.13923
70 FOR R%=1 TO 3
80 READ L(R%),CP(R%-1),ZE(R%),ZO(R%),EF(R%),LN(R%)
90 L(6-R%)=L(R%):CP(6-R%)=CP(R%-1):ZE(6-R%)=ZE(R%)
95 ZO(6-R%)=ZO(R%):EF(6-R%)=EF(R%):LN(6-R%)=LN(R%):NEXT
100 PRINT"ENTER WIDTH AND LENGTH(IN INS.) OF FIRST"
105 INPUT"8GHZ HIGHPASS INHOMOGENEOUS COUPLED LINES";ZO,LN
110 A=.0025:T=8.5E-4:B=7.534
115 ZE=B/(ZO/3.165E-2+1.08)
120 EF=1/SQR(1+12*A/(ZO-T)):EF=.5*(3.22+1.22*EF)
125 ZO=B/SQR(EF)/((ZO+T)/A+1.393+.667*LOG(1.444+(ZO+T)/A))
130 DIM A(3),B(3),C(3),D(3),A1(2),B1(2),C1(2),D1(2),Q(3),K(2)
135 W0=1.20798:W1=1.23555
140 INPUT"ENTER END FREQUENCIES AND STEPWIDTH";F1,F2,S
145 INPUT"LOW CHANNELS SCALING FACTORS";K(1),K(2):PRINT
150 IF F1<0 THEN 1000
160 PRINT"FREQ.   COMMON PORT RET. LOSS   INS. LOSS OF CHANNELS"
165 PRINT"IN GHZ.";TAB(30)"12-18GHZ  ";"8-12GHZ  ";"4-8GHZ"
170 L%=0
180 F=F1+L%*S
190 L(1)=1.11041:CP(1)=.964151
200 ZE(1)=ZE:ZO(1)=ZO:EF(1)=EF:LN(1)=LN
210 FOR R%=1 TO 3
220 A(R%)=1:B(R%)=0:C(R%)=0:D(R%)=1
230 IF R%=1 THEN 250
240 A=K(R%-1)*ATN(1/W0)/(20-4*R%):B=0:GOSUB 320
250 A1(R%-1)=A(R%):B1(R%-1)=B(R%):C1(R%-1)=C(R%):D1(R%-1)=D(R%)
260 A(R%)=1:B(R%)=0:C(R%)=0:D(R%)=1
270 A=ATN(W1)*.970874/(16-4*R%):B=1
280 IF R%<3 THEN 300
290 CP(1)=CP(4):ZE(1)=ZE(5):ZO(1)=ZO(5):EF(1)=EF(5):LN(1)=LN(5)
300 GOSUB 320:NEXT R%
310 GOTO 620
320 FOR M%=1 TO 5
330 IF B=1 THEN 390
340 D=L(M%)*F/Z(R%-1)/ATN(1/W1)*A
350 A1=COS(D)
360 B1=Z(R%-1)*SIN(D)
370 C1=SIN(D)/Z(R%-1)
380 GOTO 450
390 E=LN(M%)*F*4.25865/(16-4*R%):D=E*SQR(EF(M%))
400 A2=1/TAN(E):B2=1/SIN(E):C2=1/TAN(D):D2=1/SIN(D)
410 C1=ZE(R%)*B2-ZO(R%)*D2
420 A1=(ZE(R%)*A2+ZO(R%)*C2)/C1
430 B1=(ZE(R%)[2+ZO(R%)[2-2*ZE(R%)*ZO(R%)*(C2*A2+B2*D2))/2/C1
440 C1=2/C1
450 T=TAN(2*A*F)*W1/4
460 A2=A1-B1*CP(M%)*T
470 B2=B1
480 C2=C1+A1*CP(M%-1)*T+A1*CP(M%)*T-B1*CP(M%-1)*CP(M%)*T*T
490 D2=A1-B1*CP(M%-1)*T
500 A1=A(R%)*A2-B(R%)*C2
505 B(R%)=A(R%)*B2+B(R%)*D2
510 C1=C(R%)*A2+D(R%)*C2
515 D(R%)=D(R%)*D2-C(R%)*B2
520 C(R%)=C1:A(R%)=A1:NEXT M%:RETURN
```

```
620 FOR R%=1 TO 3
630 A1=1:A2=0:B1=0:B2=0:C1=0:C2=0:D1=1:D2=0
640 FOR M%=0 TO 2 STEP 1
650 A=A1(M%)*A1-C1(M%)*B1:B=A1(M%)*A2+C1(M%)*B2
660 B1=B1(M%)*A1+D1(M%)*B1:B2=B2*D1(M%)-B1(M%)*A2
670 A1=A:A2=B
680 A=A1(M%)*C1+C1(M%)*D1:B=A1(M%)*C2-C1(M%)*D2
690 D1=D1(M%)*D1-B1(M%)*C1:D2=B1(M%)*C2+D1(M%)*D2
700 C1=A:C2=B
710 IF M%=R%-1 THEN 790
720 B=A(M%+1)[2+B(M%+1)[2
730 A=(A(M%+1)*D(M%+1)+B(M%+1)*C(M%+1))/B
740 B=(C(M%+1)*A(M%+1)-B(M%+1)*D(M%+1))/B
750 A1=A1+B2*A-B1*B:A2=A2+B1*A+B2*B
760 C1=C1+D2*A+D1*B:C2=C2+D1*A-D2*B
770 NEXT M%
780 GOTO 820
790 A3=A1:A4=A2:B3=B1:B4=B2:C3=C1:C4=C2:D3=D1:D4=D2
800 A1=1:A2=0:B1=0:B2=0:C1=0:C2=0:D1=1:D2=0
810 GOTO 770
820 B=A1[2+A2[2
830 A=(A1*C2+C1*A2)/B:B=(A1*C1-C2*A2)/B
840 A3=A3+B4*A-B3*B:A4=A4+B3*A+B4*B
850 C3=C3+D4*A+D3*B:C4=C4+D3*A-D4*B
860 A1=A(R%)*A3-C(R%)*B3:A2=A(R%)*A4+B4*C(R%)
870 B1=B(R%)*A3+D(R%)*B3:B2=D(R%)*B4-B(R%)*A4
880 C1=A(R%)*C3+C(R%)*D3:C2=A(R%)*C4-C(R%)*D4
890 D1=D(R%)*D3-B(R%)*C3:D2=B(R%)*C4+D(R%)*D4
900 E=A1+D1+B2+C2:O=A2+D2+B1+C1
910 A=E[2+O[2
920 Q(R%)=4.34294*LOG(A/4):NEXT R%
930 A=A1-D1+B2-C2
940 B=A2-D2+B1-C1
950 A=(A[2+B[2)/(E[2+O[2)
960 A=4.34294*LOG(1/A)
970 PRINT F;TAB(12) A;TAB(30)
980 FOR R%=1 TO 3:PRINT Q(R%);:NEXT R%:PRINT
990 L%=L%+1:IF F>=F2 THEN 140 ELSE 180
1000 END
```

5.5.1). Lines 630-800 evaluate the overall transfer matrices of the networks to the left and right of this junction and store them as

$$\begin{bmatrix} A3 + jA4 & jB3 + B4 \\ jC3 + C4 & D3 + jD4 \end{bmatrix}$$

and $\begin{bmatrix} A1 + jA2 & jB1 + B2 \\ jC1 + C2 & D1 + jD2 \end{bmatrix}$, respectively.

This process is shown in Fig. 5.5.3(a). In order to find these matrices, the input admittances of the high-pass filters to the left and right of the Rth junction must be found. This is done using lines 720-740. These shunt admittances can then be considered as two-port networks in cascade with the lowpass filters, so their combined matrix can be easily found. This is effectively done using lines 750-760.

The next stage is to calculate the input admittance of the network to the right of the Rth junction, noting that this network is effectively on open circuit. This is done using lines 820 and 830 and is represented in Fig. 5.5.3(b). Next, the transfer matrix to the left of the Rth junction is modified to include the transfer matrix of this shunt admittance (see lines 840 - 850). Finally, the overall transfer matrix of this modified network and the Rth highpass is calculated and stored as,

$$\begin{bmatrix} A1 + jA2 & jB1 + B2 \\ jC1 + C2 & D1 + jD2 \end{bmatrix}$$

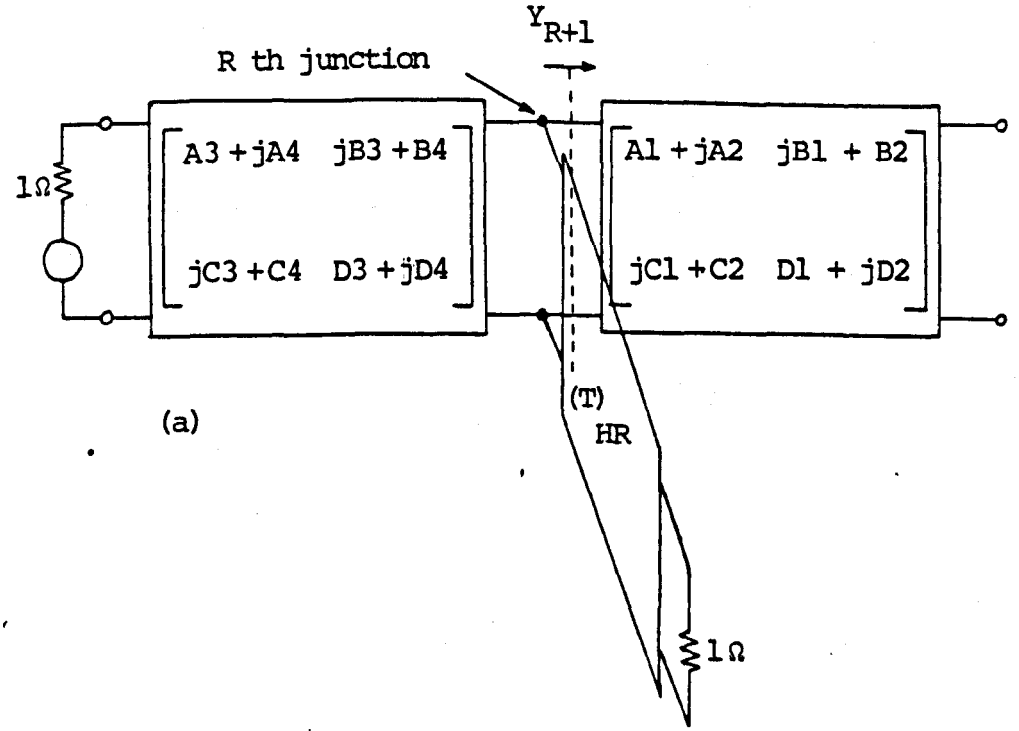

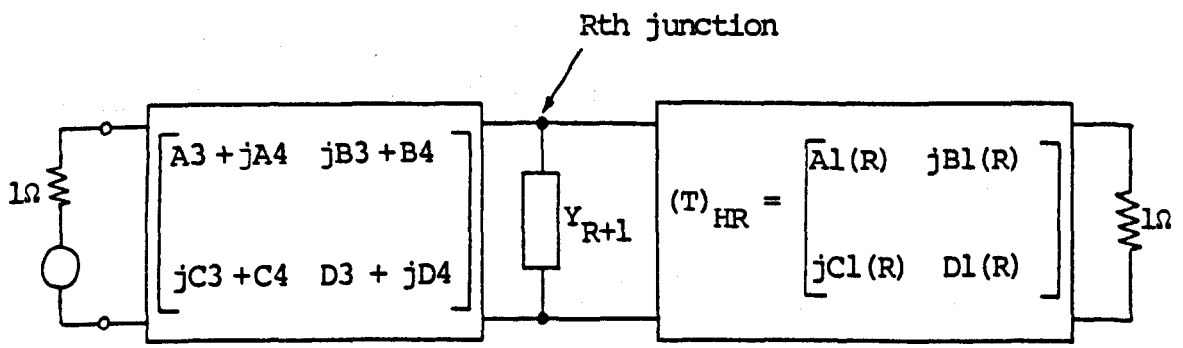

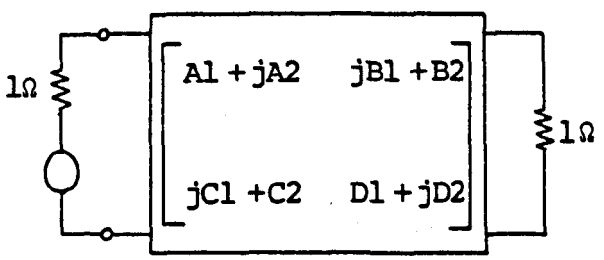

Fig. 5.5.3 Transfer matrix approach to analyse the Rth channel of a N channel multiplexer

This process is done in lines 860-890 and represented in Fig. 5.3.3(c).

The insertion loss of the Rth channel can now be found from [5.1]

$$L_{AR} = 10 \log_{10} [\tfrac{1}{4} | (A1 + jA2) \sqrt{\frac{R_L}{R_S}} + (D_1 + jD2) \sqrt{\frac{R_S}{R_L}}$$

$$+ \frac{(jB1 + B2)}{\sqrt{R_L R_S}} + (jC1 + C2) \sqrt{R_L R_S} |^2] \qquad (5.5.3)$$

where R_L and R_S are the load and source resistances respectively, which in this case are unity.
(N.b. all the analysis in this chapter has been done for 1Ω terminations)

$$\text{i.e.} \quad L_{AR} = 10 \log_{10} [\tfrac{1}{4} (E^2 + O^2)] \qquad (5.5.4)$$

where E = sum of the even parts = A1 + D1 + B2 + C2 (5.5.5)

and O = sum of the odd parts = A2 + D2 + B1 + C1 (5.5.6)

Lines 900 - 920 use these equations to find the insertion loss of the Rth channel.

The above process is performed for each high-pass junction (i.e. for R = 1,2 and 3), so the insertion loss of each channel is determined. For the last value of R (i.e. R = 3), the input port return loss of the triplexer can also be found. This is because

$\begin{bmatrix} A1 + jA2 & jB1 + B2 \\ jC1 + C2 & D1 + jD2 \end{bmatrix}$ becomes, for R = 3, the transfer matrix of the complete network between the source resistance and the load resistance of the 4 GHz highpass. Now the scattering reflection coefficient, $S_{11}(s)$, and the input impedance of the triplexer, $Z_T(s)$ are related by [5.4],

$$S_{11}(s) = \frac{Z_T(s) - 1}{Z_T(s) + 1} \qquad (5.5.7)$$

But from the overall transfer matrix,

$$Z_T(j\omega) = \frac{(A1 + jA2) + (B2 + jB1)}{(C2 + jC1) + (D1 + jD2)} \qquad (5.5.8)$$

$$\therefore \quad S_{11}(j\omega) = \frac{(A1 - D1 + B2 - C2) + j(A2 - D2 + B1 - C1)}{(A1 + D1 + B2 + C2) + j(A2 + D2 + B1 + C1)} \qquad (5.5.9)$$

Now input port return loss is defined as $10 \log_{10} (1/|S_{11}(j\omega)|^2)$, so is therefore given by

$$L_R = 10 \log_{10} \left[\frac{E^2 + O^2}{(A1 - D1 + B2 - C2)^2 + (A2 - D2 + B1 - C1)^2} \right] \qquad (5.5.10)$$

Lines 930 - 960 calculate L_R and this, together with L_{AR}, are printed using 970 - 980. Theprogram then goes back to the very beginning of this section and repeats the process for another frequency etc. Note that the analysis method described here could easily be generalised to a n channel multiplexer.

5.5.2. Results for the 4 - 18 GHz triplexer prototype

Results show that a good input port return loss is achieved over most of the 4 - 18 GHz band, but that the return loss does have a minimum of 10.85 dB at 8.1 GHz. This result is not surprising because the theory developed by Rhodes is only a first ordered solution to the diplexing problem and does not account for the different distributed frequency transformations used for the high and lowpass filters. Also, it must be remembered that the final triplexer circuit is quite complicated. The improved response shown in Figs. 5.5.4 and 5.5.5 was achieved by making the following modifications:

(i) The first series inductance in the modified lumped lowpass prototype, used for the diplexers, was reduced by 7.54%, from 1.20099 to 1.11041. This reduces the characteristic impedance of the first series stub in both filters of each diplexer by 7.54%.

(ii) The first shunt resonator capacitance in the modified lumped lowpass prototype was increased by 5.63%, from 0.912758 to 0.964151. This increases the characteristic admittance of the first shunt resonator in both filters of each diplexer by 5.63%.

(iii) The lengths of the lowpass resonators in each diplexer were reduced by 0.3%. This is essentially a tuning effect.

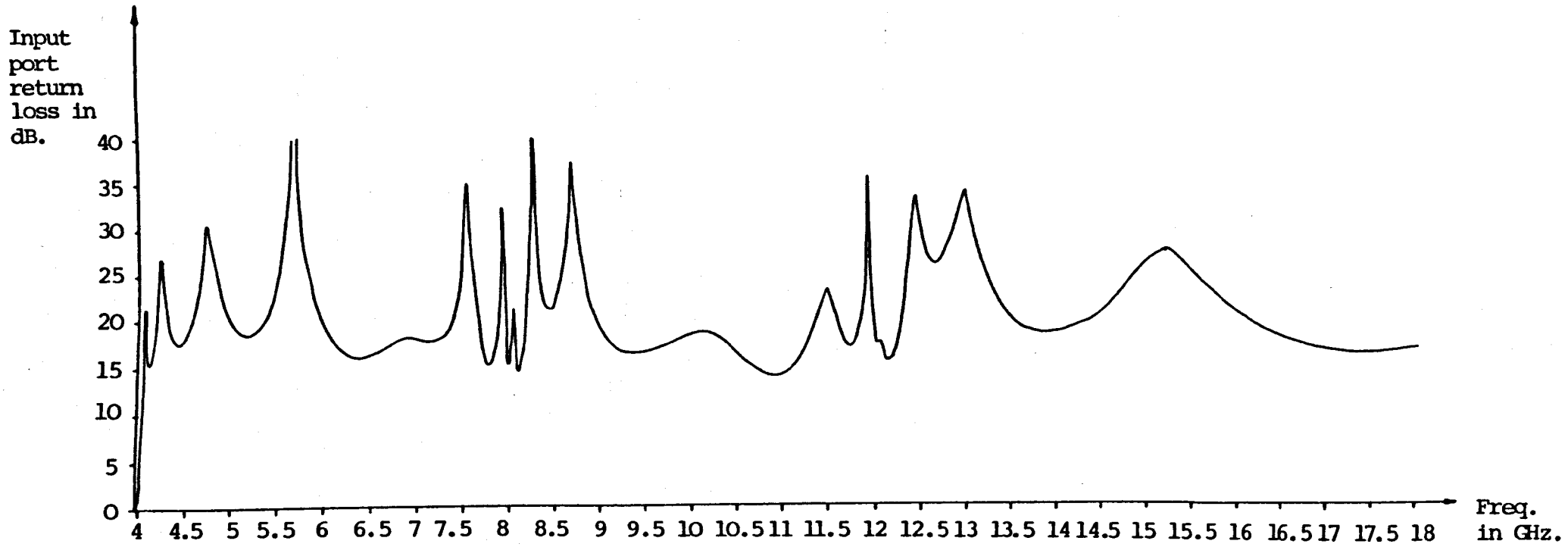

Fig. 5.5.4 Input port return loss for the 4 → 18 GHz distributed triplexer 'prototype'.

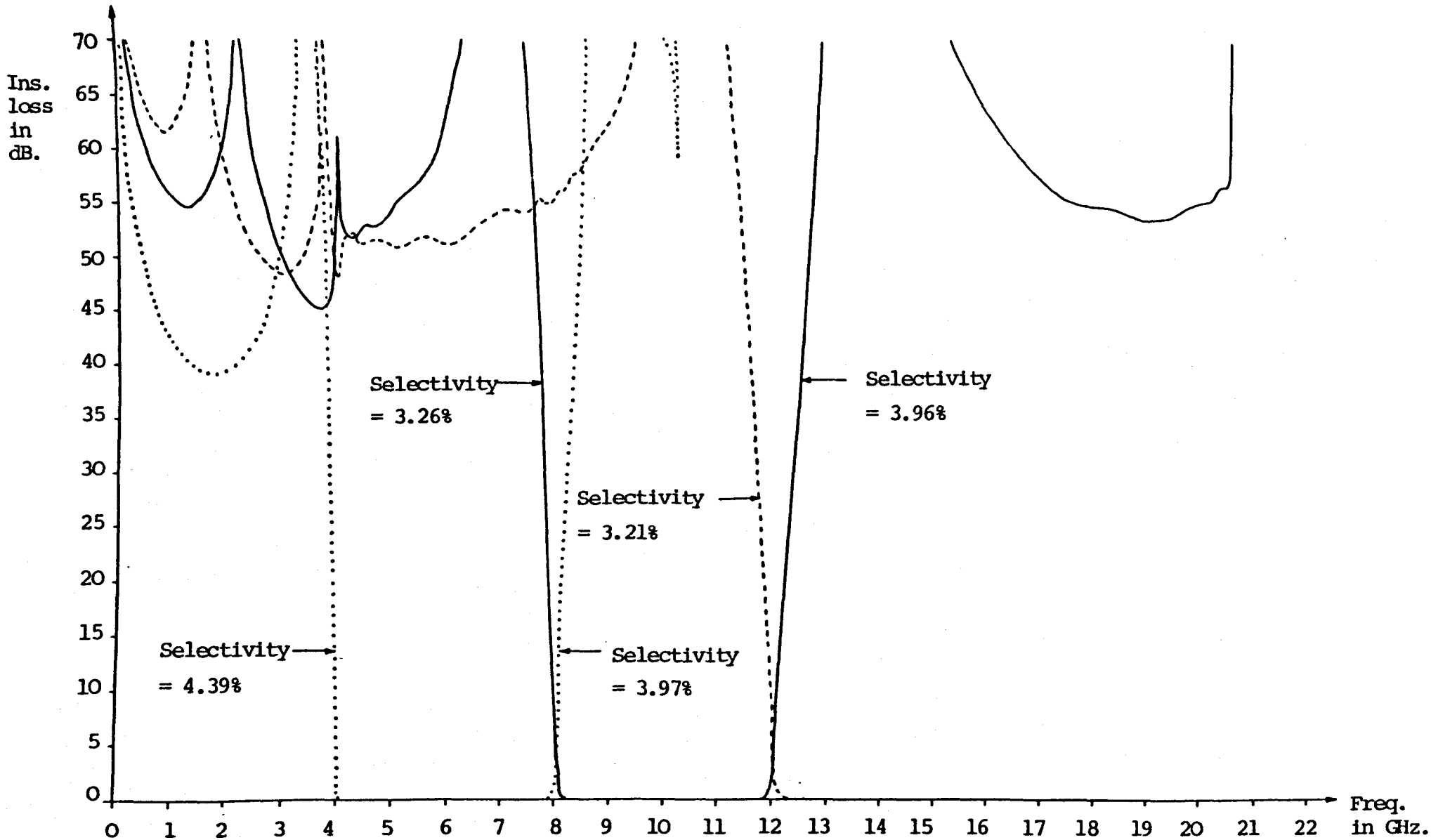

Fig. 5.5.5 Insertion loss of the three channels of the 4 → 18 GHz distributed triplexer 'prototype'

In these improved results, the bandedge frequencies (i.e. .0432 dB points) are within 2.33% of crossover. Also, the actual crossovers of the 8 and 12 GHz diplexers are, respectively, 3.092 dB at 8.020 GHz and 3.082 dB at 12.0321 GHz.

5.5.3. Analysis of 4 - 18 GHz suspended substrate triplexer

The triplexer analysed here is based on the single substrate triplexer designed in section 4.5 and the program used is shown in Fig. 5.5.2. In the analysis, the working 8 GHz highpass (Fig. 5.3.8) is used for the high channel of the 8 GHz diplexer and is scaled by factors of 8/12 and 2 respectively to form the high channel of the 12 GHz diplexer and the 4 GHz highpass. Note, however, that the first series and first shunt elements of the high channel in the diplexers must be suitably modified, according to the theory by Rhodes. The value of the first shunt resonator capacitor, given in section 5.5.2(ii), is used to determine the admittance of the first shunt resonator in these high channels. That is,

$$\begin{aligned} Y_2 &= 0.964151 \ \omega_o/2 \\ &= 0.595628 \end{aligned} \qquad (5.5.11)$$

The dimensions of the first inhomogeneous section in the highpass of the 8 GHz diplexer are supplied to the computer via an INPUT statement, so the effects of

this section on the triplexer response can be investigated. The length of this section is scaled by 12/8 to form the corresponding section in the 12 GHz diplexer. The overall transfer matrix of each highpass can then be calculated by the same methods used for the isolated highpass, discussed in section 5.3.2.

For the 12 and 8 GHz lowpass filters in the analysis program, the widths of the u.e.'s are made .0405" and .027" respectively. The characteristic impedances corresponding to these widths, for 1 Ω terminations, are 1.75098 Ω and 2.13923 Ω respectively. The widths chosen are close to those in the practical triplexer, but by making the width of every u.e. in each filter the same, the analysis is simplified. The lengths of the u.e.'s are then calculated using (2.4.17), but note that L_1 must be modified to account for the diplexing situation and the value used in the program is given in 5.5.2(i), viz. 1.11041. Note that in (2.4.17), f_{bL} = 7.888 GHz for the 8 GHz lowpass and f_{bL} = 7.888 x 12/8 = 11.832 GHz for the 12 GHz lowpass. Considering now the shunt resonators, their admittances are found using (2.2.5) but note that C_2 now takes the value in section 5.5.2(ii). The lengths of the 8 GHz lowpass resonators are given by (2.4.12), which are multiplied by 12/8 to form the resonator lengths in the 12 GHz lowpass. Using the above information, the transfer matrix of each lowpass can easily be found.

The transfer matrices of the filters are stored in arrays and the multiplexer analysis proceeds exactly as discussed in section 5.5.1. Note that runing is simulated using line 145, where the lengths of the resonators in the 12 and 8 GHz lowpass filters are scaled by factors K(1) and K(2) respectively.

5.5.4. Results for suspended substrate triplexer

The response shown in Figs. 5.5.6 and 5.5.7 is achieved for the following lowpass scaling factors and dimensions of the first inhomogeneous section in the 8 GHz highpass:

$$K(1) = .985 \quad , \quad K(2) = .991 \qquad (5.5.12)$$

$$\text{Width} = w_{1H} = .0271" \quad , \quad \text{Length} = \ell_{1H} = .0716" \qquad (5.5.13)$$

For this response, the bandedge frequencies (i.e. 0.0432dB points) are within 2.45% of crossover. Also, the actual crossovers of the 8 and 12 GHz diplexers are, respectively, 3.122 dB at 8.0123 GHz and 3.11 dB at 12.0799 GHz.

The results clearly satisfy the original specification (Fig. 1.3.3) and are in good agreement with the practical results (Figs. 4.5.3 and 4.5.4). In particular note that the insertion loss of the 8 - 12 GHz channel falls to 33.3 dB at 17.45 GHz. The insertion losses of the 8 - 12 GHz and 4 - 8 GHz channel fall below 40 dB at some frequencies between 17.2 and 20 GHz due to the

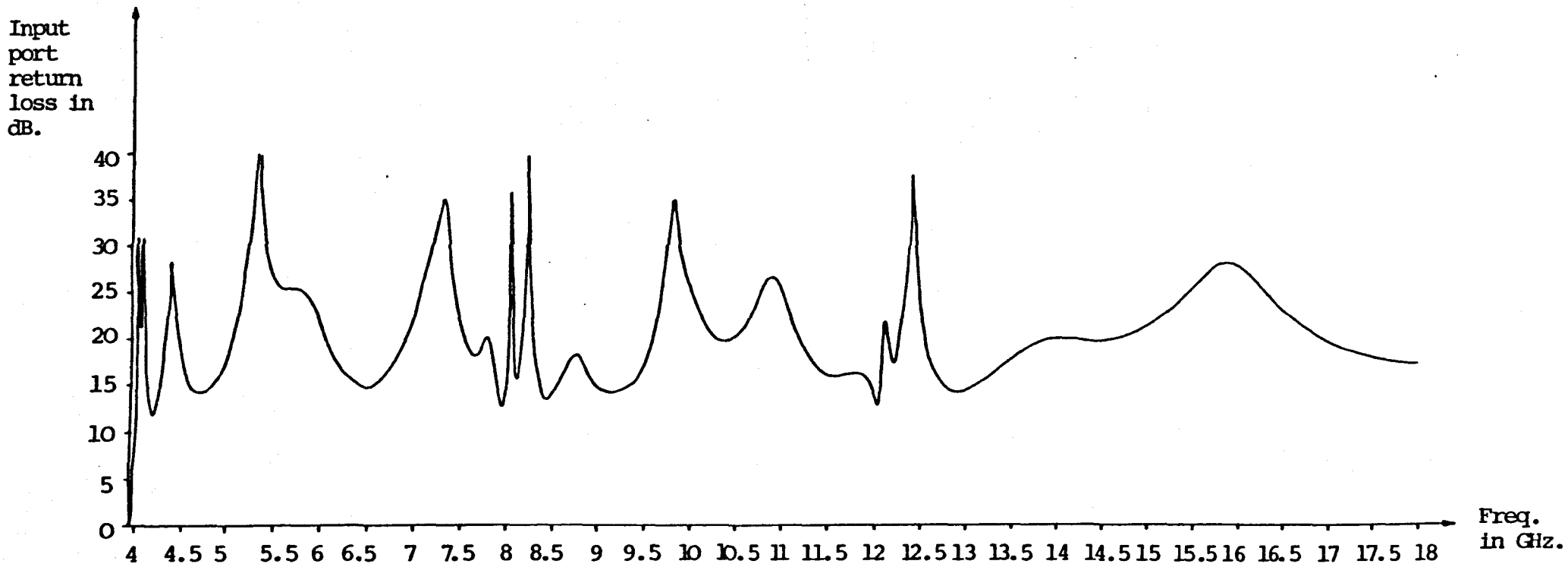

Fig. 5.5.6 Return loss for the 4 → 18 GHz single suspended substrate stripline triplexer

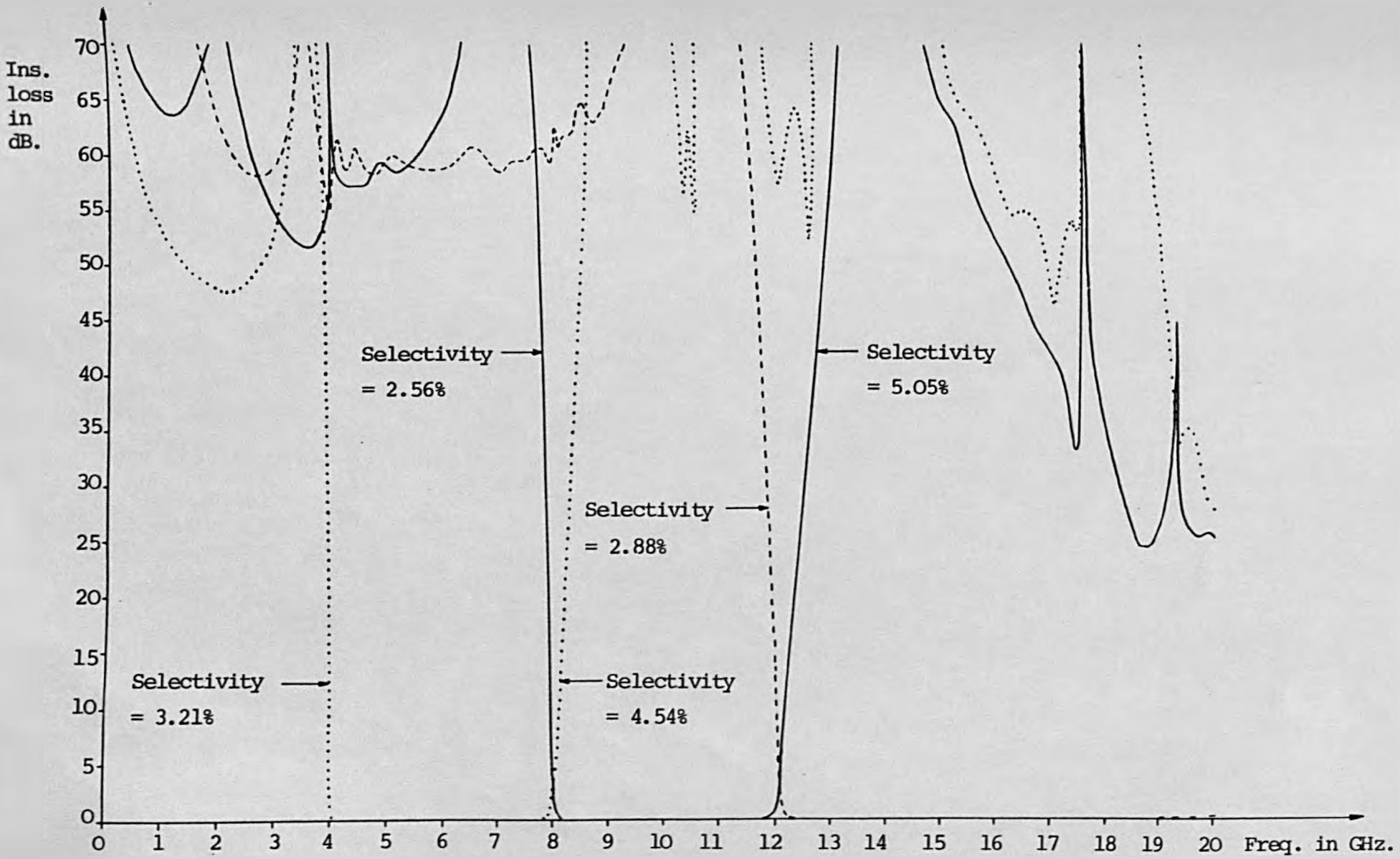

Fig. 5.5.7 Insertion loss of the three channels of the 4 → 18 GHz single suspended substrate stripline triplexer (N.B. Selectivity expresses the 40 dB frequency in terms of crossover)

insertion loss of the 12 GHz lowpass falling below 40 dB in this region. These losses could be increased to 40dB minimum up to at least 18 GHz by correctly redesigning the 12 GHz lowpass using 0.031" wide u.e.'s. (Narrower u.e.'s have a slightly broader stopband bandwidth - compare Figs. 5.2.5 - 5.2.10). Although the insertion loss of the 4 - 8 GHz channel does have a minimum around the 12 GHz crossover, it still remains above 52 dB. This is higher than the measured minimum, but we must remember that narrower u.e.'s for the 8 GHz lowpass were analysed than used in the practical triplexer and the practical minimum can be noticeably increased by slightly tuning the 8 GHz crossover. Finally, the ripples of stopband insertion loss in the 8 - 12 and 12 - 18 GHz channels, between 0 and 6 GHz, do occur in the practical triplexer and are due to interaction effects between the channels.

It should be noted that the dimensions in (5.5.13) are very similar to those of the first section in the 8 GHz highpass of the practical triplexer. This first section could be designed by solving (5.4.23) and (5.4.25). It is now understood that we are comparing the terminating impedance produced by the first imhomogeneous section with the terminating impedance produced by the first series stub of the highpass in the prototype diplexer. Due account must now be taken of the input impedance produced by the low channel. Equation (5.4.23) would be most easily solved at the frequency

where the lowpass shunt resonators become short circuits. The other equation could be simplified by justifiably neglecting the low channel.

6. CONCLUSIONS AND FUTURE WORK

Broadband, selective and low loss MIC lowpass and highpass filters have been successfully designed and constructed. Based on these filters, a contiguous multiplexer with outputs 4 - 8 GHz, 8 - 12 GHz and 12 - 18 GHz has been successfully built on a single substrate and its main results are:

(i) Input VSWR < 1.8 : 1 from 4 → 18 GHz

(ii) Stopband attenuation > 35 dB apart from within 5% of the crossover frequencies.

(iii) Passband insertion loss < 1 dB apart from within 5% of the crossover frequencies.

Several devices have been constructed to the same specification and first results suggest that a very high degree of population tracking will be achieved for both amplitude and phase. Fine tuning in the crossover regions is achieved relatively simply with capacitive tuning screws, but the main parts of the passbands are not tuned and are reproduced very accurately for all devices. Initial temperature and vibrational tests suggest that the crossover frequencies of the multiplexer will lie well within 1% of 8 and 12 GHz under most environmental conditions.

The filters used in the triplexer were designed just to meet the required specification. However, since these basic filters are not particularly complicated and are by no means at their physical limitations, higher

degree filters could be designed to produce multiplexers satisfying more difficult specifications. Indeed individual filters of higher degree and hence greater selectivity have been constructed and if used in a multiplexer would increase the attenuation level to greater than 60 dB apart from within 5% of the crossover frequencies. Due to the basic temperature variation, the 5% value cannot be readily reduced directly. To reduce this figure, it would be necessary to introduce temperature compensation techniques which are not trivial. However for most applications, 60 dB attentuation within 5% is adequate.

Recent work has been done by Professor Rhodes and S.A. Alseyab of Leeds university on a modified form of the lowpass prototype and is shown in Fig. 6.1.1. This prototype has 3 transmission zeros at infinity and (n-3) zeros at ω_o and is infact slightly more selective, for the same minimum stopband insertion loss and passband return loss, than the same degree prototype considered in this thesis. However the main advantage of it comes when it is used to design a lowpass in the distributed domain, using the techniques developed in this work. The end shunt capacitors become shunt open circuited stubs, quarter wavelength long at a frequency about 2.13 times the cut-off frequency of the filter. This produces a third ordered transmission zero at this frequency and should produce a broad stopband. Indeed experimental results for an 4 GHz lowpass show that the

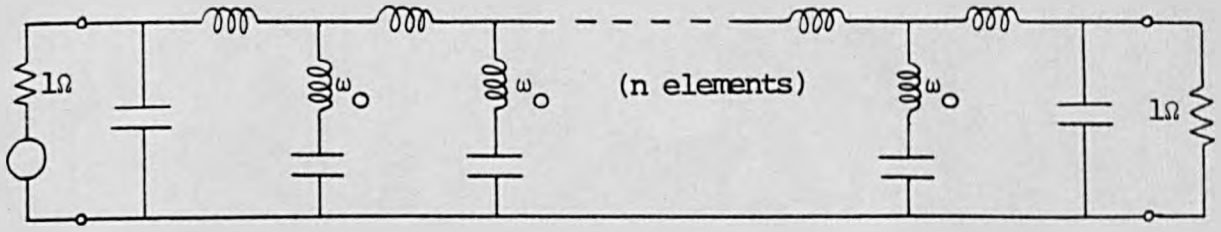

Fig. 6.1.1 The generalised Chebyshev lumped lowpass prototype filter with n-3 transmission zeros at ω_0 and 3 zeros at infinity.

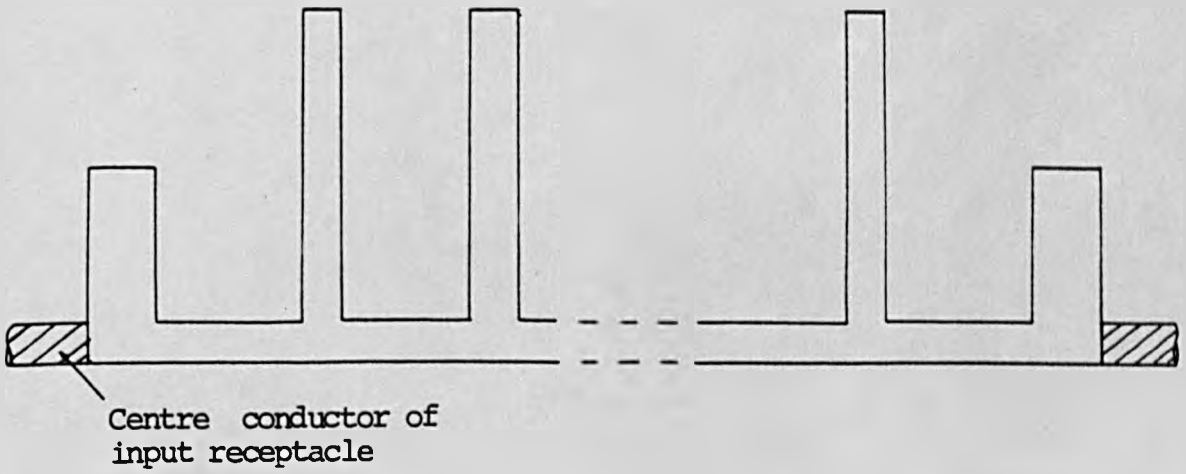

Fig. 6.1.2 Printed circuit of the distributed lowpass filter based on the above prototype

theoretical minimum stopband insertion loss is maintained up to nearly 2½ times the cut-off frequency. This bandwidth is much greater than is inherently possible from the physical lowpass structure considered in this work. The new printed form of the lowpass is shown in Fig. 6.1.2.

Using this new lowpass and the broadband highpass designed in chapter 5, it should be possible to design a multiplexer having at least octave bandwidths for each channel. A particular example would be a 4 - 8 GHz, 8 - 18 GHz diplexer. Moreover, by using a high degree design, the attenuation in each channel would be at least 60 dB apart from within 5% of the crossover frequency. This and similar devices would then have performances well in excess of those produced by the more common discrete component technology, in a fraction of the size and weight. Also, the devices would have superior population tracking properties due to the printed form.

The results presented in this thesis are comparable and in some respects are superior to the discrete component coaxial-type multiplexers. As discussed above, these results can be further improved by adding more sections or using the new lowpass prototype. Interesting results on narrowband filters and multiplexers are presently being discovered by continuing research at the university. It therefore appears that the suspended substrate structure will become one of the more important media for the realisation of microwave filters and multiplexers.

7. APPENDIX

A1 Generalised Chebyshev Diplexers

This section contains the design of contiguous generalised Chebyshev diplexers developed by Professor Rhodes. Fig. A.1.1 shows the nth degree generalised Chebyshev lumped lowpass prototype with its 3 dB frequency at $\omega = 1$.

Fig. A.1.2 shows the high-low contiguous lumped diplexer based on this prototype. The highpass in the diplexer is formed by applying the frequency transformation $\omega \rightarrow 1/\omega$ to the lowpass. By modifying the first series and first shunt elements of each filter, the diplexer can be matched at the common port at the critical resonant frequencies of the filters. The common port match should then be good at all frequencies.

Assume that the isolated lowpass is approximately matched at $\omega = 1/\omega_o$, then

$$\frac{j L_1}{\omega_o} + \cfrac{1}{Y + \cfrac{1}{j\frac{1}{\omega_o^3 C_2} + \frac{\omega_o}{j C_2}}} = 1 \qquad \text{(A.1.1)}$$

where

Y is the input admittance, at $\omega = 1/\omega_o$, seen looking to the right of the first shunt resonator of the isolated lowpass (see Fig. A.1.1)

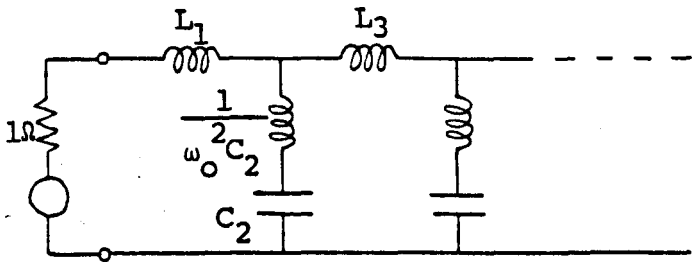

Fig. A.1.1 First few elements of the generalised Chebyshev lumped lowpass prototype filter. (Insertion loss = 3 dB. at $\omega = 1$).

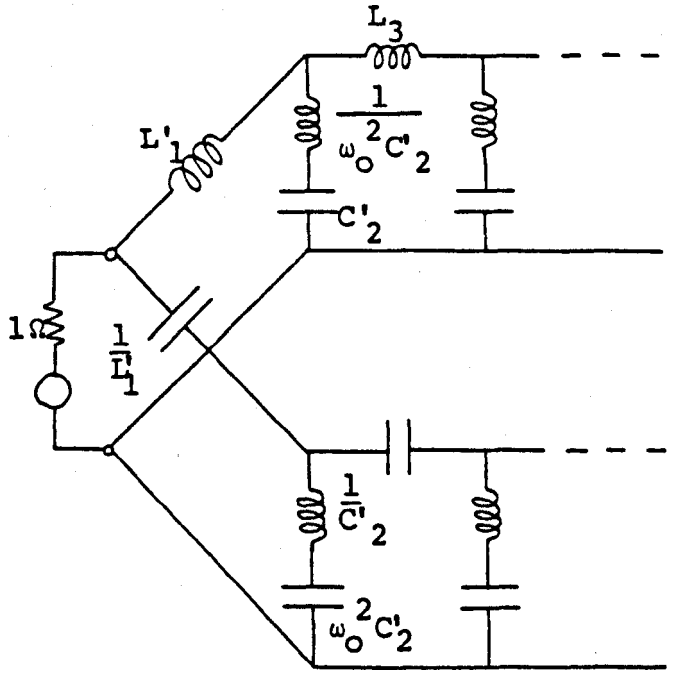

Fig. A.1.2 Lowpass -highpass contiguous generalised Chebyshev lumped diplexer.

$$\text{i.e.} \quad Y = \frac{1}{1 - j\dfrac{L_1}{\omega_o}} - j\frac{C_2\omega_o^3}{\omega_o^4 - 1} \qquad \text{(A.1.2)}$$

Using (A.1.2), the input admittance of the lowpass side of the diplexer at this frequency is,

$$Y_L = \frac{1}{j\dfrac{L'_1}{\omega_o} + \dfrac{1}{\dfrac{j\omega_o^3(C'_2 - C_2)}{\omega_o^4 - 1} + \dfrac{1}{1 - j\dfrac{L_1}{\omega_o}}}} \qquad \text{(A.1.3)}$$

For the highpass side,

$$Y_H = \frac{1}{-j\omega_o L'_1} \qquad \text{(A.1.4)}$$

To match the diplexer at the common port at this frequency, we require

$$Y_L + Y_H = 1 \qquad \text{(A.1.5)}$$

$$\text{i.e.} \quad j\frac{L'_1}{\omega_o} + \frac{1}{\dfrac{1}{1 - j\dfrac{L_1}{\omega_o}} + \dfrac{j\omega_o^3(C'_2 - C_2)}{\omega_o^4 - 1}} = \frac{1}{1 - j\dfrac{1}{\omega_o L'_1}}$$

$$\text{i.e.} \quad \frac{1}{1 - j\dfrac{L_1}{\omega_o}} + \frac{j\omega_o^3(C'_2 - C_2)}{\omega_o^4 - 1} = \frac{1 - j\dfrac{1}{\omega_o L'_1}}{1 - \dfrac{1}{\omega_o^2} - j\dfrac{L'_1}{\omega_o}} = \frac{\omega_o^2 - j\dfrac{\omega_o}{L'_1}}{\omega_o^2 - 1 - j\omega_o L'_1} \qquad \text{(A.1.6)}$$

From the real part,

$$\frac{1}{1+\frac{L_1^2}{\omega_o^2}} = \frac{\omega_o^4}{(\omega_o^2-1)^2 + \omega_o^2 L'^2_1}$$

$$\text{i.e. } L'_1 = \frac{\sqrt{(L_1^2 + 2)\omega_o^2 - 1}}{\omega_o} \qquad \text{(A.1.7)}$$

and from the imaginary part,

$$\frac{\omega_o L_1}{\omega_o^2 + L_1^2} + \frac{\omega_o^3(C'_2 - C_2)}{\omega_o^4 - 1} = \frac{\omega_o^3(L'_1 - \frac{1}{L'_1}) + \frac{\omega_o}{L'_1}}{\omega_o^2(\omega_o^2 + L_1^2)}$$

$$\text{i.e. } C'_2 - C_2 = \frac{(\omega_o^4 - 1)(L_1^2 - L_1 L'_1 + 1)}{\omega_o^2 L'_1 (\omega_o^2 + L_1^2)} \qquad \text{(A.1.8)}$$

(A.1.7) and (A.1.8) provide the modifications to the doubly terminated lowpass prototype for diplexing with a complementary filter. From this modified prototype, the distributed diplexer can be designed using the methods discussed in chapter 4.

A.2 GRAPHS FOR FINDING THE FRINGING CAPACITANCES OF COUPLED RECTANGULAR BARS, BY W.J. GETZINGER. (See Ref. [2.2])

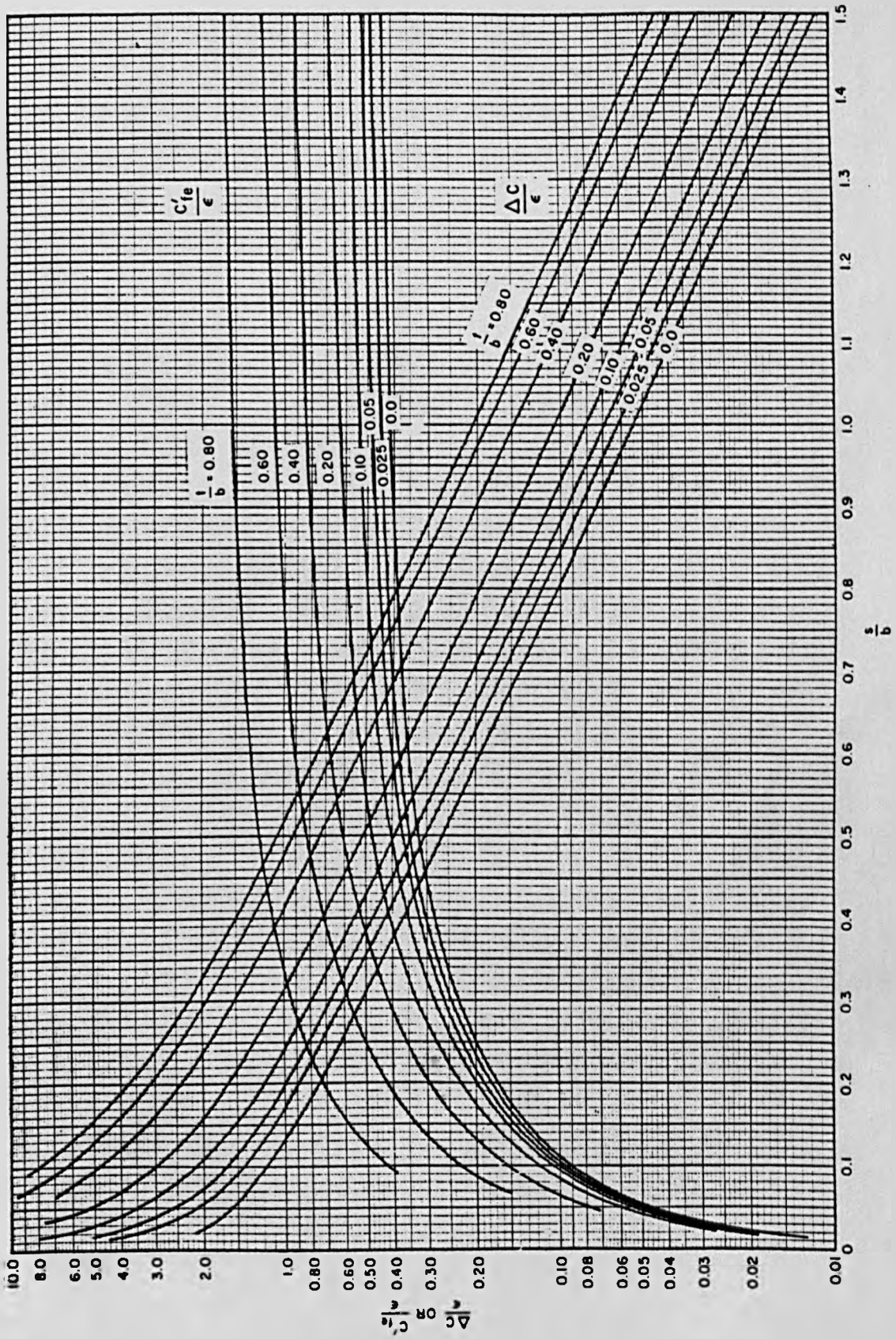

Fig. A.2.1 Normalised even-mode fringing capacitance C'_{fe}/ϵ and interbar capacitance $\Delta C/\epsilon$ for coupled rectangular bars.

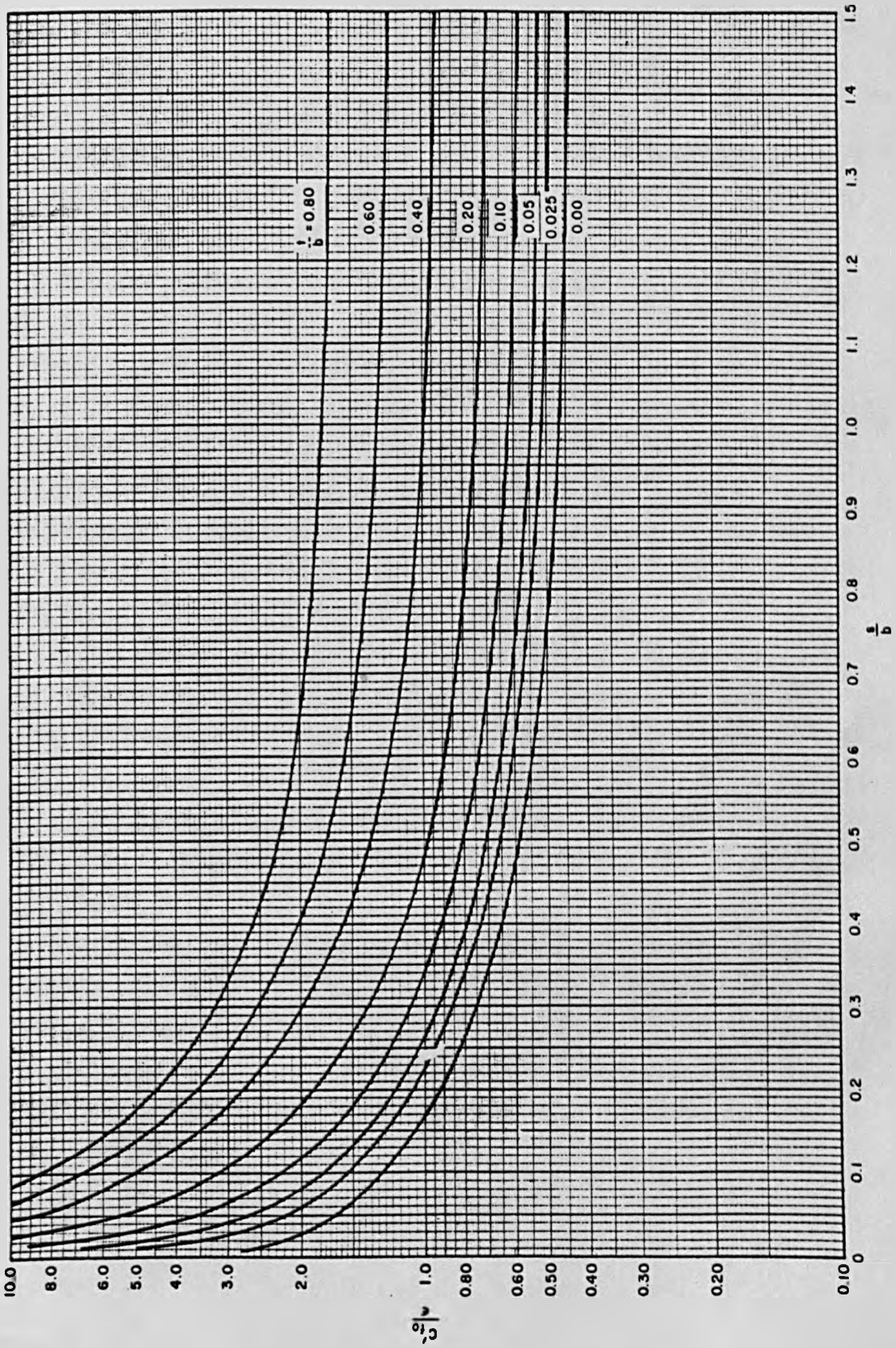

Fig. A.2.2 Normalised odd-mode fringing capacitance for coupled rectangular bars.

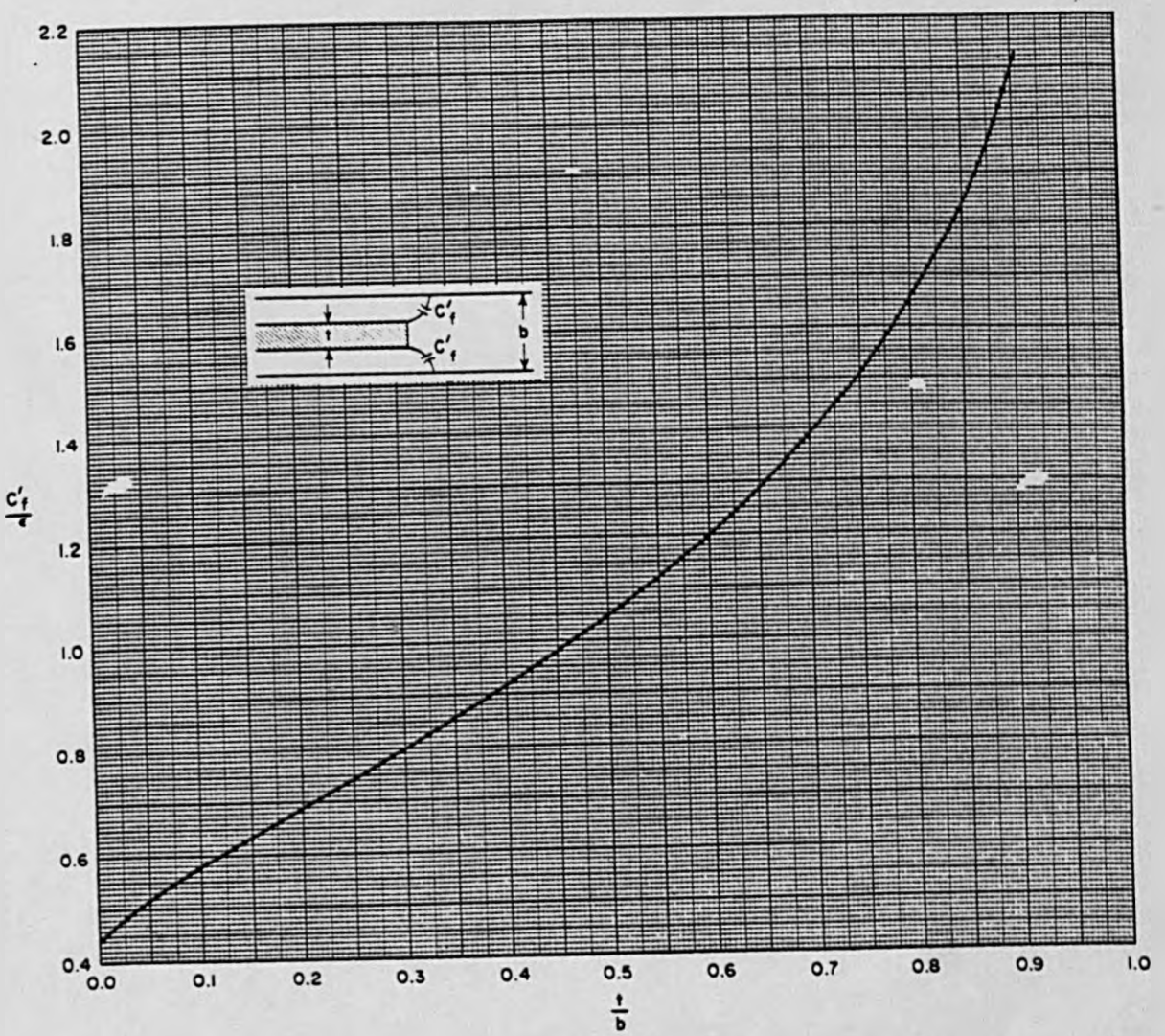

Fig. A.2.3 Normalised fringing capacitance for an isolated rectangular bar.

A3 Production and Alignment of Printed Circuits

The substrates are produced by standard printed circuit manufacturing techniques. Briefly, this involves producing an accurate photographic positive or mask of the printed circuit. This is then placed over a small piece of photo-resist coated, copper-clad duroid and exposed for a short time to ultra-violet radiation. After exposure, the board is processed in developer chemical which washes the exposed areas of resist away. The circuit can then be etched in an acid-based solution where the unexposed resist protects the circuit.

For the highpass filters and multiplexers, two masks and two exposures are required. Care must be taken to ensure that these two masks align correctly. This can be very simply achieved by fixing one mask, on a bench say, and moving the other mask over it until in correct alignment. This alignment is known from the design and by using a magnifying glass, the two masks can be very accurately located. Once in correct position, the two masks are taped together down one side to form an 'envelope' in which the duroid can be fixed. Clearly, the printed circuits on both sides of the duroid must now align and there is no need at this stage to cut the duroid to its exact size in the filter box.

To easily locate each substrate in its filter or multiplexer box, the outline of the substrate including the 0.03" groove used to support it in the box, is

drawn on the mask. This produces a copper outline on the printed circuit and shows where the circuit must be cut. Note also that the inner wall separating the two channels of a diplexer is represented by a copper rectangle on the p.c.b. This is cut away so the p.c.b. should correctly fit round the wall. The centre conductors of the receptacles also help to locate each substrate.

8. REFERENCES

1.1. H.L. Schumacher; 'Coax Multiplexers: Key to EW Signal Sorting', Microwave Systems News (MSN), Vol. 6, pp.89-93 Aug/Sept 1976

1.2. J.D. Rhodes; 'Theory of Electrical Filters', John Wiley and Sons, A Wiley-Interscience Publication, pp.12-13 and pp.30-35 (1976)

1.3. J.D. Rhodes and S.A. Alseyab; 'The Generalised Chebyshev Low-Pass Prototype', International Journal of Circuit Theory and Applications, (in press).

2.1. G.L. Matthaei, L. Young and E.M.J. Jones; 'Microwave Filters, Impedance-Matching Networks and Coupling Structures', McGraw Hill, New York, pp.360-364

2.2. W.J. Getzinger; 'Coupled Rectangular Bars Between Parallel Plates', IRE Trans. on Microwave Theory and Techniques, Vol. PGMTT-10, pp.65-72 (January 1962) (N.b. Also see Appendix, section A2)

2.3. 'Microwave Engineers Handbook', Vol. 1, Artech House Incorporated, pp.95 (1971).

2.4. Reference 2.1, pp.208-211

3.1. E.O. Hammerstad; 'Equations for Microstrip Circuit Design', 5th European Microwave Conference Proceedings, pp.268-271 (September 1975)

3.2. I.J. Bahl and R. Garg; 'Simple and Accurate Formulae for a Microstrip with Finite Strip Thickness', Proc. IEEE, Vol. 65, No. 11, pp.1611-1612 (November 1977)

3.3. Edwards and Owen; '2-18 GHz Dispersion Measurements on 10 - 100 Ohm Microstrip Lines on Sapphire', IEEE Trans. on Microwave Theory and Techniques, Vol. MTT-24, pp.506-513, (August 1976)

5.1. J.O. Scalan and R. Levy; 'Circuit Theory', Vols. 1 and 2, Oliver and Boyd, Electronic and Electrical Eng. Texts, pp.198-204, (1970).

5.2. R.A. Speciale; 'Even and Odd-Mode Waves for Non-symmetrical Coupled Lines in Nonhomogeneous Media', IEEE Trans. on Microwave Theory and Techniques, Vol. MTT-23, No. 11, pp.897-908 (November 1975)

5.3. G.I. Zysman and A.K. Johnson; 'Coupled Transmission Line Networks in an Inhomogeneous Dielectric Medium', IEEE Trans. on Microwave Theory and Techniques, Vol. MTT-17, No. 10, pp.753-759 (October 1969)

5.4. Ref. 5.1, pp.386-389.